Doctoral Dissertation
Doctoral Program in Metrology (XXXIV cycle)

Development and Experimentation of Traceable Characterization Methods for Medium Voltage Instrument Transformers for PQ and PMU Applications

By

Palma Sara Letizia
******

Supervisor(s):
Dr. Gabriella Crotti
INRIM - Istituto Nazionale di Ricerca Metrologica

Doctoral Examination Committee:
Prof. Valentina Cosentino, Referee, Università degli Studi di Palermo
Prof. Edoardo Fiorucci, Referee, Università degli Studi dell'Aquila
Prof. Jan Meyer, Referee, Technische Universität Dresden
Prof. Carlo Stefano Ragusa, President, Politecnico di Torino
Prof. Roberto Tinarelli, Referee, Alma Mater Studiorum Università di Bologna

Politecnico di Torino

2022

Declaration

I hereby declare that, the contents and organization of this dissertation constitute my own original work and does not compromise in any way the rights of third parties, including those relating to the security of personal data.

Palma Sara Letizia
2022

I would like to dedicate this thesis to my loving parents, my beloved sister.

Acknowledgements

Abstract

The International Electrotechnical Vocabulary defines Power Quality (PQ) as "the characteristics of the electric current, voltage and frequency at a given point in an electric power system, evaluated against a set of reference technical parameters". Therefore, a PQ disturbance can be identified as a change in the electric current, voltage, or frequency that interferes with the regular operation of electrical equipment and may result in failure or misoperation of customer equipment. The term "Power Quality" appeared in a scientific paper for the first time in 1968. In 1990, a study conducted by The Electric Power Research Institute evidenced that poor PQ costs the U.S. 26 billion annually.

PQ measurement is mostly performed at the Low Voltage (LV) level; however, in modern power systems, it is also gaining importance at Medium Voltage (MV). The interest in the PQ measurement at levels different from the low ones is due to the advance in the technology of switching devices and power converters that are now designed also to be directly connected to MV grids. Power converters are widely employed in distributed generation systems based on renewable energy sources and in non-linear loads. To reduce CO_2 emissions and global warming problems, the generation of energy from renewable sources is increasing more and more, and with it also the number of power converters installed in MV grids. These devices significantly contribute to injecting PQ disturbances, making PQ a critical task in MV systems. The monitoring of PQ at MV requires using Instrument Transformers (ITs) to scale MV voltage and current to suitable signals that can be fed to the input stage of PQ analyzers. Thus, assessing PQ disturbances at the MV level strongly depends on the performance of the ITs that are included into the measurement chain. For practical and economic reasons, this task is often entrusted to inductive ITs already installed in MV substations for metering and protection applications. However, currently, there are no specific standards dealing with ITs employed for PQ measurements. This issue has been partially addressed in the scientific literature, and

it has been highlighted that inductive ITs suffer from both filtering behaviour due to their dynamics and nonlinear effects produced by the iron core. As a result of the nonlinearity, the application of the principle of superposition of the effects can lead to significant errors in the ITs wideband calibration. In other words, the inductive IT frequency characterization with a sinusoidal signal sweep is not appropriate for accurately assessing their error contribution in the measurement of distorted signals and more complex test conditions are required.

The increasing number of non-linear loads and decentralized renewable generation systems have also significantly increased the power grids' complexity and instability, making substations operate under demanding conditions. Therefore, digital substations are spreading more and more to ensure stability and safety under these new complex conditions. A digital substation is an electrical substation where operations are managed among distributed intelligent electronic devices interconnected and synchronized with each other. For this reason, the first generation of analogue sensors used in power grid substantiation are going to be replaced with newer digital output sensors. However, a trade-off solution is currently taking place, and it consists of coupling conventional ITs with stand-alone merging units which are devices implementing the digitalization and time synchronization.

In this scenario, from the metrological standpoint, new measurement systems and procedures must be investigated and developed for the traceable characterization of both analog and digital ITs under distorted conditions representative of the actual ones. These characterization tests require quite complex and expensive generation and measurement systems. For this reason, it is also necessary to study and develop simplified but accurate test procedures that can be easily implemented using instrumentations already available in IT industrial laboratories.

This thesis presents the design, development and characterization of a measurement setup for the calibration of MV VTs in presence of PQ phenomenon and combinations of PQ phenomena. Starting from a deep analysis of state of the art, the thesis describes possible procedures, test waveforms and performance indices to quantify the error contribution of VTs used upstream a PQ instrument. The feasibility of the developed systems is then proved by characterizing different VTs under typical PQ phenomena. Finally, the thesis presents two different validated simplified techniques that can be performed in common industrial laboratories for assessing the frequency accuracy of inductive VTs.

Contents

List of Figures

List of Tables

Chapter 1

Introduction

1.1   Motivation

Record temperatures and frequent and unprecedented aggressive weather events are the most significant and evident signals that our world is experiencing unsustainable warming. Comparing the current temperature with the pre-industrial one, an increase of about 1.5°C is recorded, where 1°C is only due to human activities. If not well managed, global warming will dramatically compromise human life from several points of view, such as safety, health, economic growth, and social development. For these reasons, a climate conference was held in Paris in 2015 and 195 Countries, for the first time, signed a universal and legally binding global climate agreement. The agreement is mainly based on four points: long-term confinement temperature below 2°C, try not to exceed the 1.5°C, reach the maximum peak of global emissions as soon as possible and, reduce them through the most advanced scientific solutions.

The European Union aims to stop the global temperature increase and reach net-zero gas emissions by 2050. This complex but achievable goal requires extensive research and development activities in a wide variety of science and social fields. Above all, the energy one because leaving behind fossil fuels is the most critical point.

Consequently, the energy sector in each of its parts is experiencing an unprecedented revolution by introducing a vast amount of distributed energy systems based on renewable sources such as hydroelectric, thermal, nuclear, wind, solar, etc.

The decentralisation of generation, as well as the spreading of non linear and time-varying electronic loads, are the causes of two main issues:

1. the increasing complexity of power grids;

2. the significant increase of power grid disturbances.

As regards the first point, the power grid complex conditions are promoting the diffusion of digital substations to ensure the best possible stability and safety. A digital substation is an electrical substation where operations are managed among distributed Intelligent Electronic Devices (IEDs) interconnected and time-synchronized. Therefore, the digitalization of substations requires replacing the first generation of metering and protection devices with newer sensors featuring digital output and time synchronisation.

As a the second point, the degradation of the Power Quality (PQ), that expresses to which degree voltage and current conditions in an actual supply system are close to the ones of an ideal supply system, constitutes a real issue, since it may cause loss, corruption or damage of data, physical damage or ageing of sensitive devices, complete loss of the power supply. It is estimated that poor PQ has an annual cost of $119 – $188 billion for U.S. companies and €150 billion for the EU [2, 3].

Therefore, PQ monitoring is gaining more and more importance, and several international standards dealing with this topic have been produced in the past years. These standards define the characteristics and limits of the supplied voltage, methods for the PQ measurement, evaluation indices, and give prescriptions for the design and characterisation of PQ instruments (PQIs) as well as limits for their measurement uncertainty. In particular, the PQIs are built with standardised low input current and voltage levels. The choice of such low input levels is to avoid danger to operators while handling, building the PQI with economical and technologically suitable materials and sizes, and making them interchangeable.

The measurement of PQ at Medium Voltage (MV) and High Voltage (HV) levels can only be performed using suitable transducers to reduce voltage and current to levels fitting to the input stage of the PQIs. This task is commonly assigned to inductive instrument transformers (ITs), which are already installed in MV and HV grids for metering and/or protection applications.

Nevertheless, the in-force standards [4, 5] require verifying the metrological performances of inductive ITs only under rated sinusoidal conditions. From a normative point of view, only the technical report [6] provides some information in this regard. Thus, even if ITs belong to the PQ measurement chain, their errors in the measurement of PQ phenomena are not known.

The behaviour of ITs in the presence of PQ phenomena is an open issue that has been partially addressed in literature [7–10]. Some papers have highlighted that ITs can introduce significant errors in the measurement of PQ phenomena; for instance, it has been evidenced that in the measurement of harmonics, the errors introduced by a voltage transformer (VT) can reach some tens of percent or even higher depending on resonance event [8].

In this context, it is necessary to develop new measurement systems and procedures for the traceable characterisation of transducers operating on different principles, including those with digital output, under distorted waveforms representing the actual PQ conditions.

However, these measurement systems and procedures undoubtedly require accurate and costly laboratory instrumentation for generation and reference sensors. Therefore, it is also necessary to identify and develop simplified techniques that allow the accurate characterisation of ITs in industrial laboratories.

1.2 Measurement Context: The European Projects Future Grid II and IT4PQ

Most of the activities presented in this thesis are carried out in the framework of two European projects, Future Grid II and IT4PQ. Both the projects were funded from the European Metrology Programme for Innovation and Research (EMPIR) programme cofinanced by the participating States and from the European Union's Horizon 2020 research and innovation programme.

In this section, a brief overview of the two projects is given.

1.2.1 Future Grid II

The research project Future Grid II "Metrology for the next-generation digital sub-station instrumentation", funded under the EMPIR Call Industry, is a three-year project started in June 2018 and it was coordinated by the PTB, the German National Metrological Institute. The objective of the project is to provide yet missing solutions for the calibration and timing of the new type of substation instrumentation such Low Power Instrument Transformer (LPIT) and Stand-Alone Merging Unit (SAMU). As regards the LPITs, the project is focused on both digital (IEC 61850-9-2 and IEC 61869-9 compliant) and analog ouput LPIT with voltages up to $400/\sqrt{3}$ kV and current up to 2 kA.

The scientific and technical activities are developed within three technical work packages (WPs).

WP1 aims at developing calibration methods for the assessment of the behaviour, under steady-state, dynamic and transient events, of digital IT and LPIT for real-time monitoring systems which are based on synchronised PQ or PMUs measurements [11].

The aim of WP2 is to support the transition of substations with analogue, conventional IT technology, to digital substations by the introduction of suitable references for calibration of measuring instrument with a digital output. Due to the long lifetime of ITs and the high cost of replacing them, the first hybrid solution will be to upgrade the ITs to IEC 61850 gradually by use of SAMU which can 1) convert a conventional analogue IT output to a digital one and 2) implement the time synchronization.

The aim of WP3 is to assess the impact of digital real-time IEC 61850 communication on metering and grid control tasks and to investigate methods for improving the efficiency of the IEC 61850-SV protocol.

All the INRIM activities presented in this thesis belong to the first WP. In fact, INRIM main goal in FGII project is the design and development of a new laboratory reference system for traceable calibration of voltage LPITs with digital output under distorted conditions.

NOTE: *"The work presented in this thesis was partially developed within the EMPIR 17IND06 Future Grid II project, which is jointly funded by the EMPIR participating countries within EURAMET and the European Union."*

1.2.2   IT4PQ

The research project IT4PQ "Measurement methods and test procedures for assessing accuracy of Instrument Transformers for Power Quality Measurements" is a three-year project, funded within the EMPIR Call Normative 2019, which started in August 2020 and is presently ongoing and led by INRIM [12, 13].

The project's main goal is to develop a metrological framework to enable the traceable calibration of ITs to be employed for PQ measurements in electricity grids. The output results shall be used by IEC TC 38 Instrument transformers as a basis for the future standardisation about the use of ITs for PQ from IEC TC 38. Similarly to Future Grid II, also the IT4PQ activities are organised into three technical WPs. In all the WPs the analyses are focused on ITs with primary voltage and current up to 36 kV and up to 2 kA. The PQ phenomena considered are those presenting spectral components up to 9 kHz.

The first WP, is focused on the definition of accuracy and uncertainty limits of ITs for the measurement of PQ events. In other words, the WP1 activities are intended to extend the IT accuracy class concept to PQ measurements. The presently standardised IT accuracy class quantifies the maximum errors introduced at power frequency by the compliant IT as a function of the primary value of the applied voltage or current. Extension will be done by defining a new synthetic performance index that quantifies the error contribution of the IT when it is used to measure PQ disturbances.

To define the synthetic performance index, a deep knowledge and an organic classification of the IT behaviour under PQ phenomena have to be available. To this end, the objective of WP2 is the development of traceable test methods and reference measurement systems to characterise ITs under reference waveforms representative of the actual PQ disturbances. In addition, WP2 aims to study and implement architecture for simplified calibration setups and methods to characterise ITs in the industrial environment.

On site-power quality monitoring is always performed under conditions which are quite different from the controlled laboratory ones, because of the combined presence of different influence circuital and environmental factors, such as temperature, burden, grounded, floating or energized structures. So, the activities of the third WP are

devoted to evaluating the impact of separate and multiple influence factors on the ITs performances.

Although INRIM is involved in all three technical WPs, the activities contextualized in the IT4PQ project presented in this PhD thesis mainly belong to the first two. In particular:

- The identification of test waveforms and range of variation of test parameters to be used to verify the performance of IT used in PQ measurements.

- The definition of significant accuracy indices capable of quantifying the error contribution of IT that belongs to the MV PQ monitoring chain.

- The development of a generation and measurement system for accurately characterising VT of different types under single or combined PQ events.

- The investigation, development, and validation of simplified techniques for wideband characterization of IT feasible in industrial laboratories.

NOTE: *"The work presented in this thesis was partially developed within the 19NRM05 IT4PQ project which has received funding from the EMPIR programme cofinanced by the participating States and from the European Union's Horizon 2020 research and innovation programme".*

1.3 Analysed devices

This section briefly describes the most common VTs used in MV power grid applications which will be taken into consideration in the analyses presented in this thesis.

1.3.1 Inductive Voltage Transformers

Inductive VTs are electrical machines based on alternating currents (AC) and ferromagnetic material electromagnetic properties. They can produce output voltage with amplitudes proportional to those at their input. The inductive VTs schematic diagram is shown in Fig. 1.1 and, from a circuital point of view in Fig. 1.2; it consists of three main elements:

- A primary winding with N_p number of turns. It is connected to the MV power supply $(\overline{V}_p)$.

- A secondary winding with N_s number of turns. It is connected to the LV $(\overline{V}_s)$ measuring and/or protection devices.

- A core of ferromagnetic material transferring energy from the primary to the secondary winding.

- N_p/N_p is the device transformation ratio.

- Z_L is the load connected to the secondary.
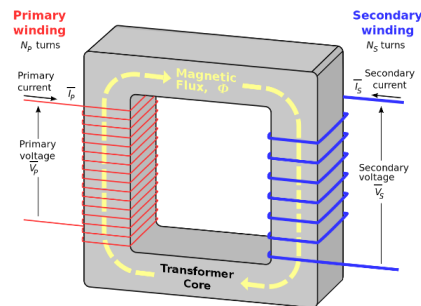
Fig. 1.1 Inductive VTs schematic diagram.
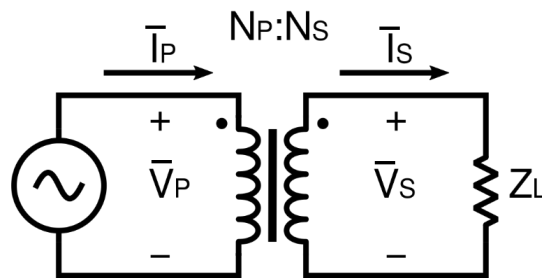
Fig. 1.2 Inductive ITs schematic circuital representation.

Considering the case of phase to ground VTs, the typical rated primary voltage $\overline{V}_p$ is chosen equal to $1/\sqrt{3}$ times the rated system voltage defined in IEC 60038. Typical values can be $30/\sqrt{3}$ kV, $20/\sqrt{3}$ kV, $11\sqrt{3}$ kV whereas the secondary voltage $\overline{V}_s$ has preferred values equal to $100/\sqrt{3}$ V or $110/\sqrt{3}$ V.

Both the primary and secondary windings have to carry current, avoiding as much as possible losses for the Joule effect. For this reason, they are commonly made up of annealed copper. The core has the task to transmit the magnetic flux reducing the losses due to magnetisation and heating. Thus, the core is built with several thin metallic layers made of Mu-metal, such as iron with 70% of nickel.

The inductive VTs working principle is rooted on Lenz's law, Faraday's law, and the conservation of energy law. Looking at Fig. 1.1, the alternating electric current $\bar{I}_\mathrm{p}$ flowing through wound conductors creates concentrated magnetic fields inside the primary windings. The ferromagnetic core provides the magnetic flux path to the secondary winding where the secondary current $\bar{I}_\mathrm{s}$ is induced. The ratio between the primary current $\bar{I}_\mathrm{p}$ and secondary currents $\bar{I}_\mathrm{s}$ depends on the number of turns of the primary and secondary winding, and it can be expressed as follow :

$$\frac{|\bar{I}_\mathrm{s}|}{|\bar{I}_\mathrm{p}|} = \frac{|\bar{V}_\mathrm{p}|}{|\bar{V}_\mathrm{s}|} = \frac{N_\mathrm{p}}{N_\mathrm{s}} \tag{1.1}$$

Even if the materials used for the VT construction are appropriately selected, problems related to losses and non-idealities are not null. In fact, from a circuital point of view, real inductive VTs can be represented as shown in Fig. 1.3:
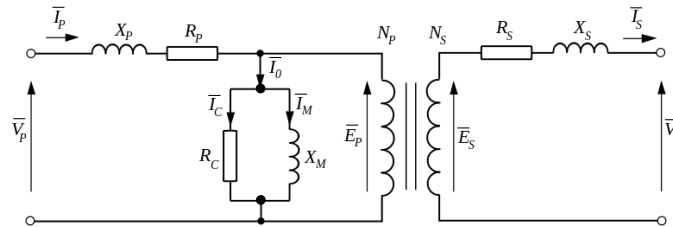
Fig. 1.3 Inductive ITs equivalent circuit.

Looking at the equivalent circuit, it is possible to identify three different sections. Two of them represent the primary and secondary windings (series parameters), and one is the iron core (magnetising branch). In detail:

- The R_p and R_s resistors represent the losses in primary and secondary windings because of the Joule effect.

- The X_p and X_s reactances are introduced to consider the flux not linked from the primary winding to the secondary (leakage flux).

- The R_c resistor models the losses in the iron core because of the Eddy currents and the nonlinearity of the magnetic material (hysteresis losses).

- The X_m reactance represents the iron core reluctance. The current $\bar{I}_M$ is necessary to establish the mutual flux inside the inductive VT core.

As a consequence of the losses listed above, Equation 1.1 is not entirely valid and is affected by an error. There is a not pure proportionality between the input current $\bar{I}_p$, and the output current $\bar{I}_s$ because of the current flowing into the magnetisation brunch ($\bar{I}_M$). The same consideration also applies to $\overline{V}_p$ and $\overline{V}_s$; in this case, the proportionality is not valid because of the voltage drops on the series elements.

Since voltage and current are phasors, the error affecting Equation 1.1 is a complex quantity, and it can be expressed in terms of magnitude and phase. These are defined as the ratio error ε and the phase error $\Delta\phi$. The errors are expressed as in Equations 1.2 and 1.3:

$$\varepsilon = \frac{k_r|\overline{V}_s| - |\overline{V}_p|}{|\overline{V}_p|} \tag{1.2}$$

$$\Delta\phi = \angle\overline{V}_s - \angle\overline{V}_p \tag{1.3}$$

where k_r is the VT rated transformation ratio defined as $V_{p,r}/V_{s,r}$ where $V_{p,r}$ and $V_{s,r}$ are the rated primary and secondary voltages at rated power frequency.

As regard the frequency behaviour of inductive VTs, several circuital model can be found in literature. The most common model that takes into account the stray capacitances among the active elements of the transformers is provided, for example, in [14]. A simplified model which highlights the stray capacitances is provided in Fig 1.4. The model takes into account the stray couplings between the primary winding and ground, the secondary winding and ground, and the primary and secondary windings are represented by C_H, C_L and C_{H-L} respectively. The presence of stray capacitances leads to inductive VT with a behavior characterized by resonance phenomena that limit the useful frequency band in which the VT can be used.
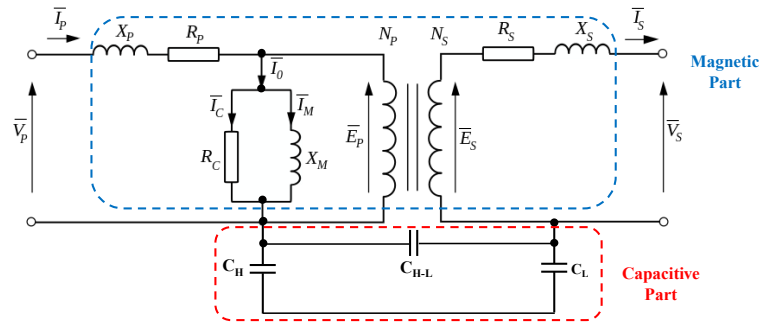
Fig. 1.4 Real circuital model of the VT with stray capacitances.

1.3.2   Low Power Voltage Transformers

The Low Power Voltage Transformers (LPVTs) are a new generation of voltage transducers. The LPVTs are defined by the Standard [1] as "arrangement, consisting of one or more voltage transformer(s) which may be connected to transmitting systems and secondary converters, all intended to transmit a low-power analogue or digital output signal to measuring instruments, meters and protective or control devices or similar apparatus". The main difference between VTs and LPVTs can be identified in the power provided at the secondary side; in fact, the LPVT can only provide power typically lower than 1 VA [1]. The use of these sensors in the measurement of the grid voltage and current has been made possible by the availability of low power electronic measurement and protection devices.

The LPVTs general block diagram provided by [1] is reported in Fig. 1.5. As can be observed, there are two types of LPVTs, the passive ones that do not require a power supply and the active ones which, on the contrary, need it.
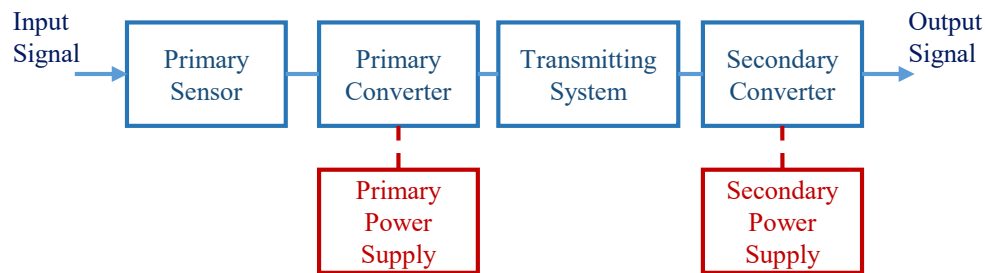
Fig. 1.5 Block diagram of an LPVT.

Moreover, from the general block diagram shown in Fig. 1.5, it follows that LPVT is not strictly based on a specific technology or operating principle. The most spread technologies employed to construct LPVTs are voltage dividers. As a general comment, the LPVT has some advantages compared to inductive VTs; they are linear, lightweight and small, not saturable, and do not suffer from ferro-resonance. Optical based technologies are now available for both the voltage and current measurements, which exploit the Pockels and Faraday effect. However, they are mainly adopted for HV measurements.

In the following, coherently with the subject of this thesis, types and characteristics of voltage dividers are briefly summarised.

Voltage Dividers

A Voltage Divider (VD) is a passive LPVT consisting of a series of two impedances $\overline{Z}_{HV}$ and $\overline{Z}_{LV}$, as shown in Fig. 1.6.
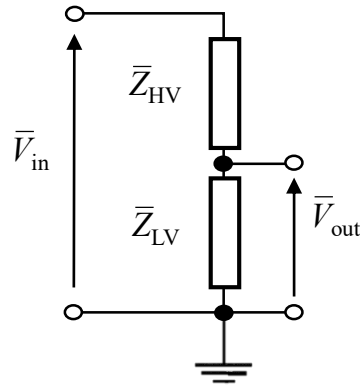
Fig. 1.6 Basic circuit representation of a voltage divider.

Based on the nature of the impedance $\overline{Z}_{\mathrm{HV}}$ and $\overline{Z}_{\mathrm{LV}}$, three different types of LPVT can be identified: the impedance can be the series of resistors (resistive divider), capacitors (capacitive divider) or the parallel connection of resistors and capacitors (resistive-capacitive divider).
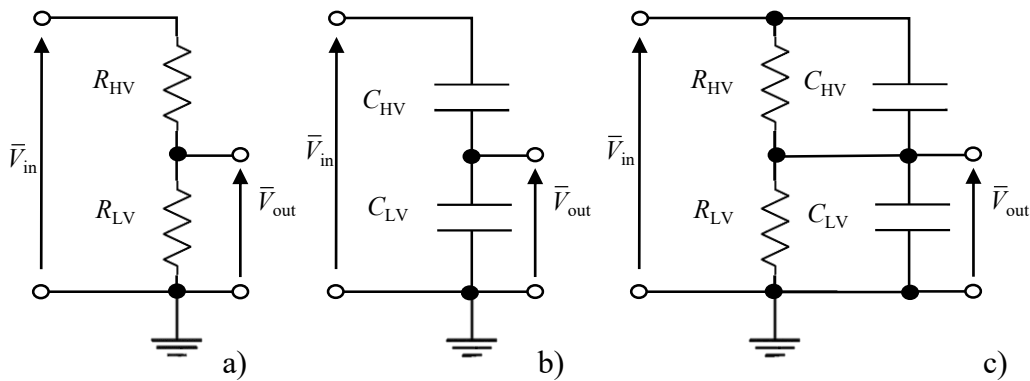
Fig. 1.7 Basic circuit representation of a) resistive, b) capacitive, and c) resistive-capacitive voltage divider.

The output voltage $\overline{V}_{\mathrm{out}}$ can be easily obtained by leveraging Ohm's Law and Kirchhoff's Voltage and Current Laws:

$$\overline{V}_{\mathrm{out}} = \overline{V}_{\mathrm{in}} \cdot \frac{\overline{Z}_{\mathrm{LV}}}{\overline{Z}_{\mathrm{LV}} + \overline{Z}_{\mathrm{HV}}} \tag{1.4}$$

Equation 1.4 shows that the output voltage is directly proportional to the input voltage and can be adequately reduced by selecting the ratio between the two impedances.

The two characteristics parameters that quantify the VD accuracy are the deviation from the nominal value of the Scale Factor (SF) K and the phase error $\Delta\phi$. The rated SF and the phase error are described by the following equations:

$$K = \frac{|\overline{V}_{\text{in}}|}{|\overline{V}_{\text{out}}|} = \frac{|\overline{Z}_{\text{LV}} + \overline{Z}_{\text{HV}}|}{|\overline{Z}_{\text{LV}}|} \tag{1.5}$$

$$\Delta\phi = \phi_{\text{out}} - \phi_{\text{in}} = \angle\overline{Z}_{\text{LV}} - \angle(\overline{Z}_{\text{LV}} + \overline{Z}_{\text{HV}}) \tag{1.6}$$

When the SF K does not depend on the frequency of the input signal $\overline{V}_{\text{in}}$, the voltage divider is defined as "compensated". This feature can be obtained by selecting the same component type for the high and low voltage branches. A resistive-capacitive divider is compensated if the resistances R_{HV} and R_{LV} and the C_{HV} and C_{LV} capacitances are chosen according to the following equation:

$$R_{\text{HV}} \cdot C_{\text{HV}} = R_{\text{LV}} \cdot C_{\text{LV}} \tag{1.7}$$

Based on their technologies, LPVTs can have very different behaviour, as shown in Fig 1.8 (source IEC TR 61869-103 [6]). The capacitive dividers can not be used for the measurement of DC or low frequency phenomena (subharmonics, for example). The resistive divider can measure the DC and low frequency voltages but they have a limited frequency bandwidth. Resistive-capacitive dividers cover a wider frequency spectrum allowing to measure voltage from DC up to 10 MHz but they have the drawback of being expensive devices as much work is required in the design stage to reduce problems associated with the resistive to the capacitive transition phase.
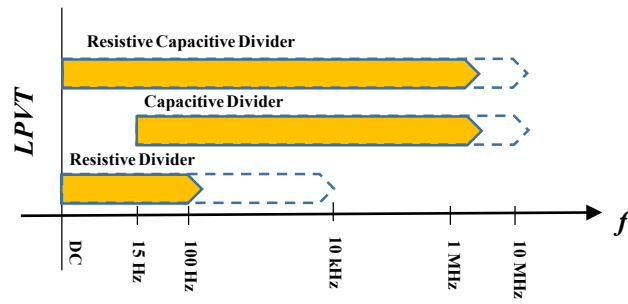
Fig. 1.8 Typical frequency bandwidths of LPVTs based on different technologies (source IEC TR 61869-103).

Chapter 2

PQ, PMU and IT: Review of International Standards and Scientific Literature

2.1 Introduction

This chapter gives a comprehensive overview of the in-force international standards dealing with Power Quality (PQ), Phasor Measurement Units (PMU) and Instrument Transformers (ITs). The considered relevant standards can be divided into five groups according to their content and/or field of applications and they are listed in Table 2.1:

Table 2.1 List and scope of considered International Standards

Standard	Parts	Scope
EN 50160/IEC 62749 *Voltage characteristics of electricity supplied by public distribution network.*	-	-Specify the main characteristics of the voltage at a network user's supply terminals in public LV, MV and HV AC electricity networks under normal operating conditions. -Introduce the limits or values within which the voltage characteristics can be expected to remain at any supply terminal in public European electricity networks.
IEEE 1159 *Recommended practice for monitoring electric power quality.*	-	-Encompasses the monitoring of characteristics of electric power systems. -Includes descriptions of conducted electromagnetic phenomena occurring on power systems. -Defines nominal conditions and deviations from these nominal conditions. -Discusses measurement techniques, application techniques, and the interpretation of monitoring results.
IEC 61000 *Electromagnetic compatibility (EMC).*	IEC 61000-4-30	-Defines the methods for measurement and interpretation of results for PQ parameters in AC power supply systems (50/60 Hz). -Measurement methods are described for each relevant parameter in terms that give reliable and repeatable results, regardless of the method's implementation. -Addresses measurement methods for in-situ measurements.
	IEC 61000-4-7	-Applies to instrument for measuring spectral components in the frequency range up to 9 kHz which are superimposed on the fundamental (50/60 Hz).
	IEC 61000-2-12	-Deals with disturbances in the frequency range from 0 kHz to 9 kHz, with an extension up to 148.5 kHz specifically for mains signalling systems. -Gives compatibility levels for public MV AC distribution systems.
IEEE/IEC 60255 *Measuring relays and protection equipment.*	IEC 60255-118-1	-Defines a PMU, synchronized phasor (synchrophasor), frequency, and rate of change of frequency measurements. It describes time tag and synchronization requirements for measurement of all three of these quantities. -Specifies methods for evaluating these measurements and requirements for compliance with the standard under both static and dynamic conditions.
IEC 61869 IEC 60044 *Instrument transformers.*	IEC 61869-2 and 3	Inductive CTs (Part 2) and VTs (Part 3) used with electrical measuring instruments and electrical protective devices at frequencies from 15 Hz to 100 Hz.
	IEC 61869-6 IEC 61869 10 and 11	Additional general requirements for LPIT (Part 6) - passive LPCT (Part 10) and passive LPVT (Part 11) - used for AC applications having rated frequencies from 15 Hz to 100 Hz covering MV, HV and EHV or used for DC applications.
	IEC 60044-7 and 8	Electronic VTs (Part 7) and CTs (Part 8) having an analogue voltage output or a digital output, for use with electrical measuring instruments and electrical protective devices at nominal frequencies from 15 Hz to 100 Hz.

In addition to the IEC/IEEE Standards listed in the Table above, a brief overview of the technical report IEC TR 61869-103 [6] is also provided. This report represents the first and only normative document concerning the issue of the use of IT in PQ applications

As regards the characterization of ITs with a view to their use in grid monitoring and control, an overview of the scientific works is also provided. The analysis is always restricted to application for MV distribution grids.

2.2 International Standard dealing with PQ and PMU

This section gives an overview of the parameters to be measured when carrying out grid measurement for PQ monitoring or measurement of grid synchrophasor by a PMU, their measurement methods and associated uncertainty.

2.2.1 Frequency deviation

The European in force standard EN 50160 [15] defines the the frequency deviation as "a variation of the nominal frequency value of the supply voltage in a distribution or transmission system of electrical energy."

A quite similar definition is provided by the technical specification TS 62749 [16], which specifies the expected characteristics of the the supply at the point of supply of public 50 Hz and 60 Hz and the power quality assessment methods, the frequency deviation is the difference between power supply frequency and nominal frequency.

The limits for the frequency variation in power grids are set by [15] and are:

- For synchronous connection to an interconnected system: ±1% during 99.5% of a year and between +4% and -6% during 100% of the time.

- For systems without a synchronous connection to an interconnected system: ±2% during 99.5% of a year and ±15% during 100% of the time.

The compatibility level given in IEC 61000-2-12 [17] for the temporary variation of frequency from the nominal frequency is ± 1 Hz. The steady-state deviation of frequency from the nominal frequency is much less.

As regards the measuring method, the IEC 61000-4-30 [18] provides "the methods for measurement and interpretation of results for power quality parameters in a.c. power supply systems with a declared fundamental frequency of 50 Hz or 60 Hz", but it does not specify how to implement it. It must be remarked that the stated measurement uncertainties refer to on-site measurements, but does not consider the contribution of the transducer, which is recognized, but not quantified being out of the scope of the standard.

According to [18], the frequency deviation of a week is evaluated by measuring the mean value of fundamental frequency over a time window of 10 s.

The IEC 61000-4-30 standard [18] identifies two different classes (Class A and S) for the measurement of the frequency deviation, and of PQ parameters in general:

- Class A is used when precise measurements are necessary, for example, for contractual applications that may require resolving disputes, verifying compliance with standards, etc.

- Class S is used for statistical applications such as surveys or power quality assessment,possibly with a limited subset of parameters. Although it uses equivalent intervals of measurement as Class A, the Class S processing requirements are much lower.

The measurement uncertainties of Class A and S devices set by [18] are:

- Class A: ±10 mHz from 42.5 Hz to 57.5 Hz for 50 Hz systems and 51 Hz to 69 Hz for 60 Hz systems.

- Class S measurement: ±50 mHz from 42.5 Hz to 57.5 Hz for 50 Hz systems and 51 Hz to 69 Hz for 60 Hz systems.

2.2.2 Supply Voltage Variation

Based on the standard EN 50160 [15], the supply voltage deviation is "a change of root mean square (r.m.s.) value of the voltage at a given time at the supply terminal, measured over a given interval".

According to [15], under normal operating conditions, excluding the periods with interruptions, supply voltage variations at MV should not exceed ± 10% of the declared supply voltage U_c. In cases of electricity supplies in networks not interconnected with transmission systems or for special remote network users, voltage variations should not exceed + 10% / - 15% of U_c.

Similar limits are also given by the IEC 62749 [16] . According to it, under normal operating conditions, during one week, the 10-minute r.m.s. values of the voltage at the point of supply terminals should comply with the following requirements:

- Voltage percentile $U_{99}\%$ does not exceed $U_c + 10\%$ of U_c.

- Voltage percentile $U_1\%$ is not lower than $U_c - 10\%$ of U_c.

- Voltage percentile $U_0\%$ is not lower than $U_c - 15\%$ of U_c.

According to the IEC 61000-2-12 [17], in normal circumstances the value of rapid voltage changes is limited to 3% of nominal supply voltage. However step voltage changes exceeding 3% can occur infrequently on the public supply network.Furthermore, following exceptional load changes or switching operations, voltage excursions outside the normal operational tolerances (e.g., $\pm$ 10% of U_c) are possible for a few tens of seconds.

According to the IEC 61000-4-30 [18], the r.m.s. of the declared voltage shall be measured over a time window equal to 10-cycles for the 50 Hz power system and 12-cycles for the 60 Hz power system. Moreover, the relative measurement uncertainty shall not exceed:

- Class A: ±0.1% over the range from 10% to 150% of the declared input voltage.

- Class S: ±0.5% over the range from 20% to 120% of the declared input voltage.

2.2.3   Voltage Unbalance

According to the international standard EN 50160 [15], the voltage unbalance is a condition in a polyphase system in which the r.m.s. values of the line-to-line voltages of fundamental component, or the phase angles between consecutive line voltages, are not all equal. The international standard IEEE 1159 includes the voltage unbalance in the category of low frequency phenomena conducted as a type of disturbance in steady state with short -term (3 s up to 1 min) variations from 2% up to 15% of the r.m.s.

The parameter that quantify the voltage unbalance is the unbalance factor introduced in the standard IEC 61000-4-30 [18] and it is the degree of the inequality expressed as the ratios of the negative and zero sequence components to the positive sequence component of fundamental. This parameter is mathematically described in Equation 2.1:

$$k_{\mathrm{u},\%} = \frac{U_{\mathrm{neg}}}{U_{\mathrm{pos}}} \cdot 100\% \tag{2.1}$$

The voltage unbalance measurement procedure is described in IEC 61000-4-30 [18]. The fundamental component of the voltage input signal is measured over a 10-cycle time interval for 50 Hz power systems or a 12-cycle time interval for 60 Hz power systems. According to [15] during each period of one week, 95% of the mean values of 10 min r.m.s. values of the negative phase sequence component of the supply voltage shall be within the range 0% to 2% of the positive phase sequence component.

2.2.4   Flicker

Based on the international standard EN 50160 [15], the flicker is the impression of instability of the visual sensation induced by a light stimulus whose luminance or spectral distribution fluctuates over time. The standard defines the flicker severity as the intensity of flicker annoyance evaluated by the following quantities:

1. Short term severity (Pst) measured over a period of ten minutes.

2. Long term severity (Plt) calculated from a sequence of twelve Pst values over a two-hour interval

Under normal operating conditions, during each period of one week the long term flicker severity Plt caused by voltage fluctuation should be less than or equal to 1 for 95% of the time.

2.2.5 Harmonic and interharmonic voltage

According to the international standard EN 50160 [15], the "harmonic voltage is sinusoidal voltage with a frequency equal to an integer multiple of the fundamental frequency of the supply voltage", whereas the "interharmonic voltage is sinusoidal voltage with a frequency not equal to an integer multiple of the fundamental". Subharmonics are special case of interharmonics characterized by frequency lower than the fundamental one.

The harmonic and interharmonic voltage can be evaluated in three ways [18]:

1. Individually, the harmonic and interharmonic voltage is related to the fundamental voltage.

2. Globally, by the total harmonic distortion factor (THD) or total interharmonic distortion factor (TIHD).

3. In delimited frequency band, using harmonic and interharmonic groups and subgroup concept provided in [19].

Harmonic and interharmonic voltages are classified by the international standard IEEE 1159 [20] in the category of low-frequency phenomena conducted in steady-state, with typical spectral content from 0 Hz to 9 kHz and voltage magnitude from 0% to 20% and from 0% to 2% for harmonics and interharmonics, respectively. According to IEC 61000-4-30 [18], the basic measurement time interval for the harmonic and interhamonic evaluation is 10-cycles for the 50 Hz power system and 12-cycles for the 60 Hz power system and, consequently, the frequency resolution is fixed (for instance, 200 ms in case of 50 Hz constant power frequency). The measurement uncertainty for the harmonic and interharmonic measurements is given by the IEC 61000-4-7 [19]. The standard [19] identifies two different accuracy

classes for instrumentation used for harmonic and interharmonic measurements; the maximum errors are:

- Class I: For $U_h \geq 1\%$ of U_{nom} max error $\pm 5\%$ of U_h. For $U_h < 1\%$ of U_{nom} max error $\pm 0.05\%$ of U_{nom}.

- Class II: For $U_h \geq 3\%$ of U_{nom} max error $\pm 5\%$ of U_h. For $U_h < 3\%$ of U_{nom} max error $\pm 0.15\%$ of U_{nom}.

Note: U_h is the amplitude of the harmonic and U_{nom} is the nominal supply voltage.

As regards the limits of harmonics and interhamonics, standard IEC 50160 [15] provides them in terms of relative amplitude versus frequency. The limits are summarised in the following Table 2.2:

Table 2.2 IEC 50160 maximum amplitude of harmonics given in percent of the fundamental voltage

Odd harmonics				Even harmonics	
Not multiples of 3		Multiples of 3			
Order h	Relative amplitude U_h (%)	Order h	Relative amplitude U_h (%)	Order h	Relative amplitude U_h (%)
5	6.0	3	5.0	2	2.0
7	5.0	9	1.5	4	1.0
11	3.5	15	1.0	6 up to 24	0.5
13	3.0	21	0.75		
17	2.0				
19	1.5				
23	1.5				
25	1.5				

The IEC 61000-2-12 standard [17] gives compatibility levels as reference values for both long-term effects and very short-term effects. The long-term effects relate mainly to thermal effects on cables, transformers, motors, capacitors, etc. They refer from harmonic levels that are sustained for 10 min or more. Very short-term effects relate mainly to disturbing effects on electronic devices that may be susceptible to harmonic levels sustained for 3 s or less. Transients are not included. In normal operating conditions, the THD of the supply voltage, including harmonics up to order 40, shall be less than or equal to 8%. The limit of harmonic voltage for each

order, with reference to long-term effects, is shown in Table 2.2. With reference to very short-term effects, the compatibility levels for individual harmonic components of the voltage are the values given in Table 2.2, multiplied by a factor $k_{\text{short}-\text{term}}$, calculated according to the following Equation 2.2:

$$k_{\text{short}-\text{term}} = 1.3 + \frac{0.7}{45} \cdot (h - 5) \tag{2.2}$$

The corresponding compatibility level for the total harmonic distortion is THD = 11%.

2.2.6 Voltage Dip

According to the international standard EN 50160 [15], the voltage dip is "a temporary reduction of the r.m.s. voltage in the electrical supply system", and it consists of two parts:

- residual voltage

- voltage dip duration

The voltage dip duration is the time between the instant the r.m.s. voltage at a point of an electricity supply system falls below the dip start threshold and the instant at which it rises to the end threshold plus a hysteresis voltage. The voltage dip residual voltage is the minimum value of r.m.s. voltage recorded during a voltage dip. According to the international standard IEEE 1159 [20], voltage dips are low-frequency phenomena defined as short periods of r.m.s. variations, usually caused by fault conditions.

The IEC 61000-4-30 standard [18] prescribes how to measure voltage dips. Dips shall be calculated considering the r.m.s. value over a time window equal to 1 cycle of the power frequency refreshed every half cycle (½), i.e. $U_{\text{rms},1/2}$.

The voltage dip detection is performed by comparing the $U_{\text{rms},1/2}$ with the voltage threshold that typically, on MV networks, is in the range of 85% - 90% of the reference voltage. The dip ends when $U_{\text{rms},1/2}$ is equal to or above the voltage threshold plus the hysteresis voltage (typically equal to 2%). The measurement uncertainty for the voltage dip measurement is given by the IEC 61000-4-30 [18]. For the two accuracy classes, the accuracy limits are:

- Class A: the measurement uncertainty related to the residual voltage shall not exceed $\pm 0.2\%$. As for the dip duration, the uncertainty is equal to the dip uncertainty (half a cycle) plus the dip conclusion uncertainty (half cycle).

- Class S: the measurement uncertainty related to the residual voltage shall not exceed $\pm 1.0\%$. As for the dip duration, the uncertainty is equal to the dip uncertainty (half a cycle) plus the dip conclusion uncertainty (half cycle). If the analysis is performed using U_{rms} instead of $U_{\text{rms},1/2}$, the uncertainty is equal to the dip uncertainty (one cycle) plus the dip conclusion uncertainty (one cycle).

The IEC 61000-4-11 [21] standard provides data from measurement campaigns in nine countries of Europe. From the data it appears that the average number of voltage dip occurrences has a maximum for residual voltage between 85% and 70%, with an associated duration between 0.02 s and 0.1 s in the case of the overhead network, whereas for the underground network between 90% and 85% with durations between 0.02 s and 0.1 s.

2.2.7   Voltage Swells

According to the international standard EN 50160 [15], the voltage swell is "a temporary increase of the r.m.s. voltage in the electrical supply system", and it consists of two parts:

- voltage swell magnitude

- voltage swell duration

The voltage swell duration is the time between the instant the r.m.s. voltage at a point of an electricity supply system exceeds the start threshold and the instant at which it falls below the end threshold plus a hysteresis voltage. The voltage swell magnitude is defined as the maximum value of r.m.s. voltage recorded during a voltage swell. According to the international standard IEEE 1159 [20], voltage swells are low-frequency phenomena defined as short periods of r.m.s. variations, usually caused by fault conditions.

The IEC 61000-4-30 standard [18] prescribes how to measure voltage swells. Swells shall be calculated considering the r.m.s. value over a time window equal

to 1 cycle of the power frequency refreshed every half cycle (½), i.e. $U_{\text{rms},1/2}$. The voltage swell detection is performed by comparing the $U_{\text{rms},1/2}$. with the voltage threshold that typically, on MV networks, is in the range of 110% of the reference voltage. The swell ends when $U_{\text{rms},1/2}$. is equal to or above the voltage threshold plus the hysteresis voltage (typically equal to 2%). The measurement uncertainty for the voltage swell measurement is given by the IEC 61000-4-30 [18]. For the two accuracy classes, the accuracy limits are:

- Class A: the measurement uncertainty related to the swell voltage magnitude shall not exceed ±0.2%. As for the swell duration, the uncertainty is equal to the swell uncertainty (half a cycle) plus the swell conclusion uncertainty (half cycle).

- Class S: the measurement uncertainty related to the swell voltage magnitude shall not exceed ±1.0%. As for the swell duration, the uncertainty is equal to the swell uncertainty (half a cycle) plus the swell conclusion uncertainty (half cycle). If the analysis is performed using U_{rms} instead of $U_{\text{rms},1/2}$, the uncertainty is equal to the swell uncertainty (one cycle) plus the swell conclusion uncertainty (one cycle).

2.2.8   Voltage Interruption

According to the international standard EN 50160 [15], voltage interruption is "a reduction of the r.m.s. voltage in the electrical supply system", and it consists of two parts:

- voltage interruptions duration

- interruptions residual voltage

The duration of the voltage interruptions is the time between the instant at which the r.m.s. voltage at a point of an electricity supply system falls below the start threshold, and the moment it rises to the end threshold. The interruption residual voltage, which is the minimum value of r.m.s. voltage recorded during a voltage interruption. Moreover, the standard [15] defines two types of voltage interruptions:

- short interruption if the duration is up to 3 minutes (included),

- long interruption if the duration is greater than 3 min.

The international standard IEEE 1159 [20] describes voltage interruptions as conducted low-frequency disturbances and classifies them by duration. According to IEC 61000-4-30 [18], voltage interruption shall be measured and detected using the declared supply voltage as reference. Typically, the line-to-line voltages on MV networks shall be considered. Conventionally, the interruption threshold equals 2% of the reference voltage. IEC 62749 [16] indicates the voltage interruption threshold between 5% and 10% of the reference voltage.

2.2.9   Synchrophasor for power systems Measurements

To better understand why standards dealing with synchrophasor for power systems measurements are included into this analysis it is worth recalling the concept and definition of synchrophasor. In AC power system analysis, phasor representation of sinusoidal signals is commonly used. The sinusoidal waveform defined in Equation 2.3 is typically represented as a phasor according to Equation 2.4 :

$$x(t) = X_{\mathrm{m}} cos(\omega t + \phi) \tag{2.3}$$

$$X = \frac{X_{\mathrm{m}}}{\sqrt{2}} e^{j\phi} = \frac{X_{\mathrm{m}}}{\sqrt{2}} (cos\phi + jsin\phi) = X_{\mathrm{real}} + jX_{\mathrm{imaginary}} \tag{2.4}$$

where $\frac{X_{\mathrm{m}}}{\sqrt{2}}$ is the r.m.s. value of the sinusoidal waveform and ϕ is the phase angle that depends on the initial time. The standard [22] defines the synchrophasor as the phasor X of Equation 2.4 where ϕ is the instantaneous phase angle relative to a cosine function at the nominal system frequency synchronized to the Universal Time Coordinate (UTC). In other words, ϕ represents the offset from a cosine function at the nominal system frequency synchronized to UTC.

The synchrophasors are measured by PMU, and they represent the foundation for real-time grid monitoring and control.

The standard [22] defines two different performance classes for the PMU:

- P class: intended for protection applications requiring fast response and mandates no explicit filtering.

- M class is intended for measurement applications that are adversely affected by aliased signals and do not require the fastest reporting speed.

Moreover, even if the PMUs are used only for measurement of synchrophasors at power frequency, the standard specifies methods for evaluating the PMU performance under both static and dynamic conditions.

In the following the tests prescribes by [22] are briefly recalled.

Steady-state test

The standard [22] provides test parameters for the verification of the PMU performance under stationary conditions. The test involves 1) the generation of a signal composed of a sinusoid with variable frequency, amplitude, and phase angle and 2) the generation of signal composed by multiple harmonic tones. The range of variation of the quantities are summarized in the Table 2.3. In the same table also the maximum errors in terms of Total Vector Error (TVE) for P class and M class PMUs are provided.

Table 2.3 Test parameters for PMU steady-state test

Influence quantity	Reference condition	Minimum range of influence quantity over which PMU shall be within given TVE limit			
		P class		M class	
		Range	Max TVE (%)	Range	Max TVE (%)
Signal frequency $f_{in} = f_0 \pm f_{dev}$	f_0 (50/60 Hz)	f_{dev} ± 2.0 Hz	1	± 2.0 Hz for $F_s < 10$ $\pm F_s/5$ for $10 \leq F_s < 25$ ± 5.0 Hz for $F_s \geq 25$	1
Voltage signal magnitude	100% rated	80% to 120% rated	1	10% to 120% rated	1
Current signal magnitude	100% rated	10% to 200% rated	1	10% to 200% rated	1
Phase angle with $|f_{in} - f_0| < 0.25$ Hz	Constant or slowly varying angle	$\pm\pi$ radians	1	$\pm\pi$ radians	1
Harmonic distortion (single harmonic)	<0.2% (THD)	1%, each harmonic up to 50th	1	10%, each harmonic up to 50th	1
Out-of-band interference (as described below)	<0.2% of input signal magnitude		None	10% of input signal magnitude for $F_s \geq 10$. No requirement for $F_s < 10$.	1.3

- F_s is the reporting rate expressed in frames per second (fps)
- f_0 is the nominal fundamental frequency of the input test signal, exactly 50 Hz or 60 Hz.
- f_{in} is the fundamental frequency of the input test signal that in the course of testing may be varied from nominal (f_0) of a quantity f_{dev}.
- Out-of-band interference testing: The passband at each reporting rate is defined as:

$$|f - f_0| < F_s/2.$$

An interfering signal outside the filter passband is a signal at frequency f where:

$$|f - f_0| \geq F_s/2$$

Dynamic test

The standard [22] prescribes dynamic tests for the determination of the PMU bandwidth. The signals for this test are represented by an amplitude and phase modulation (Equation 2.5) and a frequency ramp (Equation 2.6):

$$X_a = X_m \cdot [1 + k_x \cos(\omega t)] \cdot cos[\omega_0 t + k_a cos(\omega t - \pi)] \qquad (2.5)$$

$$X_a = X_m \cdot cos(\omega_0 t + \pi R_f t^2) \qquad (2.6)$$

where

- X_m is the amplitude of the input signal;

- f_0 is the nominal power system frequency in Hz;

- f_m is the modulation frequency in Hz;

- k_x is the amplitude modulation factor

- k_a is the phase angle modulation factor.

- $Rf(= df/dt)$ is the frequency ramp rate in Hz/s.

In the following tables the parameter values for Equation 2.5 and Equation 2.6 are reported.

Table 2.4 Test parameters for PMU amplitude and phase test

Modulation level	Reference condition	Minimum range of influence quantity over which PMU shall be within given TVE limit			
		P class		M class	
		Range	Max TVE	Range	Max TVE
$k_x = 0.1$, $k_a = 0.1$ radiant	100% rated signal magnitude, f_0	Modulation frequency	3%	Modulation frequency	3%
$k_x = 0$, $k_a = 0.1$ radiant	100% rated signal magnitude, f_0	0.1 Hz to lesser of F_s/10 or 2 Hz	3%	0.1 Hz to lesser of F_s/5 or 5 Hz	3%

Table 2.5 Test parameters for PMU frequency ramp test

Test signal	Reference condition	Minimum range of influence quantity over which PMU shall be within given TVE limit		
		Ramp rate (R_f) (positive and negative ramp)	Performance class	Ramp range	Max TVE
Linear frequency ramp	100% rated signal	± 1.0 Hz/s	P class	± 2 Hz	1%
	f_0 at the start or some point during the test		M class	Lesser of ± (F_s /5) or ± 5 Hz [a]	1%

Performance under step changes in phase and magnitude

The last test presented in [22] is the step changes in magnitude and phase. The test waveform is mathematically described by Equation 2.7.

$$X_a = X_m \cdot [1 + k_x f_1(t)] \cdot cos[\omega_0 t + k_a f_1(t)] \qquad (2.7)$$

Where $f_1(t)$ is a unit step function. In Table 2.6, the parameter values for the test Equation 2.7 are provided.

Table 2.6 Test parameters for PMU input step change test

Step change specification	Reference condition	Maximum response time, delay time, and overshoot					
		Class P			Class M		
		Response time (s)	Delay time (s)	Max Overshoot /undershoot	Response time (s)	Delay time (s)	Max Overshoot /undershoot
Magnitude 10%, $k_x = \pm 0.1$, $k_a = 0$	Nominal conditions at the start or end of the step	$2/f_0$	$1/(4 \times F_s)$	5% of step magnitude	$7/F_s$	$1/(4 \times F_s)$	10% of step magnitude
Angle $\pm 10°$, $k_x = 0$, $k_a = \pm \pi/18$	Nominal conditions at the start or end of the step	$2/f_0$	$1/(4 \times F_s)$	5% of step magnitude	$7/F_s$	$1/(4 \times F_s)$	10% of step magnitude

The response time is defined "the time to transition between two steady-state measurements before and after a step change is applied to the input". The delay time is defined as "the time interval between the instant that a step change is applied to the input of a PMU and measurement time that the stepped parameter achieves a value that is halfway between the initial and final steady-state values". The overshoot is, instead, the deviation between the maximum measured value during the step and the steady-state value (expressed in percentage of the steady-state value).

2.3   International Standard dealing with IT

This section provides an overview of the indications prescribed by the standards dealing with the accuracy verification of ITs to be used with measuring or protective instruments. The types of devices considered in the following are inductive ITs, low power ITs (LPIT) and electronic ITs. ITs performances are classified in terms of accuracy classes. The accuracy class is defined as the highest permissible percentage error at rated voltage/current and with rated burden. For each accuracy class, limits

are given for the IT ratio and phase error as a function of the applied primary quantity expressed as a percentage of the rated one and for any burden as specified.

2.3.1   Inductive Current Transformer

For inductive current transformers (CTs) the relevant standard is the IEC 61869-2 [4]. The standard requires to verify the CTs accuracy class against the indicated limits for ratio error and phase displacement for various:

- Primary current amplitudes.

- Burden conditions.

The standard accuracy classes for measuring CTs are:

$$0,1 - 0,2 - 0,2S - 0,5 - 0,5S - 1 - 3 - 5$$

For classes $0,1 - 0,2 - 0,5$ and 1, the ratio error and phase displacement at rated frequency are evaluated under sinusoidal conditions with current amplitude varying from 5% to 120% of the rated primary current. The burden can assume any value from 25% to 100% rated.

For spacial classes 0,2S and 0,5S, the ratio error and phase displacement at the rated frequency are evaluated under sinusoidal conditions with current amplitude varying from 1% to 120% of the rated primary current. The burden can assume any value from 25% to 100% of the rated one.

For classes 3 and 5, the ratio error at rated frequency is evaluated under sinusoidal conditions with current amplitude varying from 50% to 120% of the rated primary current. There are no specified requirements for the phase displacement for classes 3 and 5. The burden can assume any value from 50% to 100% of the rated one

As regards the burden power factor, two categories are identified:

- Burden Range I from 1 VA to 5 VA: the power factor is equal to 1 (resistive load).

- Burden Range II from 5 VA to 15 VA: the power factor of 0.8 lagging.

2.3.2   Inductive Voltage Transformer

For inductive VTs the relevant standard is the IEC 61869-3 [5]. It requires verifying the VT accuracy class for different values of:

- Primary voltage amplitudes.

- Burden conditions.

The standard accuracy classes for measuring VTs are:

$$0,1 - 0,2 - 0,5 - 1 - 3$$

For all the accuracy classes, the ratio error and phase displacement (not included for class 3) at rated frequency are evaluated under sinusoidal conditions with voltage amplitude varying from 80% to 120% of the rated primary voltage.

- Burden Range I from 1 VA to 10 VA: the power factor is equal to 1 (resistive load). In this case, tests can be performed with any burden value from 0% to 100%.

- Burden Range II from 10 VA to 100 VA: the power factor of 0.8 lagging. In this case, tests can be performed with burden values in the range from 25% to 100%.

2.3.3   Low Power Current Transformers

Low Power passive current Transformers (LPCTs) are coverd by IEC 61869-6 and 61869-10 Standards [1, 23]. The LPCT accuracy class is verified at different:

- Primary current amplitudes.

- Frequency

- Harmonics and interharmonics conditions.

All tests are performed at the rated burden condition, which according to [1] is the parallel connection of a 2 MΩ resistor and 50 pF capacitor. The standard accuracy classes for measuring LPCTs are:

$$0,1 - 0,2 - 0,2S - 0,5 - 0,5S - 1 - 3 - 5$$

Accuracy tests for measuring LPCT versus amplitude

For classes 0,1 – 0,2 – 0,5 and 1, the ratio error and phase displacement at rated frequency are evaluated under sinusoidal conditions with current amplitude varying from 0.05 to a factor k_{pcr} of the rated primary current.

For special classes 0,2S and 0,.5S, the ratio error and phase displacement at rated frequency are evaluated under sinusoidal conditions with current amplitude varying from 0.01 to a factor k_{pcr} of the rated primary current.

For class 3, the ratio error at rated frequency is evaluated under sinusoidal conditions with current amplitude varying from 0.20 to a factor k_{pcr} of the rated primary current. There are no specified requirements for the phase displacement.

The standard values for the rated extended primary current factor k_{pcr} are:

$$5 – 10 – 20 – 50 – 100$$

Accuracy tests for measuring LPCT versus Frequency (from IEC 61869-6)

Two frequency ranges are identified:

- for measuring LPCTs from 99% to 101% of rated frequency,

- for protecting LPCTs from 96% to 102% of rated frequency.

Tests for the evaluation of the LPCT accuracy versus frequency are performed at the two extremes of the frequency range with rated amplitude and burden.

Accuracy tests for measuring LPCT in Harmonics and Interharmonics Measurement (from IEC 61869-6)

The standard IEC 61869-6 [1] covers the accuracy limits, classes requirements and class extension for harmonics, interharmonics and low frequencies measurement. The standard identifies three different frequency applications for LPCTs and for each of them it defines different limits. The three applications are:

- LPCT for metering: limits are given for 0 Hz (optional), 1 Hz and from 2nd harmonic up to 13th and above.

- LPCT for quality metering and low bandwidth d.c. applications: limits are provided from 100 Hz to 3 kHz (extension of metering application).

- LPCT for high bandwidth d.c. applications: limits are provided from 100 Hz to 20 kHz (extension of metering application).

For the three categories, [1] defines different accuracy limits for different frequency ranges.

In an ideal case, tests for the verification of the harmonics measurement accuracy should be made with a multi-tone signal composed by the fundamental tone at rated amplitude and frequency plus tones at different frequencies with reduced amplitudes. However, arranging a test circuit that generates such a primary input signal can be complex. Therefore, the LPCT accuracy in harmonics measurement can be evaluated with a sinusoidal frequency sweep, i.e. generating one single harmonic frequency.

2.3.4   Low Power Voltage Transformers

Low Power passive Voltage Transformers (LPVTs) are covered by IEC 61869-6 and 61869-11 Standards [1, 24]. According to [24], the accuracy class has to be verified at different:

- Primary voltage amplitudes.

- Frequency

- Burden

- Harmonics and interharmonics conditions.

The accuracy classes for measuring LPVTs and protection and multi-purpose LPVTS are:

$$0,1 - 0,2 - 0,5 - 1,0 - 3$$

$$0,1P - 0,2P - 0,5P - 1P - 3P - 6P$$

Accuracy tests for LPVT versus Amplitude

For classes 0,1 – 0,2 – 0,5 – 1,0 – 3, the ratio error and phase displacement (except for class 3) at rated frequency are evaluated under sinusoidal conditions with voltage amplitude varying from 80% to 120% of the rated primary voltage.

For classes 0,1P – 0,2P – 0,5P – 1P – 3P – 6P, the ratio error and phase displacement (except for class 3) at rated frequency are evaluated under sinusoidal conditions with voltage amplitude varying from 2% to $F_{v,\%}$ of the rated primary voltage.

The standard values for the rated voltage factor $F_{v,\%}$ are:

$$1.2\% – 1.5\% – 1.9\%$$

Accuracy tests for LPVT versus Burden

The rated burden is identified by the parallel connection of a 2 MΩ resistor and 50 pF capacitor. According to the standard, the burden variations are:

- $\pm$ 5% of the resistive part of the rated burden,

- between 0% and 100% of the capacitive part of the rated burden.

Accuracy tests for measuring LPVT versus Frequency (from IEC 61869-6)

See accuracy test for LPCT versus Frequency

Accuracy tests for measuring LPVT in harmonics and interharmonics measurement (from IEC 61869-6)

See accuracy test for LPCT in harmonics and interharmonics measurement.

2.3.5 Electronic Voltage Transformers

For electronic VTs (EVTs) the in force standard is [25]. It requires to verify the accuracy class at different:

- Primary voltage amplitudes.

- Burden conditions.

- Frequency.

- Harmonics.

The standard accuracy classes for EVTs are listed below:

$$0{,}1 - 0{,}2 - 0{,}5 - 1 - 3 - 3P - 6P$$

Accuracy tests for EVT versus Amplitude

For the accuracy classes $0{,}1 - 0{,}2 - 0{,}5 - 1 - 3$, the ratio error and phase displacement (except for class 3) at rated frequency are evaluated under sinusoidal conditions with voltage amplitude varying from 80% to 120% of the rated primary voltage.

For the accuracy classes $3P - 6P$, the ratio error and phase displacement at rated frequency are evaluated under sinusoidal conditions with current amplitude varying from 2% to X% of the rated primary voltage. The standard values for the factor X are:

$$1.2\% - 1.5\% - 1.9\%$$

Accuracy tests for EVT versus Burden

As regards the burden, two burden categories are identified:

- Burden Range I: from 1 VA to 10 VA with a power factor equal to 1.

- Burden Range II: from 10 VA to 100 VA with a power factor of 0.8 lagging.

The standard reference range of burden shall be from 25% up to 100%

Accuracy tests for measuring EVT versus Frequency

Two frequency ranges are identified:

- for measuring EVTs from 99% to 101% of rated frequency,

- for protecting EVTs from 96% to 102% of rated frequency.

Tests for the evaluation of the EVT accuracy versus frequency are performed at the two extremes of the frequency range with rated amplitude and burden.

Accuracy tests for EVT versus Harmonics

Annex D of the standard [26] gives recommendations about accuracy requirements for harmonic measurements performed with electronic current and voltage transformer. The standard identifies three different frequency applications for EVTs and for each of them it defines different limits. The three applications are:

- EVT for power metering : limits are given from 2nd harmonic up to 13th.

- EVT for quality metering limits are provided for harmonics from the 2nd to 50th.

- EVT for protection for usual purposes: limits are provided from 16.7 Hz to 5th harmonic.

For the three categories, [26] defines different accuracy limits for different frequency ranges. The standard suggests to perform tests with harmonic amplitude equal to 10% of rated amplitude for harmonics from 2nd to 5th and with 5% amplitude for higher orders harmonics.

2.3.6   Electronic Current Transformers

For electronic CTs (ECTs) the in force standard is [26]. It requires to verify the accuracy class at different:

- Primary current amplitudes.

- Frequency.

- Harmonics

The standard accuracy classes for ECTs are listed below:

$$0,1 - 0,2 - 0,2S - 0,5 - 0.,5S - 1 - 3 - 5$$

Accuracy tests for ECT versus Amplitude

For the accuracy classes $0,1 - 0,2 - 0,5 - 1$, the ratio error and phase displacement at rated frequency are evaluated under sinusoidal conditions with current amplitude varying from 5% to 120% of the rated primary current.

For the accuracy classes $0,2S - 0,5S$, the ratio error and phase displacement at rated frequency are evaluated under sinusoidal conditions with current amplitude varying from 1% to 120% of the rated primary current.

For the accuracy classes $3 - 5$, the ratio error at rated frequency are evaluated under sinusoidal conditions with current amplitude varying from 50% to 120% of the rated primary current. Limits of phase error are not specified.

ECT Standard Burden values

As regards the burden, the standard values of rated burden in Ohm are:

$$2 \text{ k}\Omega - 20 \text{ k}\Omega - 2 \text{ M}\Omega$$

The total burden has to be equal to, or higher than, the rated burden.

Accuracy tests for measuring ECT versus Frequency

Two frequency ranges are identified:

- for measuring ECTs from 99% to 101% of rated frequency,

- for protecting ECTs from 96% to 102% of rated frequency.

Tests for the evaluation of the ECT accuracy versus frequency are performed at the two extremes of the frequency range with rated amplitude and burden.

Accuracy tests for ECT versus Harmonics

See accuracy test for EVT in harmonics measurement.

2.3.7   IEC TR 61869-103: a brief overview

The technical report IEC TR 61869-103 [6] represents the only normative document dealing with the issue of assessing IT performances in PQ parameters. The [6] highlights that there is a mismatch between the accuracy verification conditions required by IT standards and their actual operating conditions.

In this context, the TR examines typical PQ phenomena along with features and frequency behaviour of ITs based on several different operating principles. The first aim of this analysis is the identification of the PQ parameters whose measurement can be influenced by the IT. More specifically, the TR investigates which specific characteristics of IT (magnitude, phase or transient response) are more relevant for each PQ parameters. For example, according to the TR, the measurement of voltage dips, swells and interruption is influenced by the IT magnitude, phase and transient response, for the interharmonic the only relevant IT parameter is the magnitude response whereas for the frequency deviation none because the IT does not introduce any additional uncertainty. As following step, the TR proposes test methods, for example fundamental component at rated amplitude and frequency plus superimpose reduced amplitude distortion, and possible generation and measurement setups to be adopted for the tests of ITs.

Useful information can be also found in the two TR annexes. In particular, Annex A identifies possible test parameters points for IT characterization under non-steady-state conditions (dips, swells and interruptions). For example, according to Annex A of [6] possible test parameters could be:

- Voltage dip: 10% Un, 50% Un, 85% Un

- Voltage swell: 110% Un, 120% Un, 150% Un

- Voltage interruption: 5% Un

- Duration: 1 s, 1 min

Annex B proposes four accuracy classes for ITs intended to be used in PQ applications. Along with the accuracy class, it introduces for each PQ parameter, possible measurement methods, variation range of the investigated parameters, uncertainty and influence quantity to consider to determine the accuracy class.

2.4   Recent Literature dealing with IT and PQ

The study of PQ issues is of great interest in several technical and economical fields. For this reason, the scientific literature concerning the PQ is pervasive, and tens of thousands of papers on the subject can be found. Here the attention is focused on two categories of papers:

- Papers related to common power quality phenomena found on the grid during recent measurement campaigns.

- Papers related to ITs performances in PQ measurements.

The results of the review activity are also reported in the publication [27].

2.4.1   Measurement of PQ phenomena

The aim of this analysis to provide a picture of the "typical values" and the "extreme ones" that can be experienced in MV grids to be considered in the study of the IT performances. Information is presented per specific PQ event. For some analyzed papers presenting results of measurement campaigns, data related to the voltage levels, period of monitoring and geographical locations are summarized in Table 2.7

Table 2.7 Information of some analyzed papers dealing with on-site PQ measurements.

Paper	Year	Voltage Level	Location
[28] Analysis of voltage quality parameters in MV distribution grid	2014-2016	22 kV	Czech Republic
[29] Power Quality General Levels in Distribution Networks	2014	20 kV – 6 kV	Romania
[30] Voltage Quality in the Medium Voltage Distribution Grid with Connected Wind Power Plants	2013-2014	22 kV	Czech Republic
[31] Evaluation and Trends of Power Quality Indices in Distribution System	2007	13.8 kV-138 kV	Brazil
[32] Guidelines for power quality monitoring – measurement locations, processing and presentation of data.	2014	110 kV	-
[33] Long-Term Monitoring of Flicker and Some Other Parameters of Voltage Quality	2014	22 kV	Czech Republic
[35] Voltage Quality in the Low Voltage Distribution Grids with the High Penetration of Distributed Energy Sources	2014	400V	Czech Republic
[36] Measurement of Harmonics in Different Sectors On 11 kV Distribution Networks	2016	11 kV	Brunei Darussalam
[37] LONG-TERM POWER QUALITY MEASUREMENTS IN MEDIUM VOLTAGE NETWORKS	2011-2018	10 kV and 30 kV	Sweden
[39] Power Quality Survey of a Photovoltaic Power Plant	2013	20 kV	Spain

Supply Voltage Variation

 In paper [28], fifteen different MV (at 20 kV) supply points are monitored over three years (2014-2016) and the voltage variations recorded range from 96.6% to 107.3% of the rated voltage. In [29] the voltage reaches a maximum value of 108% of the rated voltage U_r (20 kV). In [30], the quality of voltage of nine distribution grids operating at 22 kV with connected wind power plants is investigated and the voltage reaches the maximum value of 107% of U_r and a minimum of about 98% of U_r.

Voltage Unbalance

The k_u factor, defined in [15], is used to evaluate the voltage unbalance. The standard EN 50160 [15] sets a limit for the k_u factor equal to 2%. In [28] all the k_u values lay in the range of 0.1% and 0.7%. In [31], the PQ is monitored in substations and distribution feeders at different MV and HV levels (from 13.8 kV to 138 kV). For 90% of the installations, the measured k_u factor is below 1%. In [29], all the measured unbalance factors are below the 0.5% level. A quite similar value (0.54%) is observed in [32]. In [30], the k_u maximum value is equal to 1.33%.

Flicker

This flicker is evaluated in terms of long term and short term flicker severity, P_{lt} and P_{st} respectively [15]. The paper [33] reports the results of 15 years of PQ monitoring. As a result, it has been found that the P_{lt} index often exceeds the limit imposed by the standard [15] (i.e. 1) and the maximum value is 1.7. In paper [28], the maximum measured P_{lt} is 2.5 and the corresponding P_{st} is 3. In [29], P_{lt} ranges from 1.35 to 3.53. In addition, the paper [34] presents a PQ measurements campaign lasting 64 weeks in several MV sites, P_{st} reaches a maximum value of 5 in a residential site. In paper [35], the flicker limit Plt=1 was exceeded in 53% of the analyzed cases, the maximum value is 2.45. On the contrary, in [30] and [32], all the observed P_{lt} values are below the limit and the maximum P_{lt} recorded are 0.63 and 0.3, respectively.

Harmonic and Interharmonic Voltage

Harmonic can be evaluated in two ways, i.e., the amplitude level of a single harmonic and the total harmonic distortion (THD). In [28], the THD values are below the limit set by the standard EN 50160 [15] (i.e. 8%) and they range from 1.5% to 6% with 2% mean value. The same paper gives a focus on some odd harmonics, in particular the 3rd, 5th, 7th and 15th; all their amplitudes are below the standard limits [15], except for the 5th harmonic that reaches the limit of 6% but without exceeding it. Paper [31], focuses the analysis on the THD and the 70% of the measured THDs are in the range 1% to 3%. Similar information is given by [29], where the mean value of the THD is about 2%. Correspondingly, in [30], the recorded THD values are in the range from 1% to 2.2%. Moreover, [30], gives a focus on the 15th harmonic and

the maximum amplitude is equal to 0.26%, that is half the 0.5% limit prescribed by [15]. In [34], measurement of THD and the 3rd harmonic are presented. All the measured THD values are below 8%, the measured 3rd harmonic amplitudes are below 1% in almost all the monitored sites except for one where the mean value is 2.5%. In [36], the measured THD values are quite low and they range from 0.8% up to 1%. Paper [32] reports harmonics up to the 50th and as a result it is observed that the odd harmonics are prevailing, whereas the even harmonics have amplitudes far below 0.5%. More in detail, the highest amplitude of 2% is reached by the 5th harmonic. Similar results are presented in [33], where the first eleven odd harmonics are measured. All the harmonic amplitudes are below the limits [15] and the highest amplitude is observed at the 5th one (0.33%). In [37] measurement of harmonics in 3 different MV sites (from 10 kV to 30 kV) are presented. The recorded THD values range from 0.96% to 1.39%. Moreover, the papers also reported single harmonics up to the 25th, and higher amplitudes are observed for the odd ones. As regard the interharmonics amplitude and frequency, they strongly depend on the mechanical and electrical parameters of their sources [38]. As a consequence from the literature review common values in terms of frequency and amplitude cannot be identified.

Voltage Dips

Among the PQ phenomena, the voltage dips are the most widespread [31, 39, 40]. In [32], more than 50% of the measured voltage dips has a time duration less than or equal to 5 cycles and 80% has a residual voltage in the range between 70% and 90%. In [39], almost the totality of the dip events (about 94%) has a residual voltage from 70% to 90% and their time durations range between 0 ms and 100 ms (5 cycles of 50 Hz). Similarly, in [41] 60% of the dips measured in a 22 kV substation has a residual voltage between 70% and 90% and time durations lower than 100 ms.

Voltage Swells

In [32], 70% of the detected voltage swells last less than or equal to 1 cycle and have maximum magnitude of less than 114% of the rated voltage.

Voltage Interruption

In [32], about 70% of the interruptions has a duration in the range of 30-70 cycles.

PQ Literature Summary

As output, some PQ phenomena typical values have been identified and summarized in Table 2.8.

Table 2.8 PQ phenomena typical values from Literature Review

PQ Phenomena	Typical values	Comments
Supply voltage deviation	$0.96\text{-}1.08 \cdot U_n$	-
Voltage unbalance	Voltage unbalance factor $k_u = 0.7\%$	-
Flicker	Not identified	P_{lt} and P_{st} indices frequently exceed the limit set by the standard (EN 50160).
Harmonic voltage	Total Harmonic Distortion THD from 1% to 3 %	most common events: first harmonics up to 10th and odd harmonic up to 23th
Interharmonic voltage	Not identified	interharmonics frequencies and amplitudes are strongly related to the their sources (e.g. load variation, inverter frequency…)
Voltage Dip	$U_{res} = [0.7\text{-}0.9]$ p.u. ; $t_{dip} = 5$ cycles	they occur more frequently than voltage swells and interruptions
Voltage Swell	$U_{swells} = [1.10\text{-}1.14]$ p.u. ; $t_{swells} = 1$ cycle	-
Voltage interruption	[30 -70] cycles duration	-

It is worth noting that no information about the MV VTs used to measure the PQ disturbances is provided in almost all the papers reviewed. In [32], a brief section on 100 Inductive VTs (IVTs) frequency behavior with different primary voltages are given. In [28], only the rated features of the VTs used are reported. In no paper the use of a LPVT is mentioned.

2.4.2   IT performance in PQ/PMU measurements

Most of the papers on IT involved in PQ applications deal with measuring their frequency behavior for the monitoring of harmonics and interharmonics. In general, significant differences in frequency behaviour can be observed between conventional inductive ITs and LPITs. The latter are usually characterised by a flatter frequency response [42, 7]. In contrast, inductive ITs show a worse frequency behaviour and are characterized by distinctive resonance points at decreasing frequency with increasing rated primary voltage [32]. Nevertheless, for practical and economical reasons inductive ITs are often used as transducers at the input stage of PQ instrumentations since they are already installed in MV grids for metering and protection applications. Thus, from scientific literature it is highlighted the need of characterize them for PQ applications and, because of their non-linearity, the need of identify tests conditions close to the actual ones.

Paper [43] deals with the frequency characterization of a 11 kV/$\sqrt{(3)}$ inductive VT and it shows that different ratio and phase frequency responses can be measured using two different test waveforms: a sinusoidal sweep at Low Voltage (LV) and a bi-tone signals at MV. In particular, comparing the two responses a difference close to the 1 % is observed in the measurement of the second harmonic. The same paper [43] highlights that when the VT under test is supplied under MV bi-tone signals, its frequency response assumes a discontinuous behaviour in the measurement of even and odd harmonics.

A quite similar outcome is found in [44]. In particular, the paper [44] focuses on influence factors that can impact on the frequency response of a VT. In this regard, three main categories of influences are identified: 1) influences by design (f.i, primary rated voltage), 2) influences of operating conditions (f.i., burden or temperature) and 3) influences by measurement methodology (f.i., amplitude of the test signal, number of different frequencies in the test signal). Due to the large number and the different types of impact factors, the paper results suggest to measure the frequency response individually for each VT where it is needed. To include all possible influences of the operating environment, the measurement should be carried out on-site after the final installation of the VT. Moreover, the paper states that the most realistic measuring method for the VT characterization is the use of a two-frequency test signal, consisting of a fundamental component at rated frequency and rated voltage amplitude and a second higher frequency component

with variable frequency at amplitudes of up to 10% of the rated voltage. The simplest measuring method consists in a sinusoidal frequency sweep performed at LV. The two methods are applied for the characterization of a 20 kV VT and, as a result, differences up to 1.2% are observed between the frequency response obtained by performing a sinusoidal sweep at LV and by supplying the VT with bi-tone signal with 5% harmonic component. Considering the bi-tone test conditions, the difference between the excitation with 1%, 5% and 10% of the rated voltage is lower than 0.05%. Using a single-frequency sweep, an overall accuracy better than 1% is achieved with a test signal magnitude higher than 125 V. With an excitation of 200 V, which is a handy voltage in practice, up to 3 kHz an error lower than 0.85% and up to 1.5 kHz lower than 0.5% is observed.

Also the paper [45] focuses on the frequency responses of two VTs (primary rated voltage of 10 kV and 20 kV) under the influence factors listed below:

- primary voltage

- burden

- temperature

Considering the temperature, for example, it is shown that the VT resonance frequency decreases with the increase of the temperature. Also the burden value and typology (resistive or resistive-inductive) has a no negligible impact on the VT frequency response. Thus, as main output, the paper suggests to take into account all the influence factors in the determination of MV VT frequency performance.

In [46], it is evidenced that the frequency response of VTs depends not only on the primary voltage at which the characterization is performed but on a more complex system of influence factors such as temperature, proximity, and burden. In the same paper, the authors provide an estimation of the accuracy for 20 kV VTs used in the harmonic measurement up to the 50th order:

- For $0.1 \leq f < 1\ kHz \rightarrow \pm 2\%$.

- For $1 \leq f < 2\ kHz \rightarrow \pm 4\%$.

- for $2 \leq f < 2.5\ kHz \rightarrow \pm 6\%$.

A very similar approach and findings for determining the VT accuracy in harmonic measurement is presented in [8], where harmonics up to the 100th order are considered. In paper [47], the frequency response of a 33 kV single phase inductive VT is evaluated in a frequency range from 50 Hz up to 5 kHz. The result shows that the ratio error drops as frequency increases up to 4.85 kHz where a resonance phenomenon occurs. The difference between the normalized voltage ratio at 50 Hz and that at higher frequencies is significant and the tested VT exceeds the 5% limit is around 2 kHz (40th harmonic). As a consequence, if this tested VT is used for high order harmonic measurement, the magnitudes of the harmonics will result lower than their actual values.

The paper [48] focuses on the performance of a 1000 V VT in harmonics measurement under two different tests conditions. The first test consists in the generation of a sine voltage signal and the evaluation of the total harmonic distortion (THD) at both primary and secondary side. The result is that a similar value is found (0.15%). The second test includes also additional conducted disturbances and their level is chosen so that the Total Harmonic Distortion (THD) verifies the 8% limit sets by the standard [15]. As main output it is found that the decrease of the accuracy is proportional to the degree of transferred signal distortion and IT causes additional error in determining of the harmonic distortion factor.

In [49] it is proposed a method for the accuracy specification of VTs used for harmonics measurement. The method is based on the definition and identification of a frequency threshold called "critical frequency f_{crit}". In the paper, a deep measurement campaign is reported and the frequency behaviour of more than 100 VTs is analyzed (both for MV and HV applications). Considering a fixed critical frequency value, that is $f_{crit} = 1\%$, it is evidenced that with the increasing of the rated primary voltage, the critical frequency decreases significantly. Considering the planning levels for harmonics up to the 50th order prescribed by the IEC 61000-3-6, the paper [49] shows that only all the 10 kV-VTs as well as a few 20 kV- and 66 kV-VTs meet the 1%-accuracy up to those frequencies.

Papers [9, 10, 50] introduce techniques to evaluate and compensate the inductive IT (both VT and CT) errors introduced because of the non-linearity of their iron core. All the compensation techniques presented in [9, 10, 50] share the same main target that is reducing the inductive IT errors contribution in the measurement of first harmonics.

The paper [9] shows that, due to CTs and VTs intrinsic non linearity, remarkable errors are introduced in the measurement of first 10-15 harmonic tones. To improve the ITs harmonic performance, the authors of [9] provide a compensation procedure based on a simplified theoretical model for the non linearity, which relates the non linearity at harmonic frequencies to the fundamental tone amplitude. The proposed procedure called SINDICOMP is validated testing two ITs by using distorted waveforms with different harmonic contents, and varying the secondary burden. More specifically the tested ITs are an inductive commercial CT (500/5 A/A) and an inductive commercial VT (20/$\sqrt(3)$/ 100/$\sqrt(3)$ kV/V). The results of [9] show that, due to CT and VT intrinsic non linearity errors up to 1% and 10 mrad are introduced in the measurement of harmonics amplitude and phase. Nevertheless, these errors can be compensate by supplying the ITs with a sinusoidal signal at rated voltage and frequency and measuring the spurious primary and secondary harmonics tone.

The technique presented in [10] provides compensation of harmonic distortion through polynomial modelling in the frequency domain. The determination of the compensating coefficient is based on the measurement of the IT harmonic responses under test conditions representative of the actual one that is with signal composed by a large fundamental tone at rated frequency and N harmonic tones at reduced random amplitude compliant with [15]. The compensation technique [10] has been applied for the characterization of a LV inductive VT.

As said before, also the paper [50] deals with a technique for the reduction of the non-linearity error introduced by inductive IT, with particular reference to CT. The proposed technique is based on the modelling of the complex ratio of the CT with a frequency domain model based on the frequency coupling matrix approach.

It is worth noting that in all the analyzed papers, the IT frequency response is evaluated starting from the rated frequency (50 Hz), not evaluating the performance of the ITs in the measurement of subharmonics (i.e., interharmonics with frequencies lower than the power frequency). On the other hand, it is known that DC and low-frequency components can worsen IT performance [51], in particular voltage subharmonics with frequencies from few mHz to about 5 Hz, and amplitude lower than 1% cause core saturation in transformers. Another paper dealing with subharmonics and IT is [52] where it is evidenced that very low frequencies subharmonics have the potential to cause hysteresis loop asymmetries, core saturation, and consequent amplification of the non-linear behavior. Such situations lead to

transformers higher magnetizing currents and iron losses with consequent thermal effects that lead to transformer power derating. The paper presents also experimental tests on a LV single phase transformer supplied with a fundamental tone at rated voltage and amplitude plus a 0.7% subharmonic at 1 Hz.

Other papers have investigated the performance of ITs when they are used for the measurement of PQ phenomena different from the harmonics and interharmonics. In particular, [53] provides a quantification of the impact of CTs on the measurement of synchrophasors when amplitude and phase modulations or frequency ramp are present in the input signal. As a result, it is found that the tested CTs exceed their 50 Hz accuracy classes affecting the synchrophasors measurement under particular operating conditions.

The paper [54] presents results related to the phenomenon of inductive CT additional secondary current distortion in condition of variation of their primary current r.m.s. value caused by dips and interruptions of the power line's voltage. To assess the CT accuracy in presence of such disturbances, harmonics spectrums of primary and secondary currents are compared when the CT is supplied with transient events. It is found that the variation of the inductive CT primary current r.m.s. value causes additional distortion of its secondary current. This will result in additional errors during the evaluation of current higher-order harmonics.

To summarize, many works currently suggest procedures and measurement systems to verify ITs performance for harmonics measurements and some propose compensation techniques for the low frequency errors. However, the ITs error contributions in the measurement of other PQ phenomena are not fully investigated and quantified yet.

2.5   Relevant PQ phenomena for ITs characterization

Starting from the review of in-force standards and recent literature dealing with PQ, PMU and ITs presented in the previous sections, this final section aims to propose in Table 2.9 a list of PQ phenomena and the possible range of test parameters which can be relevant for testing ITs.

Table 2.9 Relevant PQ phenomena to be employed in the testing of voltage and current ITs.

Parameter	Inductive ITs		LPITs	
	VT	**CT**	**VT**	**CT**
Voltage and current deviations	1% to 150%·V_n (k_p· V_n for protection VTs)	1% to 120%·I_n (1% to 100%·I_{th})	1% to 150%·V_n (k_p· V_n for protection VTs)	1% to 120%·I_n (1% to 100%·Ith)
Frequency deviations	±15% of rated frequency (isolated systems).			
Harmonics and interharmonics	Harmonic: 10% from 2nd up to 15th - 5% from 16th up to 50th 2% from 51th up to 9 kHz. Interharmonic: 3% from DC up to 20 Hz - 5% from 20 Hz up to 100 Hz and 1% from 100 Hz up to 9 kHz.			
	Multi-tone waveforms at rated amplitude with superimposed tones (selected from the 0.1 Hz to 9 kHz) up to 9 kHz.			
	Fundamental tone at rated amplitude with 1 superimposed tone up to 9 kHz (including harmonic phase variations from 0 to 2π).			
Modulations	Modulating frequency from 0.1 Hz up to 5 Hz , modulating factors k_x=0.1 V/V (A/A), k_a=0.1 rad (see Equation 2.5).			
Frequency ramp	Ramp rate: ±1 Hz/s; from - 5 Hz to 5 Hz from rated frequency.			
	VT and LPVT only			
Dips	10% to 90% of rated amplitude at point on wave from 0 to 1.5π by $\pi/4$ steps and ±$\pi/2$ jump at the beginnig/end of each jump			
Interruptions	5% of rated amplitude at point on wave from 0 to 1.5π by $\pi/4$ steps.			
Voltage Swells	110%, 120%, 150% of rated amplitude at point of wave from 0° up to 270° with 45° step and ±90° change at the beginning and the end of cycle.			
Transient overvoltage	Oscillatory transient with spectral content ≤9 kHz.			

Chapter 3

Generation and Measurement Setup

3.1 Introduction

This Chapter provides a description of the developed laboratory system for the performance evaluation of MV VTs and LPVTs with analog and digital output for PQ and PMU applications.

The generation and measurement setup is shown in Fig. 3.1. It can be used for the calibration of MV Voltage Transformers (VT) and Low Power Voltage Transformers (LPVTs) with primary voltage from 1 kV to 30 kV (peak value) in presence of sinusoidal and arbitrary voltage signal with frequency content from DC up to 9 kHz.
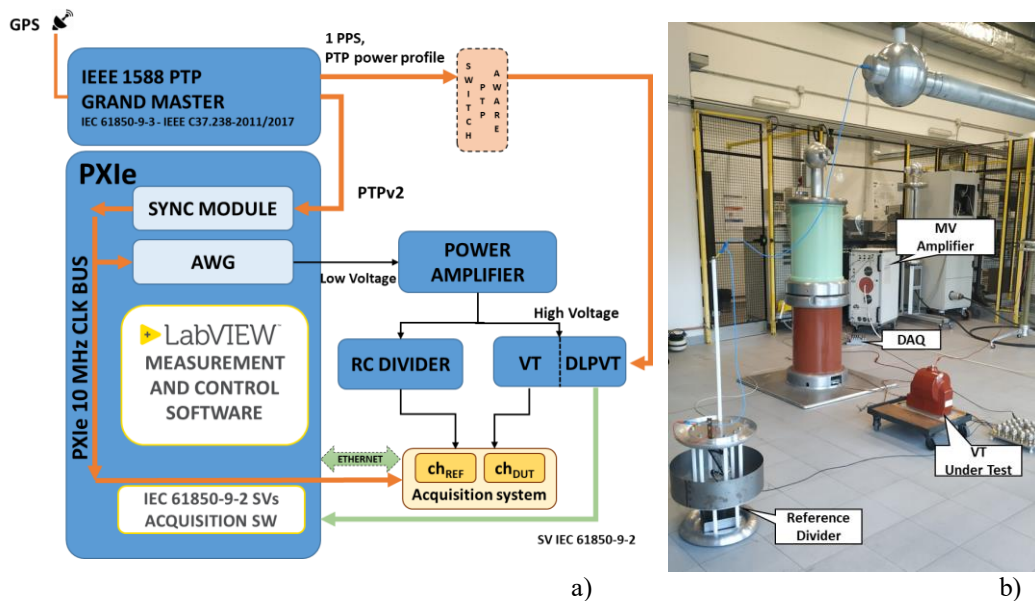
Fig. 3.1 (a) Block scheme and (b) photo of the laboratory reference system for MV VT and LPVT calibration.

The setup architecture is based on a National Instruments (NI) PCI eXtension for Instrumentation (PXI) platform and it can be divided into five different sections:

Generation: the MV test waveforms are generated by an arbitrary waveform generator (AWG) coupled with a high-voltage power amplifier.

Reference Sensor: the reference sensor is a wideband resistive-capacitive (RC) voltage divider for smart grid applications designed, built and characterized at INRIM.

Synchronization: the synchronizations system, necessary when the device under calibration is a digital output LPVT (DLPVT), is an IEEE 1588 Grand Master (GM) device synchronized to the GPS, which can provide synchronization signals such as 10 MHz,1 pulse per second (1PPS) and IEEE 1588-2008 (PTPv2).

Data acquisition: when a VT or an LPVT with analog output is calibrated, the measured reference and test signals are acquired by a comparator that includes various acquisition modules. When a DLPVT is calibrated, a single acquisition channel of a different acquisition board is used to acquire the reference signal.

Measurement and control software: The software for data processing and instrument control is developed in LabVIEW. A large variety of signals can be

generated, such as sinusoidal, fundamental plus one or *N* harmonics, amplitude and phase modulated signals, frequency ramps, PQ events from database or user simulated.

Each setup section and the relative characterization results, will be described in detail in the following subsections.

3.2   Measurement Procedure

With the aim of investigating the possible errors introduced by the VT or LPVT when they are used to sense the grid voltage and reduce it to fit the input of a Power Quality Instrument (PQI) or PMU, the measurement system configuration shown in Fig. 3.2 is assumed.

The reference sensor (REF) and the devices under test (VT/LPVT) are used to measure the same distorted voltage signal. Their outputs are acquired by the acquisition system and then processed by two instances of the same software that implement the measurement algorithms prescribed by the relevant standards for PQIs (for instance IEC 61000-4-30 [18] or IEC 61000-4-7 [19]) or PMUs (for instance IEEE/IEC 60255-118 [22]).

The accuracy of analog output VT or LPVT under calibration is evaluated in terms of complex voltage transformation ratio according to Equation 3.1:

$$\overline{k}_{\mathrm{A}}(f) = \frac{\overline{V}_{\mathrm{p}}(f)}{\overline{V}_{\mathrm{s}}(f)} \tag{3.1}$$

where $\overline{V_{\mathrm{p}}}$ and $\overline{V_{\mathrm{s}}}$ are the primary and secondary voltage phasors at the rated frequency for a sinusoidal signal or at a generic frequency for an arbitrary waveform signal, respectively.

Taking into account the measurement chain sketched in Fig. 3.2, the quantity in Equation 3.1 can be written as:
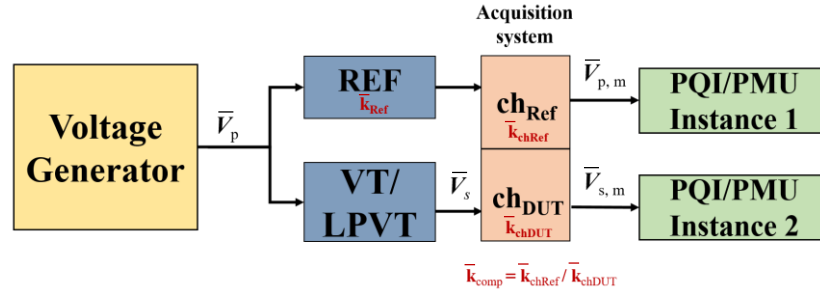
Fig. 3.2 Functional block diagram of the measurements for the analog output VT and LPVT characterization.

$$\overline{k}_{\mathrm{A}}(f) = \frac{\overline{V}_{\mathrm{p,m}}(f) \cdot \overline{k}_{\mathrm{ref}}(f)}{\overline{V}_{\mathrm{s,m}}(f)} \cdot \overline{k}_{\mathrm{comp}}(f) \tag{3.2}$$

where:

- $\overline{V}_{\mathrm{p,m}}$ is the acquired phasor of the applied primary voltage $\overline{V}_{\mathrm{p}}$ measured by the reference arm;

- $\overline{V}_{\mathrm{s,m}}$ is the acquired phasor of the DUT secondary voltage $\overline{V}_{\mathrm{s}}$;

- $\overline{k}_{\mathrm{ref}}$ is the complex transformation ratio of the reference voltage sensor;

- $\overline{k}_{\mathrm{comp}}$ is the comparator complex ratio given by the ratio of the reference ($\overline{k}_{\mathrm{chRef}}$) and DUT ($\overline{k}_{\mathrm{chDUT}}$) complex calibration factor of the acquisition device.

For a digital output DLPVT, the functional measurement chain is the one shown in Fig. 3.3. It follows that the Equation 3.1 can be rewritten as in Equation 3.3:
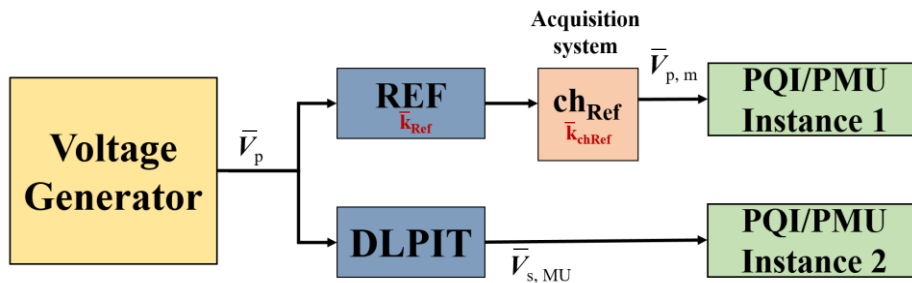
Fig. 3.3 Functional block diagram of the measurements for the DLPVT characterization.

$$\overline{k}_{\mathrm{D}}(f) = \frac{\overline{V}_{\mathrm{p,m}}(f) \cdot \overline{k}_{\mathrm{ref}}(f)}{\overline{V}_{\mathrm{s,MU}}(f)} \cdot \overline{k}_{\mathrm{chRef}}(f) \qquad (3.3)$$

where:

- $\overline{V}_{\mathrm{p,m}}$ is the acquired phasor of the applied primary voltage $\overline{V}_{\mathrm{p}}$ measured by the reference arm;

- $\overline{V}_{\mathrm{s,MU}}$ is the phasor of the secondary voltage obtained from the DLPIT digitized data;

- $\overline{k}_{\mathrm{ref}}$ is the complex transformation ratio of the reference voltage sensor;

- $\overline{k}_{\mathrm{chRef}}$ is the reference acquisition channel calibration factor.

3.3 Generation System

The NI 5421 AWG module is used to generate low voltage (LV) signals Fig. 3.4 (a). The NI 5421 AWG module can generate both user-defined and ordinary waveforms such as sinusoidal, square, triangulated, and ramp with frequency bandwidth up to 43 MHz. It has a DAC with 16-bit resolution, voltage range ± 12 V (peak value), 100 MHz maximum sampling rate, and 256 MB on-board memory.

a)   b)
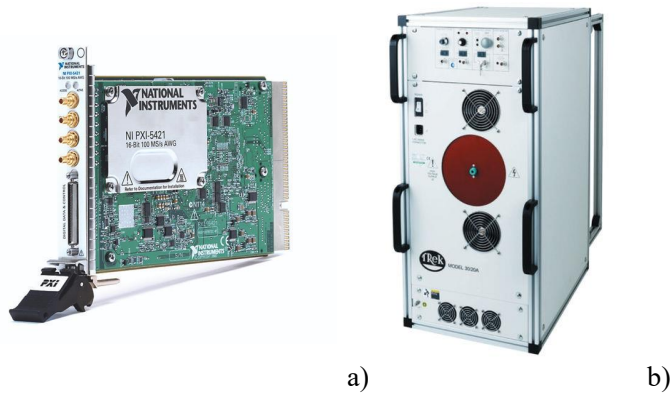
Fig. 3.4 System for the generation of reference AC and distorted waveforms for the characterization of MV VT and LPVT. (a) low voltage AWG and (b) high-voltage power amplifier.

The LV signals from the NI 5421 AWG are then amplified by a Trek high-voltage power amplifier shown in Fig. 3.4 (b). The Trek high voltage power amplifier can generate output voltage up to ±30 kV DC or peak AC, with a maximum output current of ±20 mA. It has a wide bandwidth; in particular from DC to 2.5 kHz it can be used at full voltage whereas waveforms up to 30 kHz are generated at reduced voltages. The amplifier slew rate is higher than 550 V/µs.

3.3.1   THD Quantification

The Total Harmonic Distortion (THD) of the generation setup has been measured at different primary voltages. In particular, the generation section first has been configured to generate a sinusoidal waveform at 50 Hz and the first 100th spurious harmonic tones have been considered for the THD evaluation.

Results are summarized in Table 3.1:

Table 3.1 Measured THD for the MV Generation set-up

Voltage (kV)	THD (%)
2	0.029
5	0.013
7	0.011
10	0.012
12	0.010
15	0.012

As can be observed, for all the voltage levels, the measured THD values are below 0.03%.

An estimation of the accuracy of the voltage waveform actually generated by the system with respect to the nominal one, as set by the user, is carried out. The analysis is performed by generating 100 different waveforms composed of the fundamental tone and 24 superimposed harmonic components randomly chosen. It is worth noting that all the harmonic tone amplitudes are compliant with the IEC 50160 [15] prescriptions concerning MV grids harmonic levels and, in general, the nominal THD value does not exceed the 8% limit.

The deviations between the waveform reproduced by the generation system and the imposed ones are evaluated. For sake of brevity, only the 100 differences related to the ratio of the second harmonics to the fundamental tone and of the THD values are reported in Fig. 3.5 (a) and Fig. 3.5 (b) respectively.
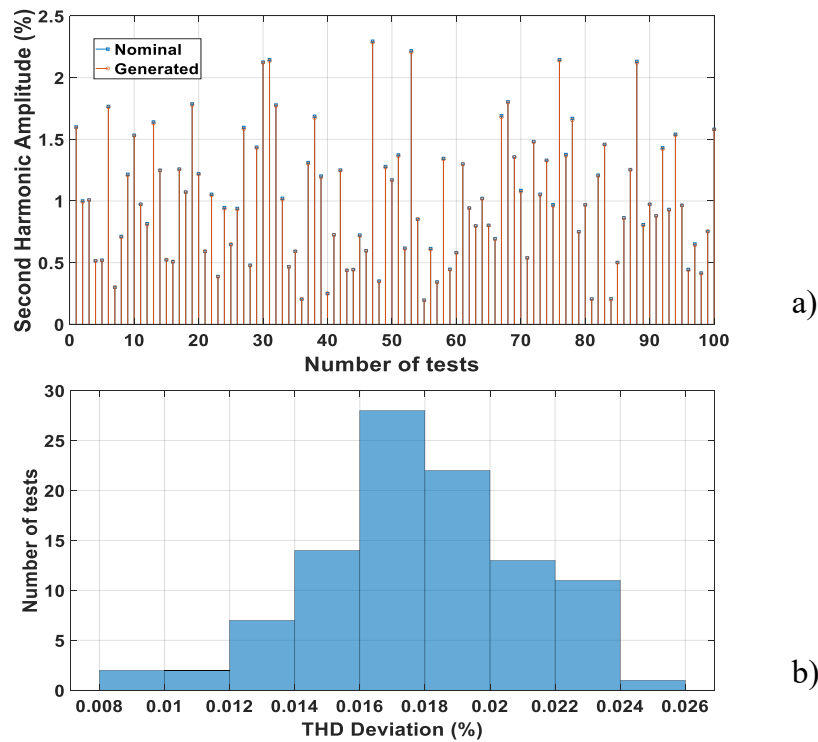
Fig. 3.5 (a) Comparison between generated and nominal second harmonic amplitudes and (b) deviation between the generated and nominal THD in %.

As can be observed in Fig. 3.5 (a) in all the 100 tests performed by varying the harmonic amplitude the generated second harmonic amplitudes are well overlapped to the nominal one and their deviations are within the measurement uncertainty (see Section 3.7). As to the THD, for about 65% of the cases, the deviations are in the [0.014-0.02]% range, also in this case within the measurement uncertainty.

3.3.2   Waveform Generation Features

The generation system can be used to reproduce a large variety of MV signals. In particular, the software for data processing and instrument control is an event-driven finite-state machine developed in LabVIEW. Several signals have been synthesized

and generated: sinusoidal, fundamental plus one or N harmonics, amplitude and phase-modulated signals, frequency ramps, voltage dip, voltage swell, and PQ events reconstructed from an available database of on-site recorded signal (comtrade files) or user simulated.

All the test waveforms are forerun and followed by a fade-in and a fade-out signal, in order to avoid the generation of large step voltage. The fade-in is obtained by multiplying the test signal by the function described by Equation 3.4

$$v_{\text{fade}-\text{in}}(t) = \frac{2}{1 + e^{-k_{\text{rise}}t}} - 1 \tag{3.4}$$

Setting the k_{rise} parameter makes it possible to choose the rise time properly. An analogue function is used for the fade-out. An example of a generated MV test signal with fade-in is given in Fig. 3.6.
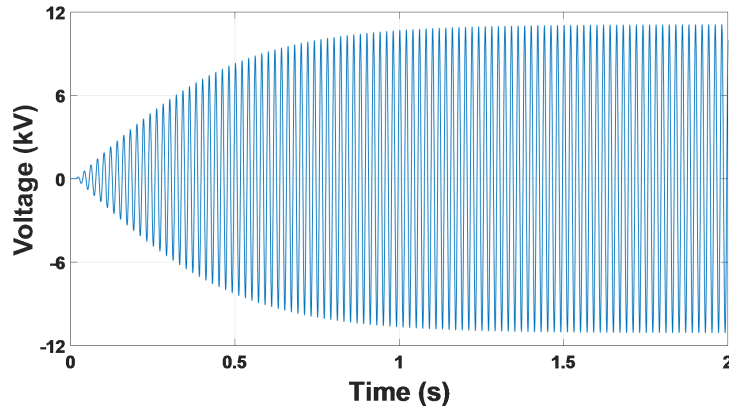
Fig. 3.6 Sinusoidal test signal with fade-in component.

Moreover, the generation software implements a real time compensation of DC component that is necessary to avoid the saturation of the VT iron core.

The software front panel for the generation and acquisition setting is shown in Fig. 3.7.
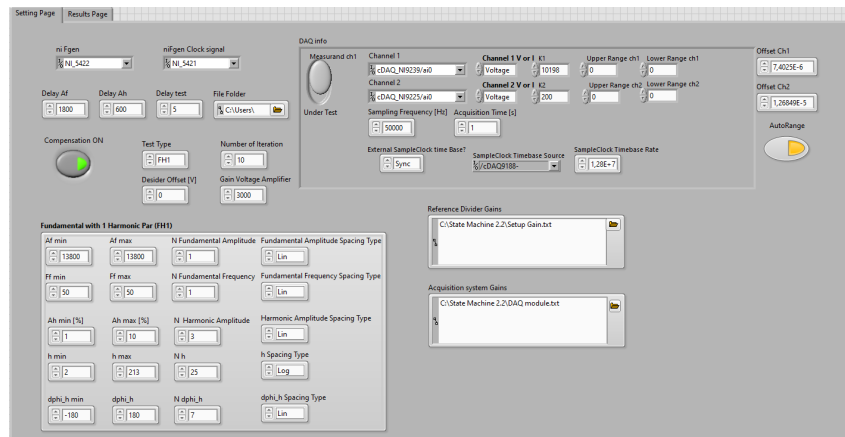
Fig. 3.7 Labview interface for the configuration of the arbitrary waveform generation and acquisition.

3.4 Synchronization System

The synchronization system is composed of a straightforward one master and two slaves architecture. The master system is based on the Meinberg microSync NTP/PTP Time Source shown in Fig. 3.8.

Fig. 3.8 Meinberg microSync NTP/PTP Time Source.

The Meinberg microSync NTP/PTP Time Source has a wide range of output signals including 1PPS, 10 MHz, IRIG timecodes, programmable pulses, and fiber optic signals. In particular, it allows the generation of several PTP profiles , which are IP/Ethernet based protocols for distributing time in a network from a Master Clock to one or more Slave Clocks, including those required for the calibration of digital LPIT:

- IEEE 1588v2 Default Profile

- IEEE C.37.238-2011 Power Profile

- IEEE C.37.238-2017 Power Profile

- IEC/IEEE 61850-9-3 Power Utility Profile

The microSync system is time-synchronized via GNS-UC (GPS and Galileo) and the accuracy associated with the timestamp is 8 ns. The internal oscillator is an OCXO DHQ and its main features are summarized in Table 3.2:

Table 3.2 MicroSync NTP/PTP Time Source OCXO DHQ oscillator main features

Short term stability T=1 s	$2 \cdot 10^{-12}$
Accuracy of PPS (pulse per second)	$< \pm 50$ ns
Phase noise	1 Hz < -80dBc/Hz
	10 Hz < -110dBc/Hz
	100 Hz < -125dBc/Hz
	1 kHz < -135dBc/Hz
Accuracy, GPS-synchronous averaged 24 h	$\pm 1 \cdot 10^{-12}$
Accuracy, free run, one day	$\pm 1 \cdot 10^{-10}$; ± 1 mHz (Note)
Accuracy, free run, one year	$\pm 1 \cdot 10^{-8}$; ± 0.1 Hz (Note)
Accuracy of time, free run, one day	± 4.5 µs
Accuracy of time, free run, 30 days	± 3.3 ms
Temperature dependant drift, free run	$\pm 2 \cdot 10^{-10}$ (5...70°C)
Note 1: The accuracy in Hertz is based on the standard frequency of 10 MHz.	

The mycroSync Time Source is used to provide the synchronization signal (1 PPS or PTP) to the device under test and to the reference measurement chain.

When the application requires to provide a PTP signal to the DUT over an Ethernet 100 FX Port Duplex LC connector, a PTP switch aware is necessary to adapt the Ethernet speed of the Meinberg mycroSync (1000 FX) to the required speed (100 FX). The PTP switch included into the setup for this purpose is the Kyland SICOM3000A Layer 2 DIN-Rail Managed Industrial Ethernet. The peer mean path delay of the PTP switch aware is 60 μs and since it is used as a transparent clock, it removes the delay from its own processing and thus compensate for delays in PTP messaging.

As regard the synchronization of the reference chain, the mycroSync provides a 1588 PTP signal to the PXIe by the means of the National Instrument NI 6683H timing and synchronization module shown in Fig. 3.9.

Fig. 3.9 National Instrument NI 6683H timing and synchronization module.

The PXI-6683H is properly configured as a PTP slave and synchronized with an accuracy <100 ns. The NI sync board features a precision 10 MHz TCXO, whose frequency accuracy and stability of this clock are better than the frequency accuracy and stability of the native 10 MHz PXIe backplane clock. For this reason, the disciplined on-board oscillator of the PXI-6683H is used to override the backplane clock of PXIe chassis. NI 6683 H main features are summarized in Table3.3.

Table 3.3 NI 6683H main features

Frequency	10 MHz
Initial accuracy	±1 ppm
Temperature stability (0 to 55 °C)	±1 ppm
Tuning range	±17.5 ppm minimum
Aging per year	±1 ppm
Duty cycle	45% to 55%

3.5   Reference Sensor

The resistive Capacitive Voltage Divider (RCVD) has been designed and built to be used as reference sensor for MV smart grid laboratory application. The RCVD primary rated voltage is equal to 30 kV and its nominal frequency band is from DC to 12 kHz.

The RCVD high voltage arm has 4 bipoles series connected with a zigzag path. In particular, each bipole is formed by the parallel connection of a 30 MΩ resistor and a 300 pF capacitor. As to the low voltage arm, it includes a 12 k Ω resistor parallel connected to a 750 nF capacitor.

The RCVD performances are assessed by carrying out a series of tests including

- evaluation of the voltage dependence of the divider Scale factor (SF), defined as the ratio of the applied to the output voltage;

- measurement of the frequency response at reduced amplitude;

- stability test at rated frequency

- proximity tests at rated frequency.

3.5.1   Voltage Dependence

The voltage dependence of the reference resistive-capacitive divider SF has been assessed both in DC and in AC (at power frequency) by comparison with a reference DC divider and different standard voltage transformers respectively.

DC voltage dependence tests are performed with both positive and negative polarity and the mean values are evaluated. Results of the DC measurement are shown in Fig. 3.10. Measurements at different voltage levels were performed after a stabilization time of 1 hour.
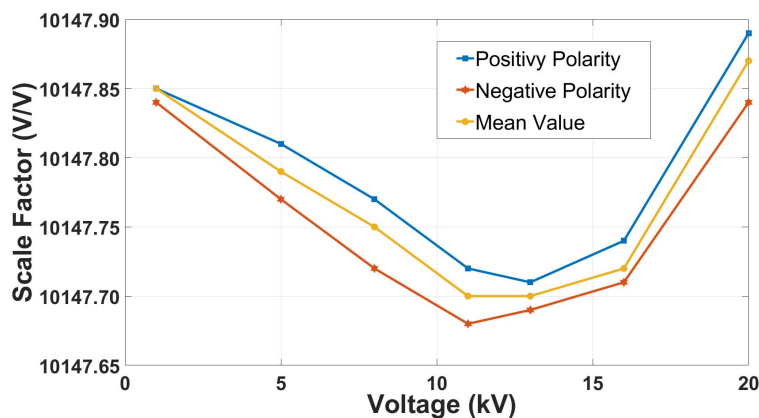
Fig. 3.10 Reference voltage divider: DC SF amplitude linearity from 1 kV up to 20 kV.

As can be observed, when the divider is acting as a pure resistive one, a variation of 16 μV/V is measured from 1 kV up to 20 kV.

As regard, the AC voltage dependence test, measured ratio and phase error variations with respect to the value measured at 11 kV at power frequency (50 Hz) are shown in Table 3.4.

Table 3.4 Reference voltage divider AC Amplitude Linearity deviation

Voltage (kV)	Ratio Error (%)	Phase Error (crad)
1	-0.012	-0.003
5	-0.008	-0.005
8	-0.001	-0.001
11	0,000	0.000
13	0.002	0.000
16	0.005	0.000
20	0.001	-0.002

3.5.2 Frequency Response

Frequency characterization of the RCVD is carried out by performing a harmonic frequency sweep at reduced amplitude, i.e. 250 V, using a Fluke 5700 A calibrator.

- the ratio error frequency response from the 120 Hz to the 9 kHz is flat within 125 μV/V (see Fig. 3.11) while

- the phase error frequency response is flat within 300 μrad.

These deviations are more than one order of magnitude lower than the limits errors indicated by the standard [1] for quality metering for high bandwidth applications for 0,1 class LPVT.
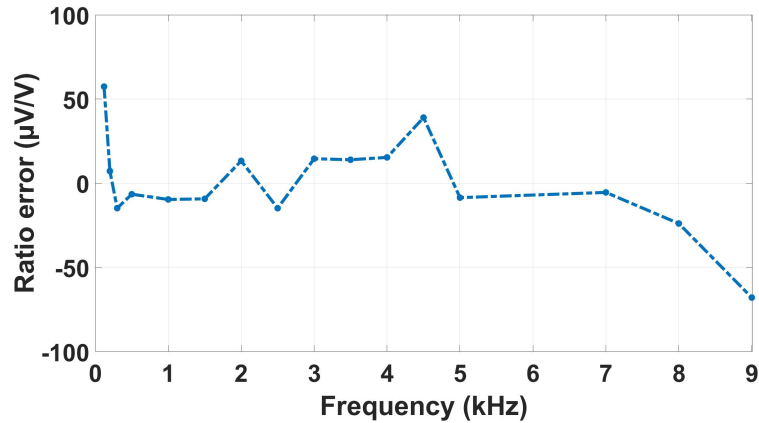
Fig. 3.11 Reference voltage divider: ratio error frequency response from 120 Hz to 9 kHz.

3.5.3 Stability

The reference divider is supplied for 90 min at 20 kV to measure the effects of the warming up on the stability of its output.

Ratio and phase errors have been measured every 30 min and the results are summarized in Table 3.5:

Table 3.5 Reference voltage divider stability test results at 20 kV

Time	Ratio Error Variation	Phase Error Variation
(min)	(μV/V)	(μrad)
0	0	0
30	31	6
60	45	7
90	50	7

As can be seen, when applying 20 kV the divider ratio error variation after 60 min is negligible for the phase error and can be assumed within a few ppm for the ratio error.

3.5.4   Proximity

As regards the proximity effect, a metallic plate of 40 cm × 50 cm size is placed at increasing distances from the divider, ratio and phase error are measured with and without the metallic plate.

The effects with the metallic structure are:

- at 60 cm within 36 µV/V and 5 µrad;

- at 100 cm 6 µV/V deviation for the ratio error and 0.5 µrad difference is found for the phase.

3.6   Acquisition system

When a VT or a LPVT with analogue output is calibrated the measured reference and the test signals are acquired by a comparator that includes a NI compact Data AcQuisition system (cDAQ) with various acquisition modules Fig.3.12 (a). When a DLPVT is calibrated, a single acquisition channel of a NI PXIe module 6124 is used Fig.3.12 (b).
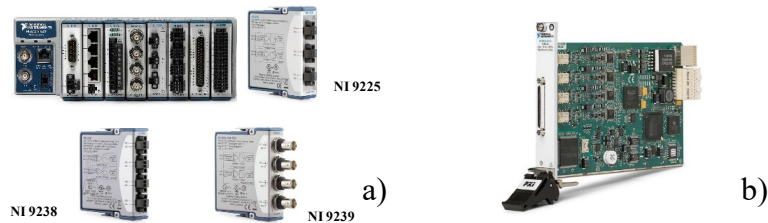
Fig. 3.12 Acquisition systems used for the calibration on a) analog output VT and LPVT and b) digital output LPVT.

The safety distance of 1 meter is kept in the measurement shown in the following sections.

3.6.1   Acquisition system for the calibration of VT and LPVT with analogue output

The comparator used for the calibration of VT and LPVT with analogue out includes the following modules:

- NI 9238: 4 channels, analogue input ±0.5 V

- NI 9239: 4 channels, analogue input ±10 V

- NI 9225: 3 channels, analogue input ±425 V

All the acquisition boards have 24 bit and 50 kHz maximum sampling frequency.

The comparator has been characterized for two use-cases:

The first case (*Case A*) occurs when the device under test has a scale factor (SF) value quite close to the RCVD one (SF_{REF}=SF_{DUT}). In this case, two channels of the same acquisition module can be used to acquire two comparable voltage amplitudes.

The second case (*Case B*) occurs when the device under test and the reference sensor have different scale factor values ($SF_{REF} \neq SF_{DUT}$). In this case, depending on the voltages levels, two channels of the same board or two different boards are used to acquire two different levels signals.

Details are given in the following subsections.

Case A

For this first case, the comparator is characterized both in amplitude and phase performing a single test type.

Sinusoidal signals at various amplitudes and frequencies are generated by a reference Fluke 5700 A calibrator (DC up to 1.2 MHz, up to 1100 V) calibrated at INRIM, the same test voltage is acquired by two channels of the same acquisition module and ratio and phase errors are evaluated according to Equation3.5 and 3.6, respectively:

$$\varepsilon_{comp,A} = \frac{U_{ch1} - U_{ch0}}{U_{ch0}} \tag{3.5}$$

$$\Delta\phi_{\text{comp,A}} = \phi_{\text{ch1}} - \phi_{\text{ch0}} \tag{3.6}$$

The subscripts ch0 and ch1 refer to the quantities measured by comparator channel 0 (Ref channel) and channel 1 (DUT channel), respectively. It follows that:

- U_{ch0} and U_{ch1} are the root mean square values of the test sinusoidal signal measured by channel 0 and channel 1.

- ϕ_{ch0} and ϕ_{ch1} are the phase angle measured by channel 0 and channel 1.

Results for the first two channels of NI 9239 are provides in Fig. 3.13 for the ratio error and in Fig. 3.14 for the phase error.
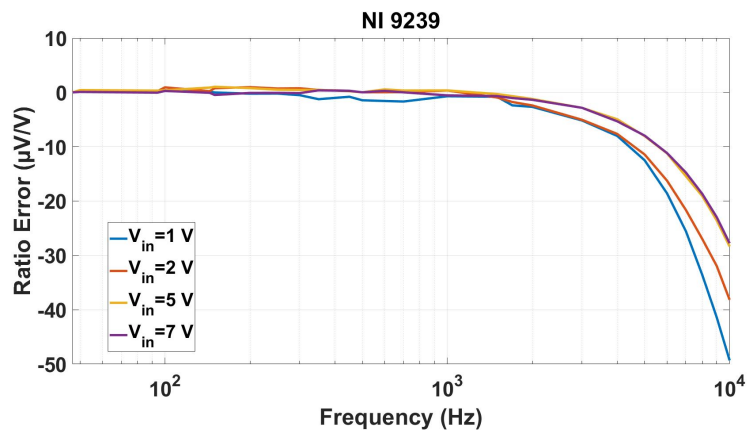
Fig. 3.13 Ratio error between 2 channels of NI 9239 when they are used to acquire the same voltage signal.
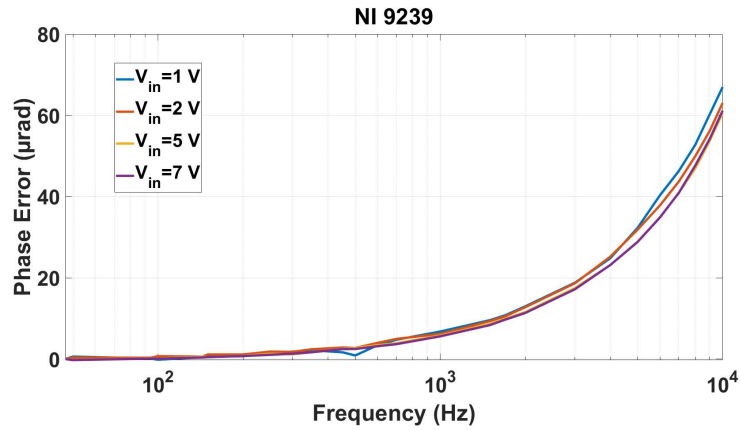
Fig. 3.14 Phase error between 2 channels of NI 9239 when they are used to acquire the same voltage signal.

As regard NI 9225, results are shown in Fig. 3.15 for the ratio error and in Fig. 3.16 for the phase error.
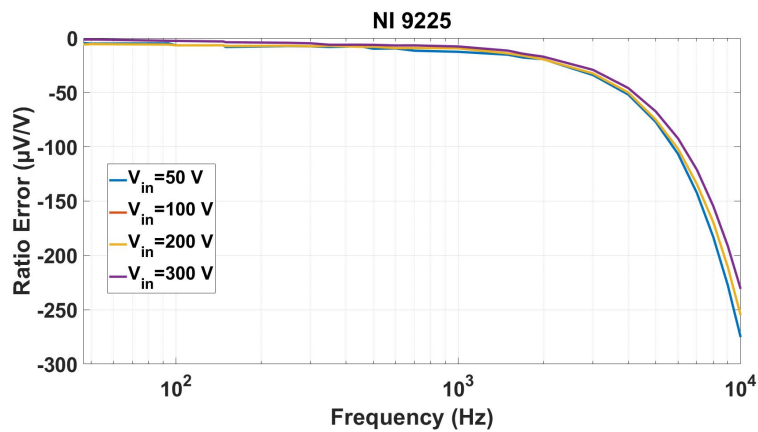
Fig. 3.15 Ratio error between 2 channels of NI 9225 when they are used to acquire the same voltage signal.
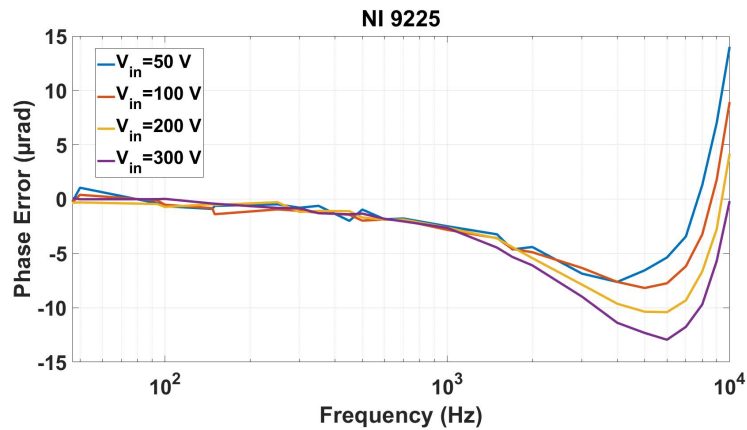
Fig. 3.16 Phase error between 2 channels of NI 9225 when they are used to acquire the same voltage signal.

The characterisation is carried out with compensation of the systematic errors by channel swapping and gives standard uncertainties within 1 µV/V and 0.5 µrad for the ratio and phase error measurement, respectively

Case B

For this case the comparator is characterized in two steps.

The characterization performed in the first step is equal to the one performed for the case A, i.e. a sinusoidal voltage is given to the two channels under test, the amplitude of the sinusoidal waveform is chosen to be compliant with both the analogue inputs of the 2 channels and the frequency varies from 50 Hz to 9 kHz.

The second step consists in a sinusoidal frequency sweep performed from power frequency up to 400 Hz interposing between the two channels a reference inductive voltage divider as shown in Fig.3.17:
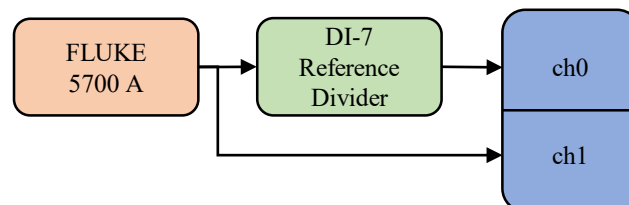
Fig. 3.17 Functional block diagram of the characterization of the comparator for Case B.

The reference inductive voltage divider is the CONIMED DI-7 and its main features are summarized in table Table 3.6:

Table 3.6 CONIMED DI-7 Reference inductive voltage divider main features

Number of decades	7
Voltage / frequency	5 V / Hz
Reference Voltage:	250 V
Reference Frequency:	50 / 60 Hz
Frequency Range:	40 - 400 Hz
Linearity:	± 0,0002 %, ± 10 μrad

The DI-7 reference divider is used to test the two channels with different voltage ratio, the ratio and the phase errors are evaluated according to the following relations:

$$\varepsilon_{comp,B} = \frac{U_{ch1} - U_{ch0} \cdot k_{DI-7}}{U_{ch0} \cdot k_{DI-7}} \tag{3.7}$$

$$\Delta\phi_{comp,B} = \phi_{ch1} - \phi_{ch0} \tag{3.8}$$

The subscripts ch0 and ch1 refer to the quantities measured by comparator channel 0 and channel 1, respectively. It follows that:

- U_{ch0} and U_{ch1} are the root mean square values of the test sinusoidal signal measured by channel 0 and channel 1.

- ϕ_{ch0} and ϕ_{ch1} are the phase angle measured by channel 0 and channel 1.

- k_{DI-7} factor is the nominal ratio of the DI-7 reference inductive divider.

Results related to the ratio error between ch0 of NI 9225 and ch0 of NI 9239 are shown in Fig.3.18.
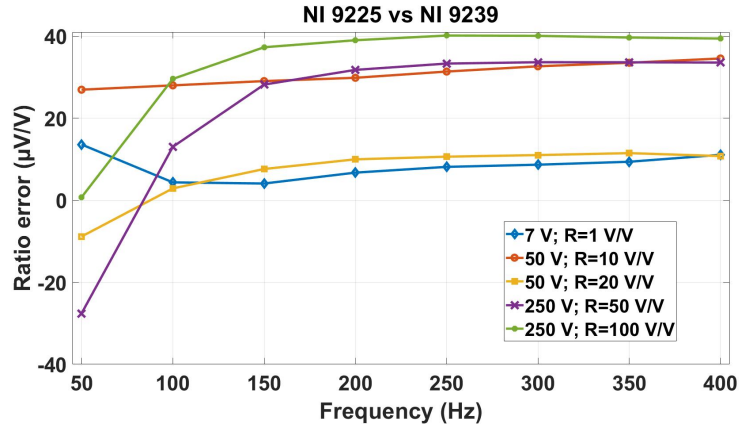
Fig. 3.18 Ratio error between 1 channel of NI 9239 and 1 channel of NI 9225 when they are used to acquire the same voltage signal (R=1 V/V- blue curve) and 2 different amplitude voltages (R from 10 V/V to 100 V/V).

As regard the time delay between ch0 of NI 9225 and ch0 of NI 9239 a mean value of $\Delta\tau_\mathrm{m}$= 0,28 μs is measured. The standard uncertainties are obtained by combining Fluke 5730A uncertainties and the repetitions contributions. For NI 9239 the standard uncertainties are within [25-35] μV/V while for NI 9225 are [28-36] μV/V.

3.6.2 Acquisition system for the calibration of LPVT with digital output

The first channel of NI 6124 ($\pm$10 V, 16 bit, maximum sampling rate 4 MHz) has been characterized at various amplitudes (from 1 V to 7 V) and frequencies (from 50 Hz up to 9 kHz).

Two different test procedures are performed for the evaluation of the module performance in amplitude and phase measurement, respectively.

The amplitude calibration is performed using the Fluke 5700A calibrator as reference system. Several voltages sinusoidal signals are generated and, for each of them, the ratio error described in Equation3.9 is evaluated:

$$\varepsilon_\mathrm{DAQ} = \frac{U_\mathrm{meas} - U_\mathrm{r}}{U_\mathrm{r}} \tag{3.9}$$

where U_{meas} and U_{r} are the root mean square of the measured and reference sinusoidal voltage signals, respectively.

Results related to the calibration of NI 6124 ch0 are shown in Table3.7 for various amplitude and frequency values.

Table 3.7 NI 6124 First Channel Amplitude Calibration

Ratio error (μV/V)					
Amplitude (V)	Frequencies (Hz)				
	50	500	1000	5000	9000
1	16	1	-4	-1	-6
3	-1	-4	-6	6	3
5	-1	1	2	1	3
7	10	2	-5	-4	3

Particular attention has been paid to the measurement of the absolute phase error of the input channels of the comparator.

In [55], the concept of absolute phase errors of digitizers and the related measurement method for its evaluation are introduced. The device tested in [55] is the same used as acquisition board when a DLVP is calibrated. It is a digitizer employing a Successive Approximation Register (SAR) Analog-to-Digital Converter (ADC), that is an architecture showing a very low time delay between input and output, so resulting in a low absolute phase error, especially at low frequencies.

Results related to the measurement of the absolute phase error of the channel 0 from 50 Hz to 20 kHz for amplitudes from 1 V to 10 V exhibit an absolute phase error lower than 10 mrad up to 10 kHz. The expanded uncertainty associated with the method described in [55] is about 4 μrad at 50 Hz and 150 μrad at 20 kHz. This last uncertainty value is a conservative one compared to the 9 kHz frequency range investigated in the thesis.

Acquisition of Sampled Values according to IEC 61850 protocol

To acquire the Sampled Values (SVs) provided by a SAMU or an LPVT with digital output, a specific software was created in the LABVIEW environment front panel in

Fig. 3.19. The acquisition section of the software is conceptually divided into two parts: the acquisition and the decoding of the SVs.

Regarding the acquisition, it has been used a subroutine Virtual Instrument (SubVI) working as an interface between LabVIEW and Winpcap. Thanks to this subVI, it is possible to detect and acquire SV ethernet packets. In particular, as outputs it provides the raw data of the packet as a hexadecimal string and the timestamp information for each packet.

As the second step, starting from the prescriptions given by the IEC 61850-9-2 [56], a subVI devoted to decoding the raw data of the SV packet according to the standard coding rules has been written in Labview. The Labview subVI works with SVs at frequency rate from 4 kHz (metering applications) up to 14.4 kHz (quality metering applications).
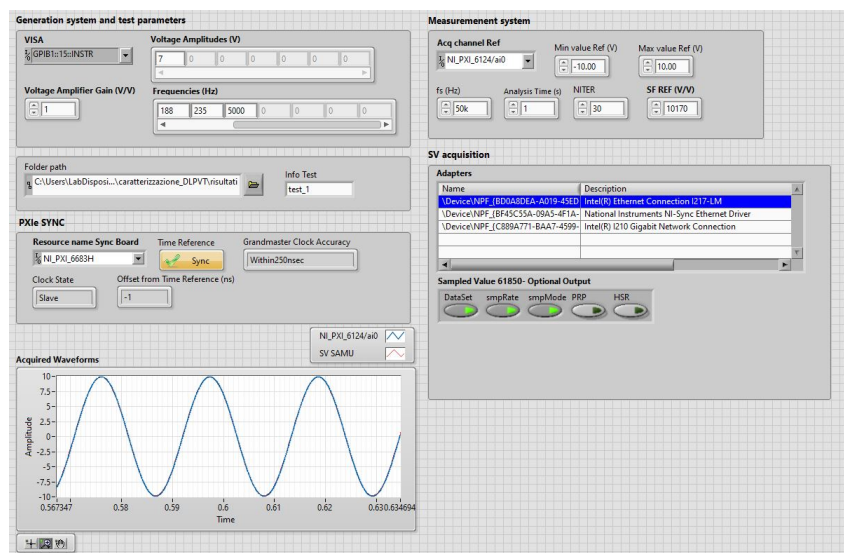
Fig. 3.19 Front Panel of the Labview software for testing DLPVTs.

3.7   Uncertainty Budget

Starting from the analysis of the systematic errors and the uncertainty sources for the system components (RC divider and acquisition system), as detailed in previous subsections, the measurement models and the uncertainty budgets for the ratio and phase errors are provided below.

Ratio error

From the schematic representation of Fig. 3.2, the measurement model for the ratio error ε_{VT} of the VT under calibration can be described as:

$$
\begin{aligned}
\varepsilon_{\text{VT}} &= k_{\text{n}} \cdot \frac{V_{\text{s}}}{V_{\text{p}}} - 1 \\
&= k_{\text{n}} \cdot \frac{k_{\text{chDut}} \cdot V_{\text{s,m}}}{k_{\text{Ref}} \cdot k_{\text{chRef}} \cdot V_{\text{p,m}}} - 1 \\
&= k_{\text{n}} \cdot \frac{k_{\text{comp}} \cdot V_{\text{s,m}}}{k_{\text{Ref}} \cdot V_{\text{p,m}}} - 1
\end{aligned}
\tag{3.10}
$$

The uncertainty associated with the ratio error ε_{VT} is expressed according to the Equation 3.11:

$$
\begin{aligned}
u^2(\varepsilon_{\text{VT}}) =\ & k_{\text{n}}^2 \cdot \frac{1}{k_{\text{Ref}}^4} \cdot \left(\frac{V_{\text{s,m}}}{V_{\text{p,m}}} \right)^2 \cdot k_{\text{comp}}^2 \cdot u^2(k_{\text{Ref}}) + \\
& k_{\text{n}}^2 \cdot \frac{1}{k_{\text{Ref}}^2} \cdot k_{\text{comp}}^2 \cdot u^2\!\left(\left(\frac{V_{\text{s,m}}}{V_{\text{p,m}}} \right) \right) + \\
& k_{\text{n}}^2 \cdot \frac{1}{k_{\text{Ref}}^2} \cdot \left(\frac{V_{\text{s,m}}}{V_{\text{p,m}}} \right)^2 \cdot u^2(k_{\text{comp}})
\end{aligned}
\tag{3.11}
$$

Considering that ε_{VT} assumes values close to zero, the following assumption (Equation 3.12) can be considered valid:

$$
k_{\text{n}} \cdot \frac{k_{\text{comp}} \cdot V_{\text{s,m}}}{k_{\text{Ref}} \cdot V_{\text{p,m}}} \cong 1
\tag{3.12}
$$

Thus, combining Equation 3.11 and Equation 3.12, the following Equation 3.13 is derived :

$$
u^2(\varepsilon_{\text{VT}}) \cong u_r^2(k_{\text{Ref}}) + u_r^2\!\left(\left(\frac{V_{\text{s,m}}}{V_{\text{p,m}}} \right) \right) + u_r^2(k_{\text{comp}})
\tag{3.13}
$$

where the subscript "r" refers to the relative uncertainty.

As regard the term k_{Ref}, from all characterization tests performed on the reference RCVD, the assumed model is the one provided by Equation 3.14:

$$k_{\text{ref}} = k_{\text{cal}} \cdot \delta k_{\text{V--dep}} \cdot \delta k_{\text{freq}} \cdot \delta k_{\text{prox}} \cdot \delta k_{\text{stability}} \tag{3.14}$$

Considering all the test results, the obtained uncertainty for the ratio error at 50 Hz from 5 kV up to 20 kV is 70 μV/V. For frequencies higher than 50 Hz the uncertainties are quantified in Table 3.8.

Table 3.8 Ratio error standard uncertainty contributions from 5 kV to 20 kV and from 100 Hz to 9 kHz

Uncertainty Source	Standard Uncertainty (μV/V)
RCVD calibration (k_{cal})	30
Voltage dependence ($k_{\text{V-dep}}$)	45
Frequency response (k_{freq})	65
Proximity effect (k_{prox})	21
Stability ($k_{\text{stability}}$)	6
Repeatability ($V_{\text{s,m}}/V_{\text{p,m}}$)	5
Acquisition system (k_{comp})	30
Expanded uncertainty (level of confidence 95%): 185 μV/V	

Phase error

By the same model the expression for the VT phase error is obtained as:

$$u^2(\Delta\phi_{\text{VT}}) = u_r^2(\Delta\phi_{\text{Ref}}) + u_r^2\left(\angle\left(\frac{\overline{V}_{\text{s,m}}}{\overline{V}_{\text{p,m}}}\right)\right) + u_r^2(\Delta\phi_{\text{comp}}) \tag{3.15}$$

where $\Delta\phi_{\text{Ref}}$ is obtained as:

$$\Delta\phi_{\text{Ref}} = \Delta\phi_{\text{cal}} + \delta\phi_{\text{V--dep}} + \delta\phi_{\text{freq}} + \delta\phi_{\text{prox}} + \delta\phi_{\text{stability}} \tag{3.16}$$

The uncertainty for the phase error at 50 Hz from 5 kV up to 20 kV is 70 μrad. For frequencies higher than 50 Hz the uncertainties are quantified in Table3.9.

Table 3.9 Phase error standard uncertainty contributions from 5 kV to 20 kV and from 100 Hz to 9 kHz

Uncertainty Source	Standard Uncertainty (μrad)
RCVD calibration ($\Delta\phi_{cal}$)	30
Voltage dependence ($\Delta\phi_{V\text{-}dep}$)	16
Frequency response ($\Delta\phi_{freq}$)	150
Proximity effect ($\Delta\phi_{prox}$)	9
Stability ($\Delta\phi_{stability}$)	1
Repeatability ($\angle(\overline{V}_{s,m}/\overline{V}_{p,m})$)	5
Acquisition system ($\Delta\phi_{comp}$)	38
Expanded uncertainty (level of confidence 95%): 320 μrad	

Note: the expanded uncertainty with the level of confidence 95% is calculated as two times the root square of the sum of the squared standard uncertainties [57].

Chapter 4

Measurement System Applications

4.1 Introduction

The developed generation and measurement setup has been used to assess the performances of MV inductive VTs, LPVTs and DLPVTs under different test conditions. In particular, it has been used to generate four categories of signals:

- steady-state (harmonics),

- dynamic (amplitude and phase modulations, frequency ramp),

- transient (voltage dips) and

- combinations of PQ disturbances (harmonics and subharmonics).

For each category of test signals, the indices used to evaluate the performances of the selected DUTs are introduced. Then, test waveforms and test parameters are described. Finally some experimental results are shown.

In Table 4.1, the devices considered for the different test conditions are listed and described.

Table 4.1 List of the devices tested under the different test conditions

Devices under test	Test Conditions					
	Harmonics and interharmonics			Amplitude and Phase Modulations	Frequency Ramp	Transient: Voltage Dip	
	FH1	FHN	FHS			Simulated	From DOE/EPRI database
Inductive VT$_A$ -U$_{p,rated}$ 20/√3 kV; -U$_{s,rated}$ 100/√3 V; -rated burden 30 VA; -accuracy class 0.5.	✗		✗	✗			
Inductive VT$_A$ plus SAMU Commercial SAMU with 0.2 accuracy class configured for power quality applications (sampling frequency equal to 14.4 kHz).	✗						
Resistive Capacitive LPVT (LPVT$_A$) gas-insulated divider with the following features: -measuring range ± 45 kV; -rated SF 10000 V/V; -0.2 % accuracy class at 50/60Hz -1 MHz bandwidth.		✗		✗	✗		✗
Resistive LPVT (LPVT$_B$) portable precision high voltage divider for DC and 50/60 Hz applications: -measuring range ±28 kV; -rated SF 1000 V/V; -0.1% accuracy class at 50/60Hz. -no bandwidth declared		✗			✗		✗
Inductive VT$_B$ -U$_{p,rated}$ 11/√3 kV; -U$_{s,rated}$110/√3 V; -rated burden 50 VA; -accuracy class 0.5.			✗				
Inductive VT$_C$ -U$_{p,rated}$ 20/√3 kV; -U$_{s,rated}$100/√3 V; -rated burden 30 VA; -accuracy class 0.5.						✗	

4.2   Steady State Tests

4.2.1   Performance Indices

This subsection introduces the accuracy indices used to evaluate the VT performances in the measurement of stationary PQ phenomena, referring specifically to the case of harmonics.

Two different categories of indices are defined:

1. Indices for the evaluation of the VT accuracy at specified harmonic frequency hf_0, i.e. the harmonic ratio error ε_h and harmonic phase error $\Delta\phi_h$:

$$\varepsilon_h = \frac{k_r \cdot U_{s,h} - U_{p,h}}{U_{p,h}} \tag{4.1}$$

$$\Delta\phi_h = \phi_{s,h} - \phi_{p,h} \tag{4.2}$$

where:

- $k_r = U_{p,r} / U_{s,r}$ is the rated transformation ratio ($U_{p,r}$ and $U_{s,r}$ are the rated primary and secondary voltages at fundamental frequency f_0);

- $U_{p,h}$ and $U_{s,h}$ are the rms values of the primary and secondary h-order harmonic voltage;

- $\phi_{p,h}$ and $\phi_{s,h}$ are the phase angle the primary and secondary h-order harmonic voltage.

2. A synthetic index to quantify the VT performance over a specific harmonic range, i.e. the THD deviation ΔTHD:

$$\Delta THD = THD_p - THD_s \tag{4.3}$$

where:

- THD_p and THD_p are defined as in the following Equations 4.4 and 4.5, respectively.

$$THD_{\mathrm{p}} = \frac{\sqrt{\sum_{h=2}^{N} U_{\mathrm{p},h}}^{2}}{U_{\mathrm{p},1}} \qquad (4.4)$$

$$THD_{\mathrm{s}} = \frac{\sqrt{\sum_{h=2}^{N} U_{\mathrm{s},h}}^{2}}{U_{\mathrm{s},1}} \qquad (4.5)$$

The harmonic amplitudes ($U_{\mathrm{p},h}$, $U_{\mathrm{s},h}$) and phases ($\phi_{\mathrm{p},h}$, $\phi_{\mathrm{s},h}$) are obtained performing the Discrete Fourier Transform (DFT) over non-overlapped time frames of 10-cycles of 50 Hz power frequency, according to [19] for a 50 Hz power system.

4.2.2   FH1: Fundamental Plus 1 Harmonic

Test signal description

The FH1 test signal waveform consists of two voltage components: a fundamental component at power frequency and one superimposed harmonic tone. The FH1 signal is mathematically described by Equation 4.6:

$$v_{\mathrm{FH1}}(t) = \sqrt{2}U_{\mathrm{n}}sin(2\pi f_0 t) + \sqrt{2}U_h sin(2\pi h f_0 t + \phi_h) \qquad (4.6)$$

where:

- U_{n} is the root mean square (rms) value of the rated primary voltage,

- f_0 is the power frequency,

- U_h is the rms value of the h-harmonic order tone,

- ϕ_h is the phase delay between the fundamental tone and the h-harmonic order tone.

For each generated frequency tone, harmonic ratio and phase errors are evaluated according to Equations 4.1 and 4.2, respectively.

Experimental Results

A. Devices under test

According to Table 4.1, the device under test is the inductive VT_A with and without a commercial Stand Alone Merging Unit (SAMU). In this way, it is possible to compare the performance in harmonics measurement of a conventional MV inductive VT and of the same VT equipped with a digitalizing stage.

B. Results

Considering the FH1 test signal described by Equation 4.6, the generated fundamental tone has amplitude U_n equal to $20/\sqrt{3}$ kV and frequency f_0=50 Hz. The harmonic components have fixed amplitude U_h of 10% and harmonic order variable from the 2nd to the 100th.

Results are shown in Fig. 4.1 where the FH1 responses of the VT with and without the SAMU are compared.
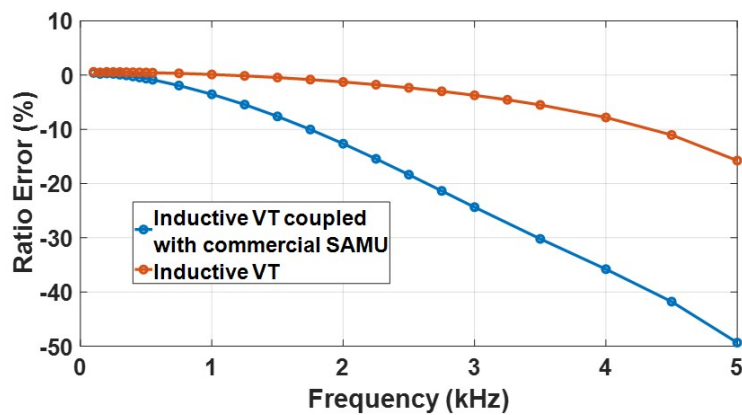
Fig. 4.1 FH1 test results of the inductive VT with and without the SAMU.

Tables 4.2 and 4.3 provide the limits for 0.5 accuracy class LPVTs required by [1] for measuring and quality metering applications, respectively.

It can be seen that the presence of the SAMU produces a worst frequency response, especially at higher harmonic orders. In fact, the VT alone frequency performance complies with the limits set by the standard [1] for both measuring and quality applications. On the contrary, the VT-SAMU combination complies with

the limits for measuring applications up to the 50th harmonic, whereas for quality applications, only the limits of the first two frequency ranges are met and the DUT exceeds the 10% at 1750 Hz.

Table 4.2 LPVT measuring accuracy classes from [1].

Accuracy class	Ratio error at low frequency		Ratio error (+/–) at harmonics					Phase displacement (+/–) at low frequency	Phase error (+/–) at harmonics			
								Degrees	Degrees			
	0 Hz	1 Hz	2nd to 4th	5th and 6th	7th to 9th	10th to 13th	Above 13th	1 Hz	2nd to 4th	5th and 6th	7th to 9th	10th to 13th
0.1	+1% -100%	+1% -30%	1%	2%	4%	8%	+8% -100%	45	1	2	4	8
0.2	+2% -100%	+2% -30%	2%	4%	8%	16%	+16% -100%	45	2	4	8	16
0.5	+5% -100%	+5% -30%	5%	10%	20%	20%	+20% -100%	45	5	10	20	20
NOTE 0 Hz in the first column means d.c. coupling is allowed but not required.												

Table 4.3 LPVT accuracy classes extension for quality metering and low bandwidth d.c. applications from [1].

Accuracy class	Ratio error (+/–) at frequencies shown below (%)			Phase error (+/–) at frequencies shown below		
				Degrees		
	$(0,1 \leq f < 1)$ kHz	$(1 \leq f < 1,5)$ kHz	$(1,5 \leq f < 3)$ kHz	$(0,1 \leq f < 1)$ kHz	$(1 \leq f < 1,5)$ kHz	$(1,5 \leq f < 3)$ kHz
0.1	1	2	5	1	2	5
0.2	2	4	5	2	4	5
0.5	5	10	10	5	10	20

4.2.3   FHN: Fundamental Plus *N* Harmonics

Test signal description

The FHN test signal is an extension of the FH1 one. In this case, the voltage waveform consists of a multi-tone signal composed of a fundamental component at

power frequency plus N superimposed harmonic tones. The mathematical description is provided in Equation 4.7

$$v_{\text{FHN}}(t) = \sqrt{2}U_{\text{n}}sin(2\pi f_0 t) + \sqrt{2}\sum_{h=2}^{N} U_h sin(2\pi h f_0 t + \phi_h) \qquad (4.7)$$

Harmonic tone amplitudes (U_h) are randomly chosen with a uniform distribution between 0% and the limits indicated by the standard [15], while the phases ϕ_h are independent and uniformly distributed between $-\pi$ and π.

In this case the VTs performances are again evaluated, for each generated frequency tone, by the harmonic ratio (Equation 4.1) and phase errors (Equation 4.2) and globally by the ΔTHD (Equation 4.3).

Experimental Results

A. Devices under test

According to Table 4.1, the performances of two different LPVTs in harmonics measurement are evaluated and compared under FHN test conditions. The two devices are both voltage dividers but based on different technologies: $LPVT_A$ is a resistive-capacitive divider designed and built for frequency applications whereas $LPVT_B$ is a resistive divider for DC and 50/60 Hz applications.

B. Results

Results of this analysis are also reported in the paper [11]. Considering the Equation 4.7, the generated fundamental tone has amplitude U_n equal to 13 kV and frequency f_0=50 Hz. Nine superimposed tones in the range from the 2nd to the 23th harmonic order are injected and their amplitudes U_h and phases ϕ_h are listed in Table 4.4. The time behaviour of the FHN test signal is shown in Fig.4.2. The generated signal has THD equal to 7.73% as measured by the reference chain, close to the THD limit prescribed by [15], that is 8%.
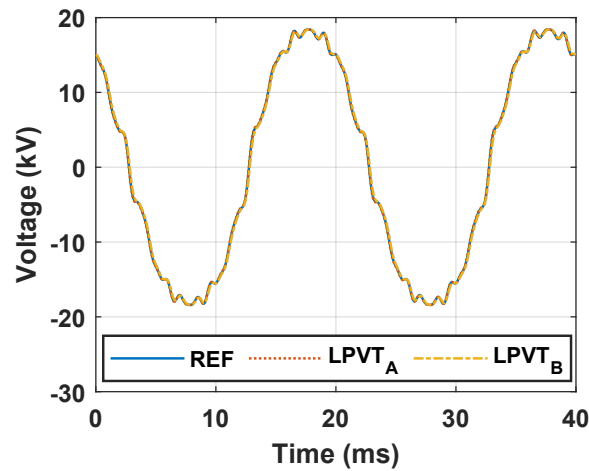
Fig. 4.2 FHN test time domain signal.

For each generated frequency, the harmonic ratio and phase errors evaluated according to Equations 4.1 and 4.2 are reported in Table 4.4.

Table 4.4 Measured THD for the MV Generation set-up

FHN Test Parameters			LPVT$_A$		LPVT$_B$	
Frequency (Hz)	Amplitude (% of rated amplitude)	Phase Displacement $(\Delta\varphi_h - \Delta\varphi_f)$ (rad)	Ratio Error (%)	Phase Error (mrad)	Ratio Error (%)	Phase Error (mrad)
50	100	0	0.025	3.20	0.029	-22.39
100	2	2.33	0.25	6.96	-0.16	-44.74
150	5	-1.65	0.58	7.75	-0.45	-66.24
200	1	0.67	0.85	7.11	-0.83	-88.21
300	0.5	-0.98	1.17	4.12	-1.88	-130.53
450	1.5	-0.32	1.37	2.03	-4.15	-191.11
550	3.5	-1.97	1.43	0.26	-6.00	-229.13
650	3	-2.23	1.45	-2.72	-8.11	-264.79
850	2	-0.64	1.51	-6.04	-12.89	-328.37
1150	1.5	0.69	1.55	-9.79	-20.82	-401.89

The THD measured by the LPVT$_A$ is equal to 7.81% whereas the THD value measured by the LPVT$_B$ is equal to 7.39%. Thus, the LPVT$_B$ introduces a deviation of 0.34% in the THD measurement. As can be seen comparing the Table 4.4 with the [1] limits provided in Table 4.2, it does not fulfil the phase error accuracy requirements for 0.1% class device in harmonics measurement and it respects the

limits for the ratio error only for harmonics up to the 6th order. This result can be explained considering that LPVT$_A$ is a resistive-capacitive divider and it is designed and built to perform frequency measurement. On the contrary LPVT$_B$ is a pure resistive divider optimized for DC and 50/60 Hz measurement.

4.3   Dynamic tests

4.3.1   Performance Indices

The VT and LPVT performances in presence of dynamic disturbances are evaluated using as test waveforms those indicated in the standard [22] for PMU performance verification. For this reason, also some of the VT performance indices are based on the indices used for the PMU characterization: the ratio error (Eq 4.8), the phase error (Eq 4.9), the Total Vector Error (TVE) (Eq 4.10), the Frequency Error (FE) (Eq 4.11) and the Rate Of Change Of Frequency error (ROCOF) (Eq 4.12).

$$\varepsilon = \frac{k_{\mathrm{r}} \cdot |V_{\mathrm{s}}| - |V_{\mathrm{p}}|}{|V_{\mathrm{p}}|} \tag{4.8}$$

$$\Delta\phi = \angle V_{\mathrm{s}} - \angle V_{\mathrm{p}} \tag{4.9}$$

$$TVE = \sqrt{\frac{[Re(k_{\mathrm{r}} \cdot V_{\mathrm{s}}) - Re(V_{\mathrm{p}})]^2 + [Im(k_{\mathrm{r}} \cdot V_{\mathrm{s}}) - Im(V_{\mathrm{p}})]^2}{Re(V_{\mathrm{p}})^2 + Im(V_{\mathrm{p}})^2}} \tag{4.10}$$

$$FE = f_{0,\mathrm{s}} - f_{0,\mathrm{p}} \tag{4.11}$$

$$RFE = \frac{df_{0,\mathrm{s}}(t)}{dt} - \frac{df_{0,\mathrm{p}}(t)}{dt} = ROCOF_{\mathrm{s}} - ROCOF_{\mathrm{p}} \tag{4.12}$$

where:

- $k_{\mathrm{r}} = U_{\mathrm{p,r}} / U_{\mathrm{s,r}}$ is the rated transformation ratio ($U_{\mathrm{p,r}}$ and $U_{\mathrm{s,r}}$ are the rated primary and secondary voltages);

- V_p and V_s are the fundamental voltage phasors at VT primary and secondary side, respectively;

- $f_{0,p}$ and $f_{0,s}$ are the fundamental frequencies measured at VT primary and secondary side, respectively.

The fundamental primary and secondary synchrophasors V_p and V_s are estimated via DFT on an observation interval of four cycles of the fundamental frequency (i.e. 0.08 s) with a reporting rate of 50 Hz in accordance with [22].

4.3.2 Amplitude Modulated Signal

Test signal description

The voltage signal used for the VT performance evaluation under amplitude modulated condition is described in Equation 4.13. It is composed of a fundamental tone at power frequency (i.e. the carrier) and a cosinusoidal amplitude modulating component:

$$v_{AM}(t) = \sqrt{2}U_n[1 + k_{AM}cos(2\pi f_{AM}t)] \cdot cos(2\pi h f_0 t) \tag{4.13}$$

where:

- k_{AM} is the amplitude modulation factor,

- f_{AM} is the modulation frequency.

Experimental Results

A. Devices under test

The devices considered for this analysis are an inductive VT (VT_A) and the $LPVT_A$. In this way, it is possible to compare the performance under amplitude modulation of a conventional inductive VT and a LPVT built for frequency applications.

B. Results

The LPVT and the inductive VT have been tested under amplitude modulated voltage signals with fundamental component at f_0=50 Hz and U_n= 20/$sqrt$(3) kV. The amplitude modulation factor k_{AM} is set to 0.1 V/V and six different modulation frequencies f_{AM} have been generated: 0.1 Hz, 0.2 Hz, 0.5H z, 1 Hz, 2 Hz, 5 Hz, in accordance with [22].

The obtained results show the presence of time oscillations of the ratio error (Eq 4.1), phase error (Eq 4.2) and TVE (Eq 4.10). In particular, are reported from Fig. 4.3 to Fig. 4.5.

The phenomenon has been explained by performing LabVIEW simulation. A numerical amplitude modulated signal is software-generated, the numerical signal is processed by two virtual ITs that model the reference divider and the device under test. The reference divider is modelled as a linear and ideal sensor, with a flat frequency response both for the amplitude and the phase. The DUT is simulated as a class 0.1 VT. A time delay between the two simulated devices is produced setting two slightly different time-bases. From the simulation it follows that the phenomena under analysis is due mainly to the following reasons:

- the primary and secondary synchrophasors are obtained performing the spectral analysis over four cycles of the power frequency 50 Hz (i.e. 80 ms) whereas

- the period of the test signals varies from 10 s (f_{AM}=0.1 Hz) to 200 ms (f_{AM}=5 Hz), moreover

- the VT and LPVT introduce phase delay with respect to the reference device, which can be determined by carrying out a calibration under sinusoidal conditions.

Thus the performance indices are obtained by comparing, for each 80 ms frame, two different not integer portions of signals. As a consequence, the VT and LPVT errors are due to their rated frequency phase error and the use of a not adeguate signal processing.

Moreover, it can be observed that the variations of the performance indices are quite constant with respect to the modulating frequency f_{AM} and, on the contrary, their frequency is equal to the modulating frequency f_{AM}.

Looking at the results, it can be noticed that in all the cases the variations of the VT indices are one order of magnitude grater than the LPVT ones. In fact for the VT

the variations are about 200 μV/V for the ratio error and TVE and 200 μrad for the phase for amplitude modulated test. For the LPVT the variations are about 20 μV/V for the ratio error and TVE and 20 μrad, lower than the measurement uncertainty. This difference can be explained considering that:

- the LPVT (class 0.2) has a lower phase error at power frequency compared to the one of the inductive VT (class 0.5).

- the amplitude modulated input signals implies a higher input amplitude that increases the magnetic flux of the VT iron-core and, thus, the non-linear phenomena that are not present in LPVT.

Some of this results are also reported in the paper [58].
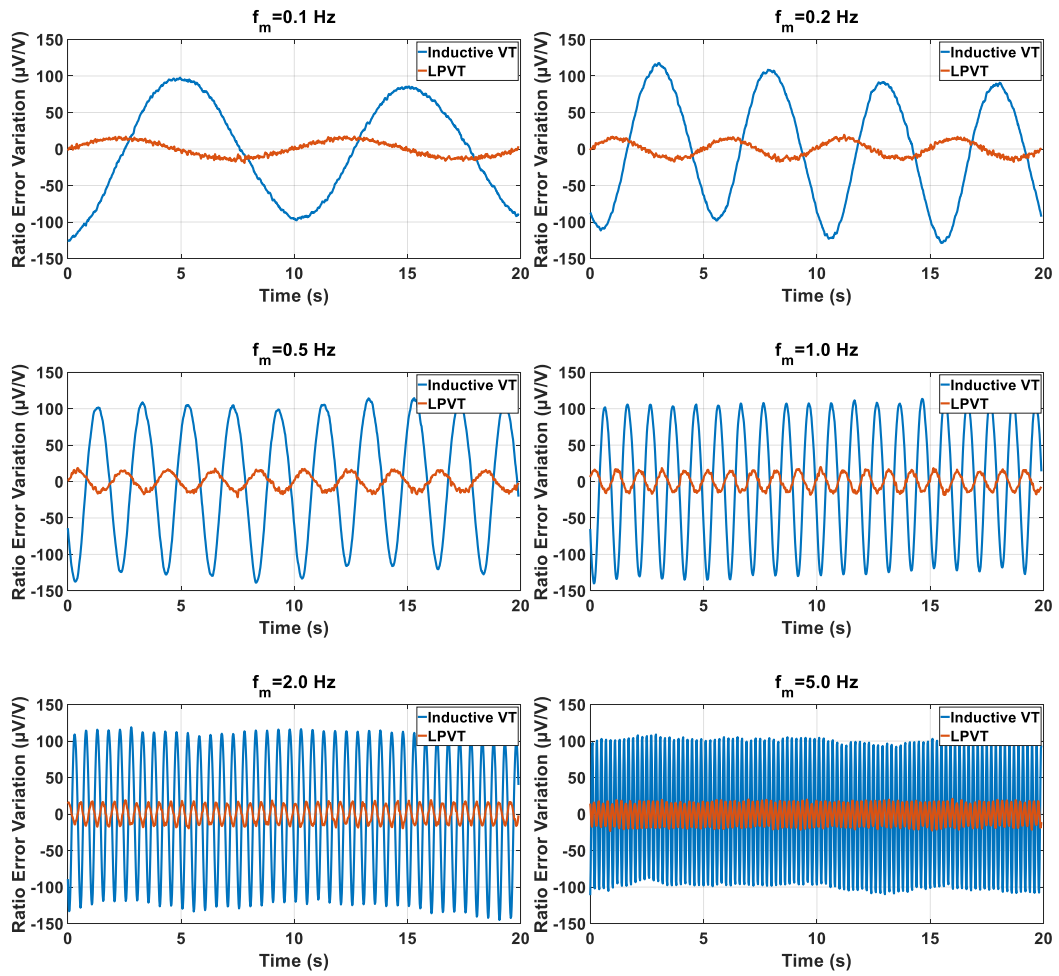
Fig. 4.3 Ratio error variations of VT (blue line) and LPVT (red line) with AM modulation at various frequencies.
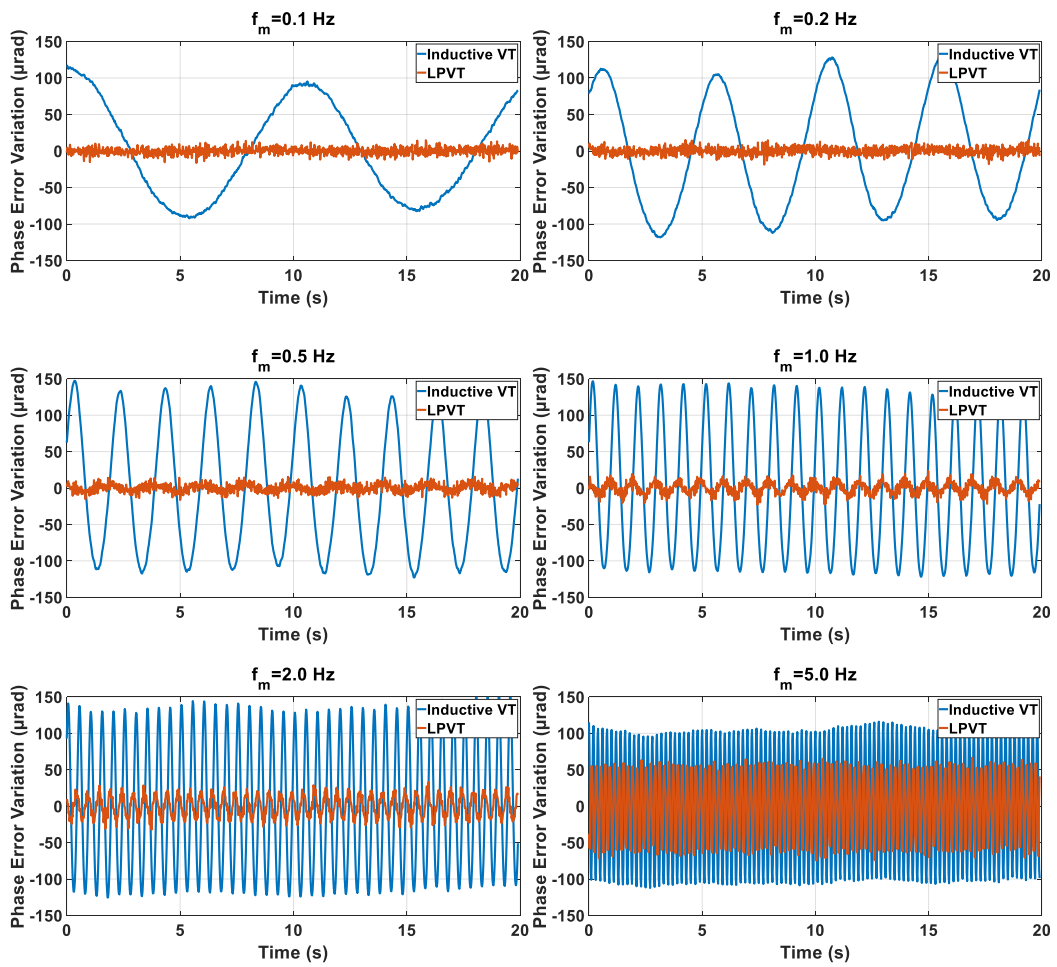
Fig. 4.4 Phase error variations of VT (blue line) and LPVT (red line) with AM modulation at various frequencies.
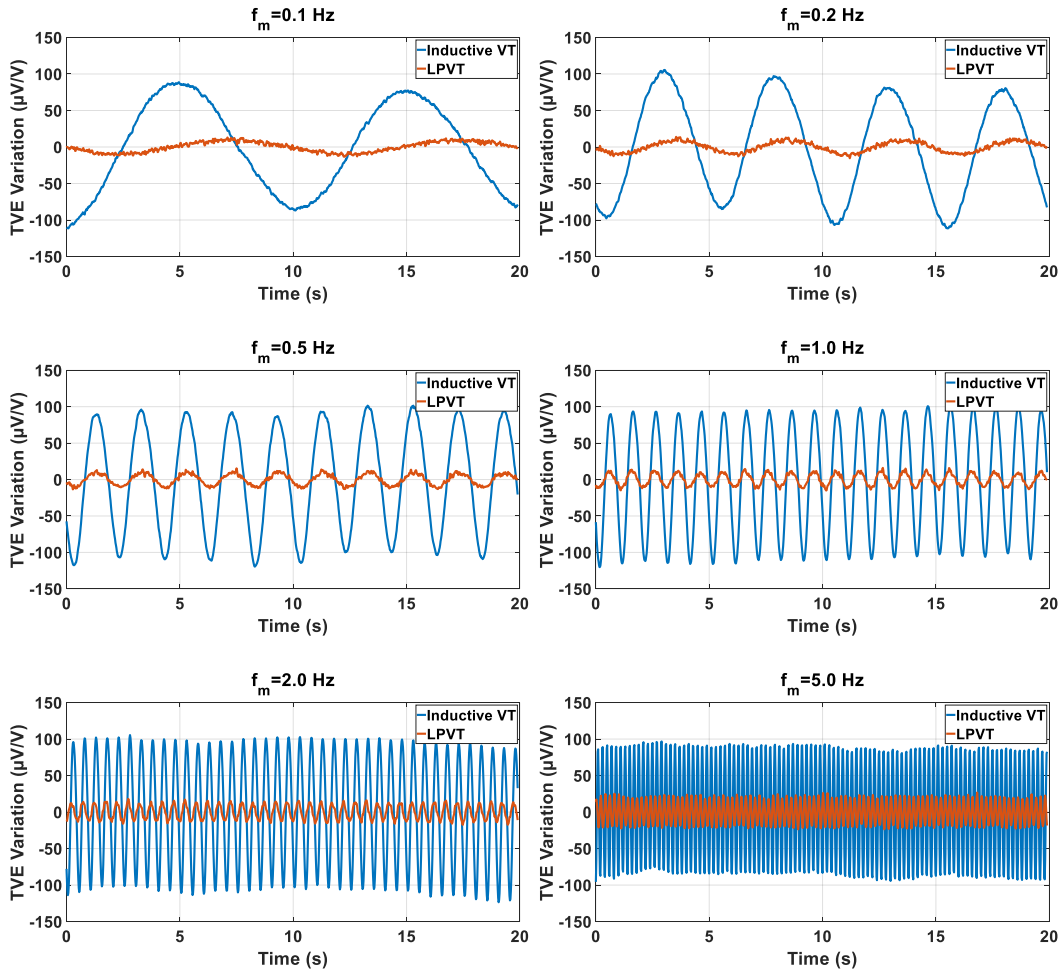
Fig. 4.5 TVE variations of VT (blue line) and LPVT (red line) with AM modulation at various frequencies.

4.3.3   Phase Modulated Signal

Test signal description

The test signal used for the assessment of the VT/LPVT performances in presence of phase modulation, is described in Equation 4.14

$$v_{\mathrm{PM}}(t) = \sqrt{2}U_{\mathrm{n}}cos[2\pi h f_0 t + k_{\mathrm{PM}}cos(2\pi f_{\mathrm{PM}}t - \pi)] \qquad (4.14)$$

where k_{PM} and f_{PM} are the phase modulation factor and the phase modulation frequency, respectively.

Experimental Results

A. Device under test

The device considered for this analysis is the VT_A.

B. Results

The inductive VT has been tested under phase modulated voltage signals with fundamental component at f_0=50 Hz and U_n= 20/$\sqrt{(3)}$ kV. The phase modulation factor k_{PM} is set to 0.1 rad and six different modulation frequencies f_{PM} have been generated: 0.1 Hz, 0.2 Hz, 0.5 Hz, 1 Hz, 2 Hz, 5 Hz, in accordance with [22]. The results are similar to those observed for the amplitude modulation tests. In fact also in this case there are time oscillations behaviour of the ratio error (Eq 4.1), phase error (Eq 4.2) and TVE (Eq 4.10). In particular, their mean values are equal to the values measured under rated sinusoidal conditions and their oscillations are reported, only for the ratio error with modulation at 5 Hz in Fig. 4.6. As can be observed in this case, the amplitude of the oscillations is about one order of magnitude lower to those observed under amplitude modulation test.
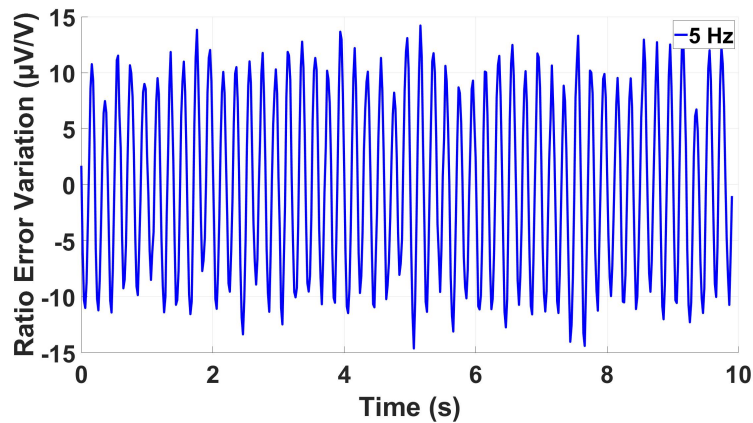
Fig. 4.6 Ratio error variations of VT with phase modulation at 5 Hz.

4.3.4   Frequency Ramp

Test signal description

The test signal for the evaluation of the VT and LPVT performances in presence of frequency ramp is described in Equation 4.15

$$v_{\text{FR}}(t) = \sqrt{2}U_{\text{n}}cos(2\pi h f_0 t + \pi R_{\text{f}} t^2) \tag{4.15}$$

where R_{f} is the frequency ramp rate.

Experimental Results

A. Devices under test

According to Table 4.1, the performances of two different LPVTs are evaluated and compared under frequency ramp.

B. Results

The frequency ramp r.m.s. voltage amplitude is set equal to 13 kV, f_0 is fixed at 50 Hz and two values of R_{f} are tested, i.e. ± 1 Hz/s and the investigated ramp range Δf is 5 Hz. Thus, for $R_{\text{f}} = 1$ Hz/s the frequency ramp goes from 50 Hz up to 55 Hz while for $R_{\text{f}} = -1$ Hz/s from 50 Hz to 45 Hz.

The FR test results for LPVT$_{\text{A}}$ and LPVT$_{\text{B}}$ are shown in Table 4.5 and they are compared with the limits stated for the M class PMUs [22].

Table 4.5 FR Test Results

Measured Quantities	LPVT$_{\text{A}}$	LPVT$_{\text{B}}$	Limits for M class PMU
Ratio Error (%)	0.025	0.029	
Phase Error (mrad)	3.85	-21.46	
TVE (%)	0.44	2.10	1
FE (mHz)	0.0094	0.057	5
RFE (mHz/s)	0.063	0.0039	200

As regard the FE and RFE, mean values for both LPVTs, are far below the limits required by [22]. As the TVE, the mean value of $LPVT_A$ cannot be considered negligible (about 50%) with respect to the maximum error prescribed for the M class PMU while the TVE of the $LPVT_B$ is outright twice as much the value imposed for M class PMU by [22].

Furthermore, by the analysis of ratio error, phase error and TVE measured values in function of the analysed frames, the time behaviours shown from Fig. 4.7 to Fig. 4.9 are observed. The analysed indices have a linear variation with a superimposed oscillation, the phenomenon gradient but not his amplitude depends on the R_f sign.
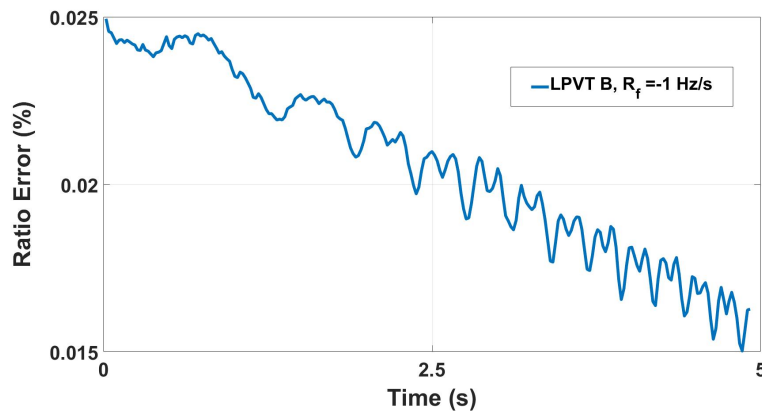
Fig. 4.7 $LPVT_B$ ratio error for for R_f =-1 Hz/s versus time.
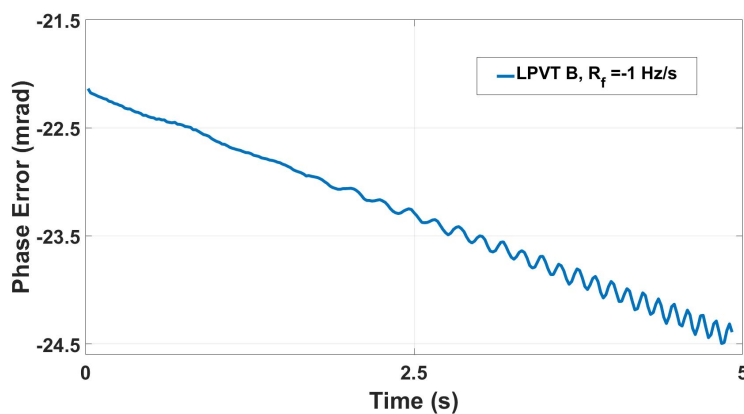
Fig. 4.8 $LPVT_B$ phase error for for R_f =-1 Hz/s versus time.
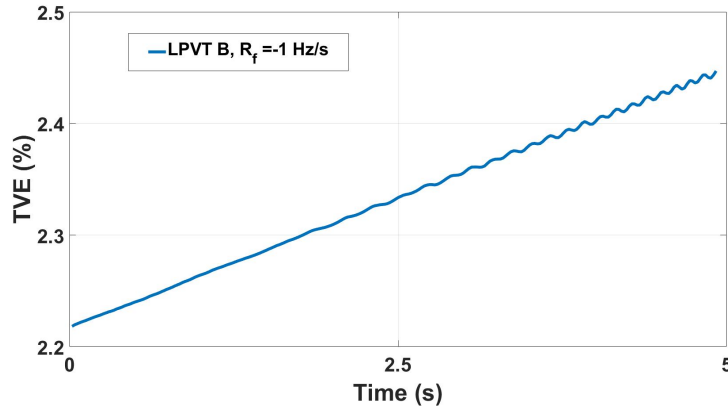
Fig. 4.9 LPVT$_\mathrm{B}$ TVE for for R_f =-1 Hz/s versus time

As LPVT$_\mathrm{A}$, the variation amplitudes are 0.016% for the ratio error, 0.38 mrad for the phase error and 0.035% for TVE. For the LPVT$_\mathrm{B}$ the measured variation amplitudes are 0.010% for the ratio error, 2.39 mrad for the phase error and 0.23% for the TVE.

The linear trend of these indices is explained considering that the phase delay $\Delta\phi$ increases (decreases) over the observation time window because of the frequency linear variation from 50 Hz to 55 Hz (50 Hz to 45 Hz).

4.4   Transient event: Voltage Dips

Two different cases of voltage dips have been implemented:

1. voltage dip synthesized by the user

2. voltage dip from database and/or comtrade files

4.4.1   Performance Indices

According to the standard [15], voltage dips characteristic quantities are the residual voltage and the voltage dip duration. Starting from these quantities the residual error defined in Equation 4.16 and the dip duration deviation in Equation 4.17 are introduced:

$$\varepsilon_\mathrm{res} = \frac{k_\mathrm{r} \cdot U_\mathrm{s,res} - U_\mathrm{p,res}}{U_\mathrm{p,res}} \tag{4.16}$$

$$\Delta\tau_{\text{dip}} = \tau_{\text{s,dip}} - \tau_{\text{p,dip}} \qquad\qquad (4.17)$$

where:

- $U_{\text{p,res}}$ and $U_{\text{s,res}}$ are the residual voltages at VT/LPVT primary and secondary side, respectively;

- $\tau_{\text{p,dip}}$ and $\tau_{\text{s,dip}}$ are the voltage dip duration measured at VT/LPVT primary and secondary side, respectively;

The residual voltage ($U_{\text{p,res}}$ and $U_{\text{s,res}}$), and the voltage dip duration ($\tau_{\text{p,dip}}$ and $\tau_{\text{s,dip}}$) are measured according to the IEC 61000-4-30 [18] prescriptions for class A instrumentation. In particular, the rms values over a time window equal to 1 cycle of the power frequency and refreshed each half-cycle, i.e. $U_{rms(1/2)}$, is evaluated and then compared with the dip threshold set to 90% of the rated primary voltage U_{r} to identify the beginning of the voltage dip and to the threshold of 90% of the rated primary voltage U_{r} plus 2% hysteresis to detect the end of the event [18].

4.4.2   User simulated Voltage dips

Voltage dips with residual voltages from 80% to 30% have been laboratory reproduced. Two different dip durations have been generated: 0.02 s and 0.20 s, i.e. 1 cycle and 10 cycles of the 50 Hz power frequency.

An example of generated voltage dip with rated residual voltage of 30% and time duration of 20 ms is provided in Fig. 4.10
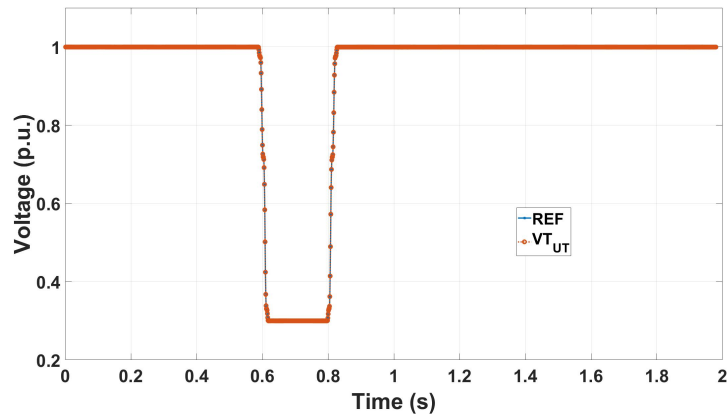
Fig. 4.10 VT and Reference $U_{\mathrm{rms},1/2\mathrm{cycle}}$ (p.u.) measured during a voltage dip with residual voltage of 30% and 200 ms time duration.

A. Device under test

The device under test is a phase-to-ground MV inductive VT_C:

B. Results

The VT under test has been preliminary characterized under rated conditions and the observed ratio and phase error at power frequency are -0.01% and 0.76 mrad, respectively.

As the voltage dip tests, the results in terms of residual errors are provided in Fig. 4.11 whereas for the time duration, in all the analyzed cases, no error have been detected ($\Delta\tau_{\mathrm{dip}}$=0 s).
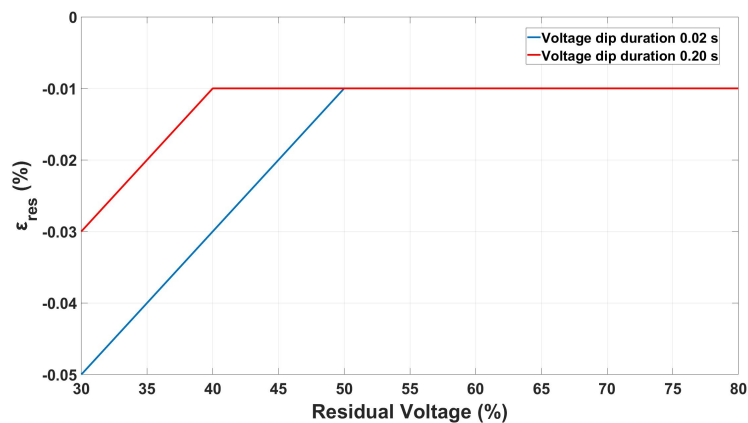
Fig. 4.11 VT error contribution to the measurement of dip residual voltages.

An interesting result can be observed by analyzing the time behaviour of the VT ratio error. In fact, from the Fig. 4.12, it can be seen that even if the error during the voltage dip is quite close to the value measured under rated conditions and prior to the PQ phenomenon, however more significant variations (0.12%) can be observed during the voltage falling and rising phases. This phenomenon can be explained by considering the excited broadband during the descent and ascent phases. However, for the analayzed VT the variations are one order of magnitude greater than the measured ratio error but a small fraction of the accuracy class.
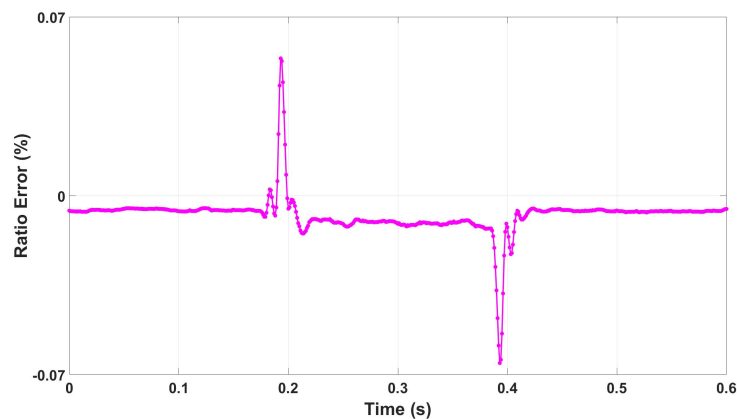
Fig. 4.12 VT ratio error measured during a voltage dip with residual voltage of 30% and 200 ms time duration.

4.4.3   Voltage dips from DOE/EPRI database

A short duration PQ disturbance from a database repository of power system events has been chosen and rescaled to have a fundamental component amplitude U_n=13 kV and reproduced by the reference set-up. The generated PQ event is shown in Fig. 4.13 and it is classified as a voltage dip.
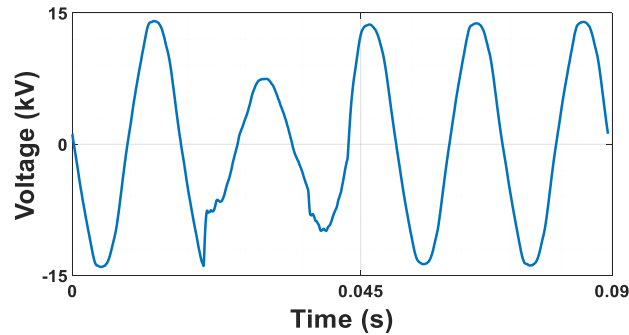
Fig. 4.13 Real voltage dip laboratory reproduced.

A. Devices under test

The devices considered for this type of test are the two LPVTs according to Table 4.1.

A. Results

For the measured τ_{dip}, no difference is detected between the reference value and that measured by the LPVTs under test. The residual voltage error (Equation 4.16) associated with the LPVT$_A$ is equal to 0.21% while that of LPVT$_B$ is 0.19%. As the result of LPVT$_B$ the measured error is quite higher considering the LPVT$_B$ rated accuracy (0.1%) and, if compared to prescription for PQ measurement instruments, its absolute value is about half of the uncertainty required for class A instrument.

4.5   Combination of PQ phenomena: Harmonics and Subharmonics

The results here provided are also presented in [59].

Scientific literature highlights that voltage subharmonics are PQ disturbances mainly related to renewable energy sources and no-linear loads and, therefore, they can be considered a growing issue in the modern power grid. For this reason, special attention has been focused on this PQ phenomenon. In particular, the research activity presented in this section investigates and quantifies the impact of subharmonics on the accuracy of MV inductive VT in harmonic measurements.

4.5.1 Subharmonics: sources and typical characteristics from literature and standard review

Given the peculiarity of this subject, in the following section the review of scientific literature and standards has been deepened to identify typical range of variations of power system subharmonics amplitudes and frequency with the aim of performing experimental tests under realistic conditions. The injection of subharmonics is mainly due to energy generation systems and modern loads.

Among the distributed energy generation systems, the main contributors to subharmonics injection are wind farms because of the tower to blade interaction [60, 61], hydro-powers for the long-time constants of their hydraulic components [62–65], and photovoltaic (PV) plants, especially when they directly supply MV AC bus bars through MV DC/AC inverters [66–68].

As regards the loads, the subharmonic generation is due to arc furnaces [69, 70], cycloconverters [71–73], automated spot-welders, adjustable speed drives, fluctuating motors driving cyclic loads, power supplies to traction systems [74, 75]. Subharmonics and, generally, low-frequency oscillations can also occur when there is a mismatch between the generated and demanded power. This power mismatch is caused by quite common events such as increase of large loads, loss of tie lines, or loss of generating units. As a result, a transient phenomenon characterized by Low-Frequency Oscillations (LFOs) may start [76].

For subharmonics generated by wind farms [60, 61], the frequencies range from 0.40 Hz to 49 Hz, and the most common values are found for frequencies lower than 17 Hz. As to the disturbances introduced by the hydropower, their frequencies are typically lower than 0.1 Hz and are classified as Ultra Low Frequency Oscillations (ULFOs) [62–65]. In [64] ULFOs with frequencies down to 0.01 Hz have been observed. Both [69] and [70] show that subharmonics generated by arc furnaces can have frequencies lower than 10 Hz. In [71], it is demonstrated that cycloconverters can inject subharmonics with 10 Hz frequency and 0.15% amplitude on an MV line whereas in [72] and [73] the cycloconverters produce subharmonics with frequencies from 5 Hz to 35 Hz. Regarding the LFOs, the literature review indicates that their frequency can vary in the (1 - 2) Hz range if they are related to a single generator or in the range of (0.1 - 1) Hz if they are associated with a group of generators [76–78]. In [79], a measurement campaign focused on subharmonic voltages in an LV

distribution system shows subharmonic components with amplitudes greater than 1%. The activity presented in [80] has the target of assessing the performances of Phase-Locked Loop systems (PLLs) in the presence of some power grid disturbances; among them, subharmonics from 0 Hz up to the power frequency with a fixed amplitude of 1% are considered. In [81], a subharmonic of 1 Hz and 10% is assumed among the possible grid disturbances. In [82] the impact of subharmonics on a single-phase transformer is studied. The authors considered subharmonics with 0.9% fixed amplitude and frequency variables from 1 Hz to 10 Hz to perform this analysis. The scientific paper [83] has also evidenced that subharmonics can be generated in electrical grid with PV panels connected. These two electrical systems are interconnected by the means of dc-ac inverter: the dc input is characterized by a time varying behaviour because of the continuous action of the Maximum Power Point Tracking (MPPT) control whereas the ac output can exhibit variations because of the various grid supply conditions. The interconnection of these two nonsynchronous subsystems with power electronic interfaces can cause significant level of intehrarmonic distortion.

The international standards provide some additional indications related to typical subharmonics amplitude and frequency ranges of variations.

Both the IEEE standards [84, 20] and IEC standards [85–87] refer to the subharmonics as interharmonics since they define the latter as "voltages or currents having a frequency that is not an integer multiple of the frequency at which the supply system is designed to operate." In [84], for systems operating from 1 kV up to 69 kV, the amplitude limit identified for the interharmonics with frequency lower than 25 Hz is 3%. In [20], a voltage amplitude below 2% is assumed for interharmonics with a frequency from 0 Hz to 9 kHz. Another low frequency disturbance presented in [20] is the voltage fluctuation. It is described as a phenomenon having spectral content at frequencies lower than 25 Hz and a typical magnitude ranging from 0.1% to 7%. Standards [85–87] discuss possible LV and MV sources of interharmonics and subharmonics. As output, in [85], it is mentioned that discrete frequencies of 0 Hz to 2500 Hz can be found on the grid, and their possible amplitudes are equal to 0.5% or even more. In [86], a conservative planning level for interharmonics in MV grids is set to 0.2%.

Based on these considerations, in Table 4.6 subharmonics are grouped basing on frequency and amplitude levels.

Table 4.6 Possible subharmonic amplitudes and frequencies.

Group	Frequency (Hz)	Amplitude (%)
I	0.01 – 0.05	0.1
II	0.1 – 0.5	0.1 – 0.3
III	1 – 20	0.1 – 3

4.5.2   Background considerations

According to the Faraday's law [88], when a transformer is working in no-load conditions and is supplied with a sinusoidal voltage source at primary winding, it produces a sinusoidal flux. The amplitude of the flux is directly proportional to the applied voltage and inversely proportional to the frequency. To sustain the flux, a magnetizing current is generated in the primary winding. The magnetizing current is related to the flux via the magnetization characteristic [89] of the transformer ferromagnetic core. Due to the non-linearity of the ferromagnetic core, the magnetizing current is far from sinusoidal. In fact, as it can be seen from Fig. 4.14 (blue bars), the spectrum of the magnetizing current includes harmonic distortion even when a sinusoidal at rated voltage and rated frequency is applied to primary winding, especially the third harmonic (0.05% of the fundamental). As a result, also the secondary voltage presents spurious harmonic tones.
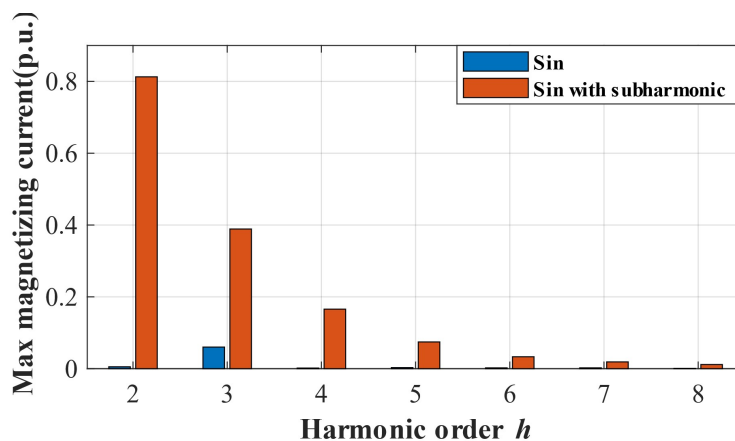
Fig. 4.14 Harmonic contenent of the magnetizing current given in p.u. of fundamental component without subharmonic (left blue columns) and with a subharmonic with amplitude of 0.1% and frequency of 0.01 Hz (right orange columns).

If a low frequency sinusoidal voltage is superimposed to the rated voltage at the fundamental frequency, the total flux is the sum of two components: the first component is given by the fundamental tone and the second is given by the low-frequency voltage [82]. In this condition, a higher flux must be sustained by a higher magnetizing current; therefore, its spectral content increases as can be observed from Fig. 4.14 (red bars). As a result, the voltage at the secondary winding is more distorted. Furthermore, the low frequency oscillation of the primary voltage generates an oscillation of the total flux. For this reason, the magnetization curve changes with a periodicity given by the characteristics of the low frequency component and the harmonic components of the magnetizing current are not constant in time.

In fact, as it can be seen in Fig. 4.15, when a low-frequency voltage is superimposed on the fundamental component, the measured amplitude of the 2nd harmonic of the magnetizing current oscillates, while it is constant in time in the sinusoidal case. In conclusion, if an inductive VT is supplied with a waveform composed by the fundamental tone, harmonic components and subharmonic tones, the harmonic components of the secondary voltage are the result of the vector sum of:

1. the actual harmonics superimposed on the primary voltage (modified by the systematic VT ratio and phase errors at the specific harmonic frequency);

2. the spurious harmonic components due to both the fundamental and the low frequency components.
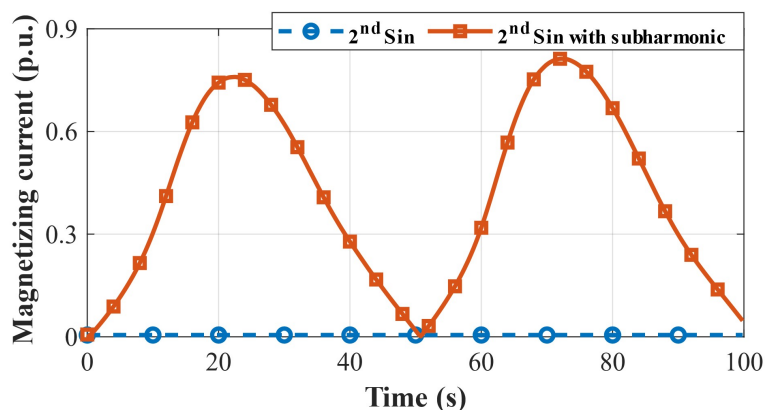
Fig. 4.15 Amplitude of 2nd harmonics of magnetizing current given in p.u. of fundamental component without 0.01 Hz subharmonic (circle markers) and with subharmonic (square markers).

4.5.3 FHS: Fundamental Plus 1 Harmonic and 1 Subharmonic

This section describes the test carried out to analyze how the accuracy of harmonic measurements performed through inductive VTs is affected by the presence of subharmonics in the input voltage and the indices used to quantify this impact. The FHS test signal waveform consists of three voltage components: a fundamental component at power frequency, one superimposed harmonic, and one subharmonic. It follows that the FHS test signal is described by Equation 4.18:

$$v_{\text{FHS}}(t) = \sqrt{2}U_{\text{n}}sin(2\pi f_0 t) + \sqrt{2}U_h sin(2\pi h f_0 t + \phi_h) + \sqrt{2}U_s sin(2\pi f_s t + \phi_{\text{s}})$$
(4.18)

The ratio and phase errors at the h-order harmonic are evaluated according to Equation 4.1 and 4.2, respectively. The evaluation is performed over an integer number of periods of the FHS signal in non-overlapped 200 ms time frames, according to [19] for a 50 Hz power system.

To quantify the effect of the subharmonic voltage on the harmonic the following indices are introduced:

$$\xi_h = \max\left(\bigcup_{w_i=1}^{N} |\varepsilon_{h,i} - \overline{\varepsilon_h}| \right)$$
(4.19)

$$\psi_h = \max\left(\bigcup_{w_i=1}^{N} |\phi_{h,i} - \overline{\phi_h}| \right)$$
(4.20)

where:

- $\displaystyle\bigcup_{w_i=1}^{N}$ is the union of time frames in which ratio and phase errors are evaluated. Each w_i is equal to 10 cycles of fundamental frequency and N is always chosen in order to evaluate at least an integer multiple of the period of the subharmonic.

- $\varepsilon_{h,i}$ and $\phi_{h,i}$ are the ratio and phase errors at h-order harmonic, evaluated on the different time frames w_i;

- $\overline{\varepsilon_h}$ and $\overline{\phi_h}$ are the mean values of ratio and phase errors at h-order harmonic evaluated under FH1 test conditions.

In practice, ξ_h and ψ_h quantify the maximum absolute increment of the harmonic ratio and phase error caused by the presence of the subharmonic.

4.5.4   Experimental Results

A. Devices under test

The analyzed VTs are two commercial resin insulated VT_A and VT_B provided in Table 4.1.

The VTs main features are summarized in Table 4.1.

B. Results

This section presents the results of the FHS tests performed on VT_A and VT_B to assess their performance in fundamental and harmonic measurement in the presence of a subharmonic component.

The VTs tests presented in this section are carried out in null burden conditions. Next subsection will analyze the impact of different choices for fundamental amplitude, harmonic amplitude and burden.

As mentioned before, a subharmonic component in the VT input voltage produces spurious harmonic phasors in the VT secondary voltage. These harmonic phasors, evaluated over non-overlapped observation windows of 200 ms according to [19] for a 50 Hz power system, have a periodic behavior and thus cause time varying ratio and phase errors at the considered harmonic frequency. A practical example is given in Fig. 4.16, where the time behavior of the VT_A second harmonic ratio error is shown in the presence of a 0.1%, 0.01 Hz subharmonic. To better evaluate the impact of the subharmonic, the time behavior of the second harmonic ratio error measured under the FH1 test is also reported in Fig. 4.16. The oscillation characteristics are strongly related to the subharmonic parameters. In particular, the oscillation period is equal to the subharmonic period, whereas the oscillation amplitude depends on both the subharmonic amplitude and the frequency.
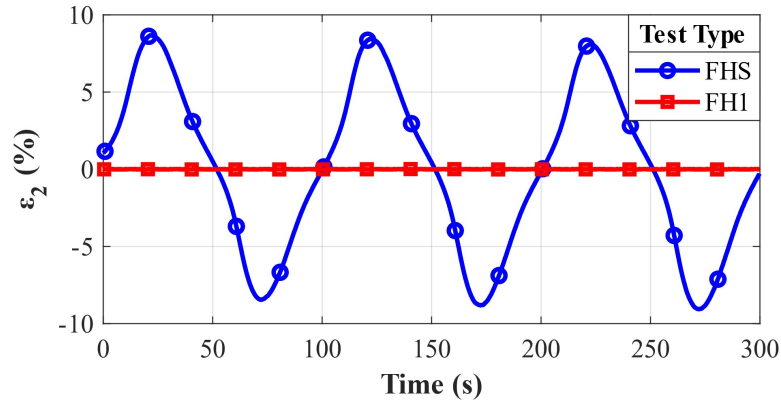
Fig. 4.16 Ratio errors of VT_A at second harmonic with (blue line circle markers) and without (red line square marker) subharmonic component at 0.01 Hz and 0.1%.

A comprehensive overview of the VT_A and VT_B behaviours is provided from Fig. 4.17 to Fig. 4.26. The maximum absolute increments of ratio and phase errors in the various test conditions are shown.

In particular, Figures 4.17 and 4.18 show the VT_A and VT_B performance results in fundamental tone measurement. In this case, the test waveform comprises a fundamental rated amplitude and frequency, a subharmonic component with amplitude and frequency according to Table 4.6 and no harmonic tones. The subharmonic presence has a low impact on the measurement of the fundamental tone for both the VTs under test, being in some cases lower then the measurement uncertainty. For VT_A, the maximum values of ξ_1 and ψ_1 are equal to 0.05% and 0.40 mrad and they are observed in the presence of a 0.3%, 0.1 Hz subharmonic. For VT_B, the maximum values of ξ_1 and ψ_1 are close to 0.05% and 0.41 mrad and are found in the presence of a 0.1% and 0.01 Hz subharmonic. The measured increments represent a small fraction of the 0.5 accuracy class limits, which are 0.5% and 9 mrad, respectively, for ratio and phase errors. Thus, even in the presence of subharmonics, an MV VT remains compliant with its accuracy class limits regarding the fundamental tone measurements.

Fig. 4.17 Maximum absolute increments of VT_A ratio errors (a) and phase errors (b) at fundamental frequency, in presence of subharmonics with various amplitudes and frequencies.

Fig. 4.18 Maximum absolute increments of VT_B ratio errors (a) and phase errors (b) at fundamental frequency, in presence of subharmonics with various amplitudes and frequencies.

From Fig. 4.19 to Fig. 4.26, the maximum absolute error increments (ξ_h and ψ_h) are shown for each generated harmonic, subharmonic frequency, and fixed subharmonic amplitude. It is worth noting that for all these figures, a logarithmic scale has been chosen for the y-axes since the error increments extend over a wide range of values.

Looking at all the figures from Fig. 4.19 to Fig. 4.26, it is evident that, regardless of subharmonic parameters, the most affected harmonics are the firsts, in particular the second and the third harmonics. As a general consideration, analyzing the single h harmonic, it can be observed that ξ_h and ψ_h increase with a monotonous behavior when the subharmonic frequency decreases.

Looking at any single harmonic in Fig. 4.19 (VT_A) and Fig. 4.23 (VT_B), it can be observed that the maximum error increments caused by the presence of a 0.1% subharmonic vary up to two orders of magnitude, depending on the subharmonic frequency. More in particular, considering the (VT_A) results (Fig. 4.19), ξ_2 and ψ_2 in presence of a 0.1%, 0.01 Hz subharmonic are equal to 9.00% and 32.05 mrad, whereas they significantly decrease to 0.02% and 0.14 mrad if a 0.1% but 20 Hz subharmonic is considered. For VT_B, the 0.1%, 0.01 Hz subharmonic makes ξ_2 and ψ_2 equal to 10.42% and 27.28 mrad; these values decrease to 0.04% and 0.31 mrad when the effect of a 0.1% but 20 Hz subharmonic is evaluated. As regards the subharmonic amplitude effect, higher values of ξ_h and ψ_h are found for higher value of subharmonic amplitudes. In order to prove this consideration, it is considered the case of 1 Hz subharmonic with three different amplitudes, equal to 0.1% (Fig. 4.19 for VT_A and Fig. 4.23 for VT_B), 1% (Fig. 4.21 for VT_A and Fig. 4.23 for VT_B) and 3% (Fig. 4.22 for VT_A and Fig. 4.26 for VT_B) and it is analyzed ξ_2 and ψ_2 i.e. at the second harmonic. For VT_A, with the increase of subharmonic amplitude from 0.1% to 1% and 3%, ξ_2 increases from 0.13% to 1.22% and 8.70%, respectively, whereas ψ_2 increases from 0.65 mrad to 4.80 mrad and 29.65 mrad, respectively.
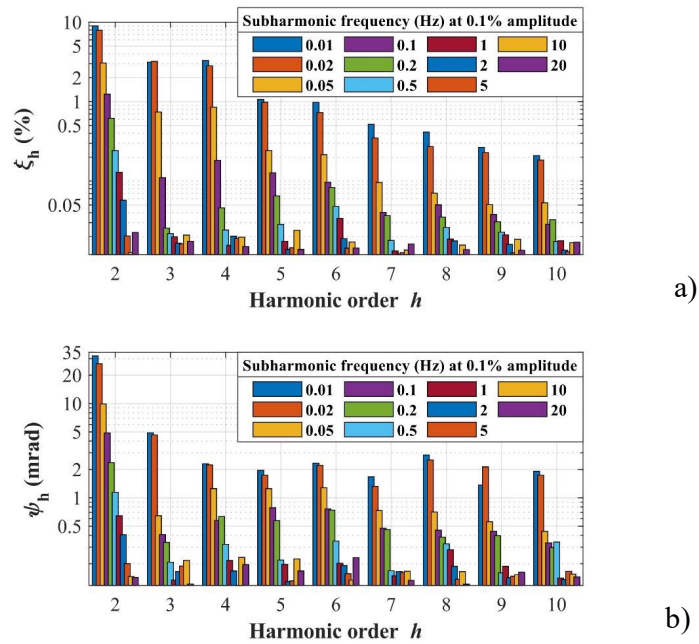
Fig. 4.19 Maximum absolute increments of VT$_A$ ratio errors (a) and phase errors (b) at harmonic order h, in presence of subharmonics with 0.1% amplitude and various frequencies.
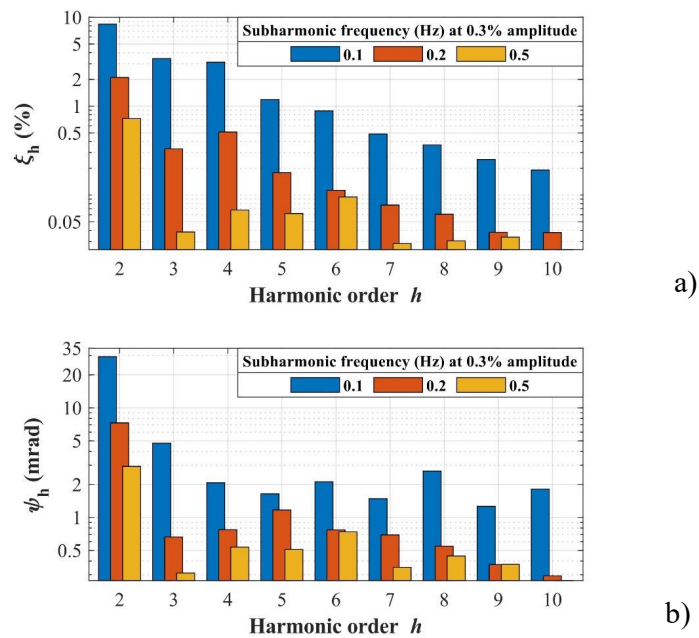
Fig. 4.20 Maximum absolute increments of VT$_A$ ratio errors (a) and phase errors (b) at harmonic order h, in presence of subharmonics with 0.3% amplitude and various frequencies.
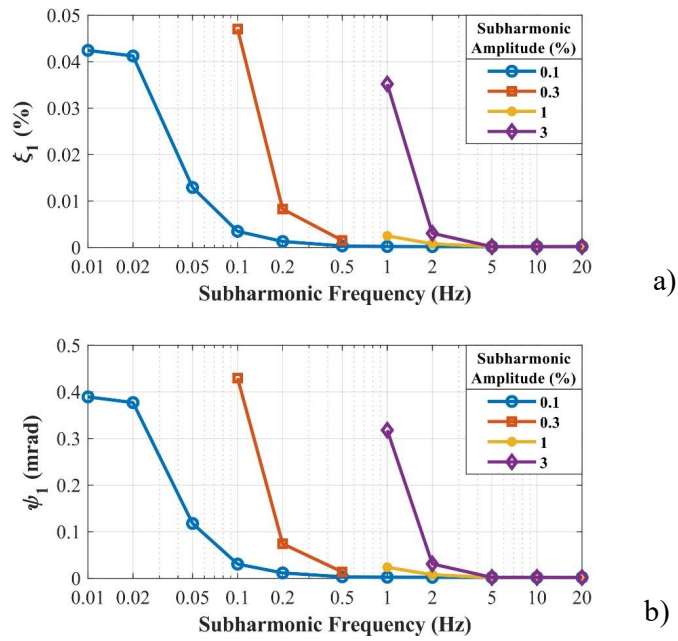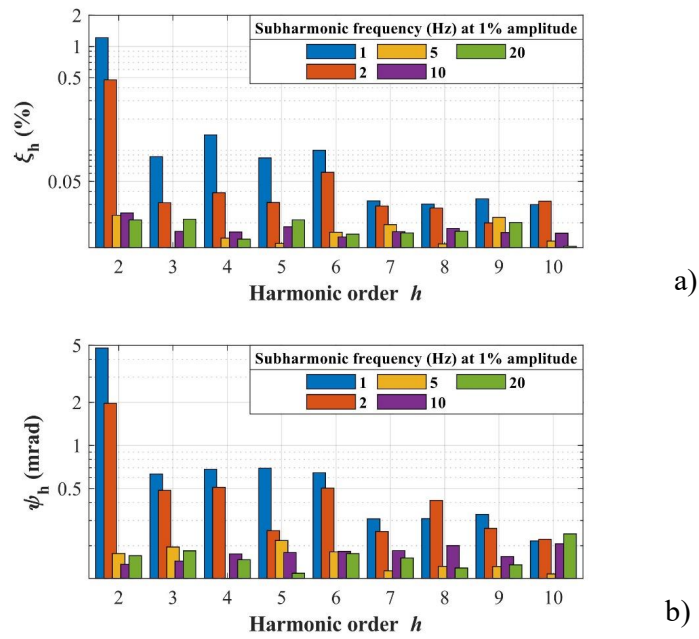
Fig. 4.21 Maximum absolute increments of VT$_A$ ratio errors (a) and phase errors (b) at harmonic order h, in presence of subharmonics with 1% amplitude and various frequencies.
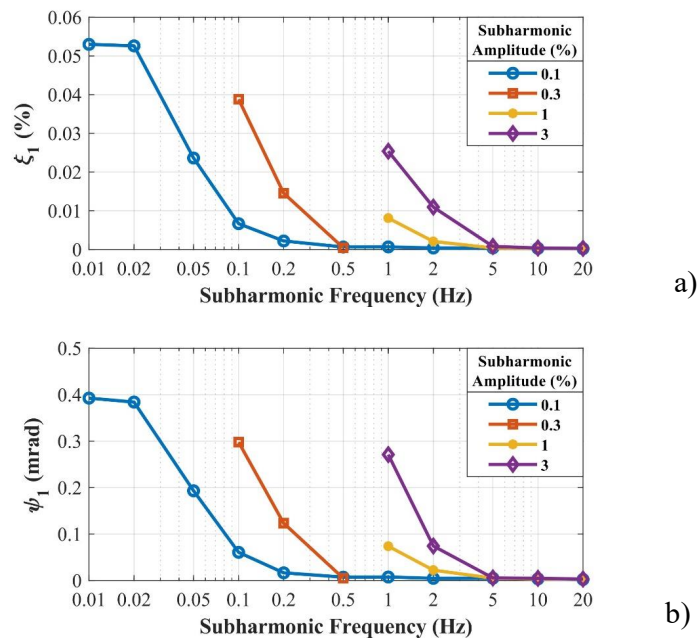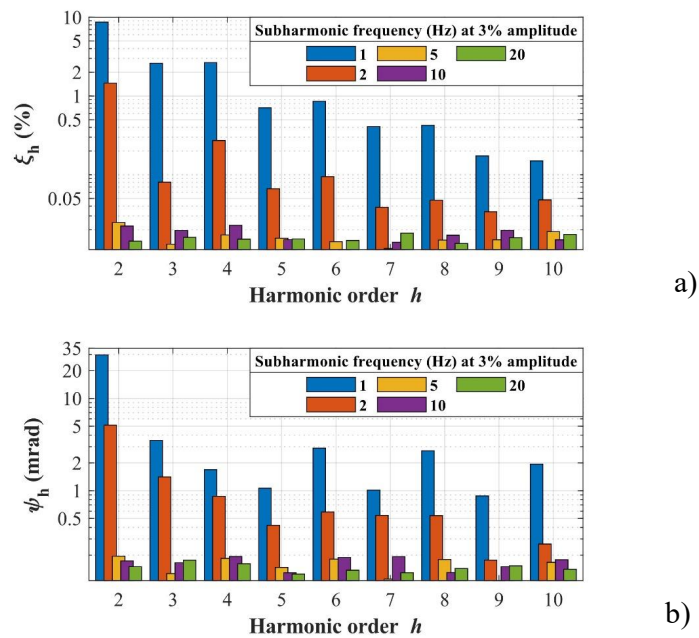

Fig. 4.22 Maximum absolute increments of VT$_A$ ratio errors (a) and phase errors (b) at harmonic order h, in presence of subharmonics with 3% amplitude and various frequencies.

For VT_B, instead, ξ_2 increases from 0.26% to 1.55% and 4.80%, respectively, whereas ψ_2 increases from 1.31 mrad to 6.21 mrad and 12.36 mrad, respectively.
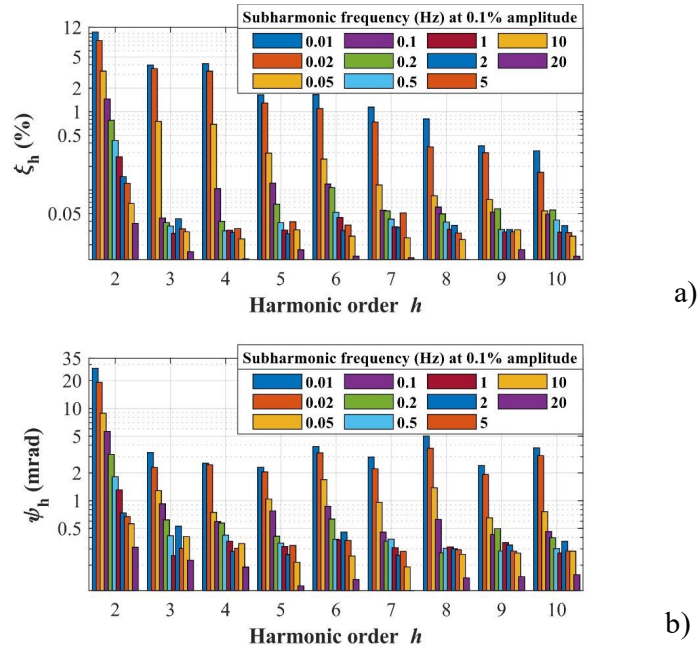
Fig. 4.23 Maximum absolute increments of VT_B ratio errors (a) and phase errors (b) at harmonic order h, in presence of subharmonics with 0.1% amplitude and various frequencies.
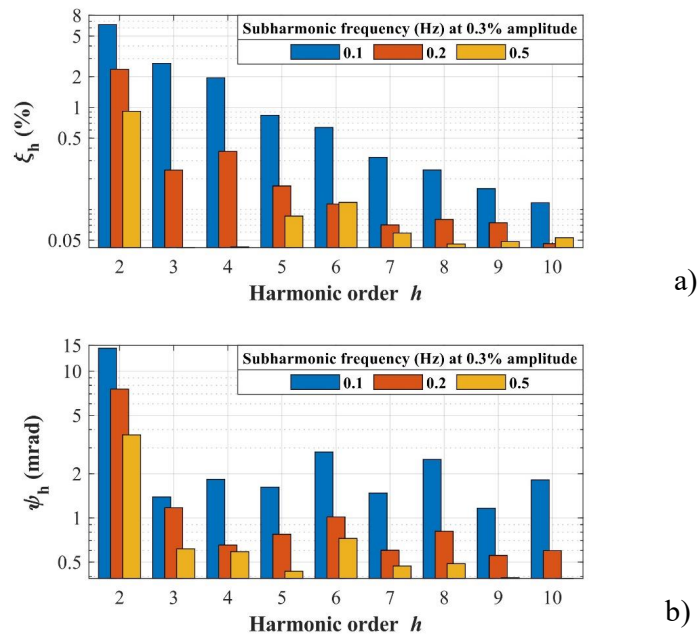
Fig. 4.24 Maximum absolute increments of VT_B ratio errors (a) and phase errors (b) at harmonic order h in presence of subharmonics with 0.3% amplitude and various frequencies.
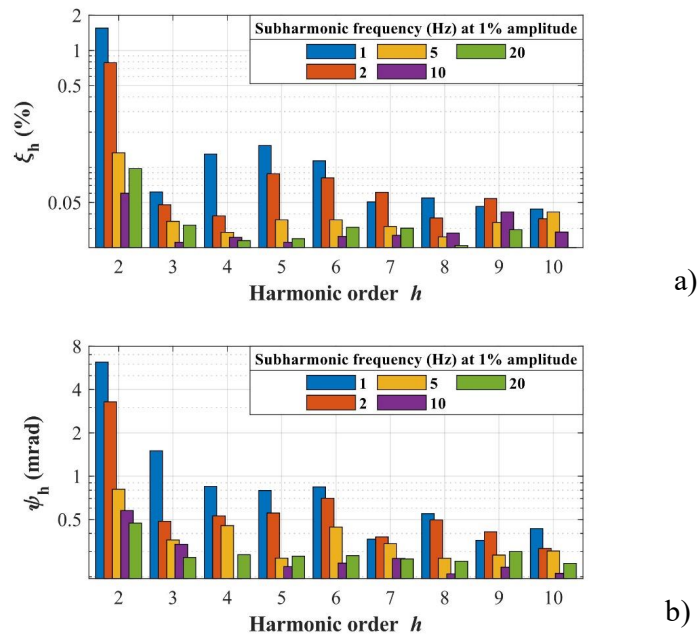
Fig. 4.25 Maximum absolute increments of VT_B ratio errors (a) and phase errors (b) at harmonic order h in presence of subharmonics with 1% amplitude and various frequencies.
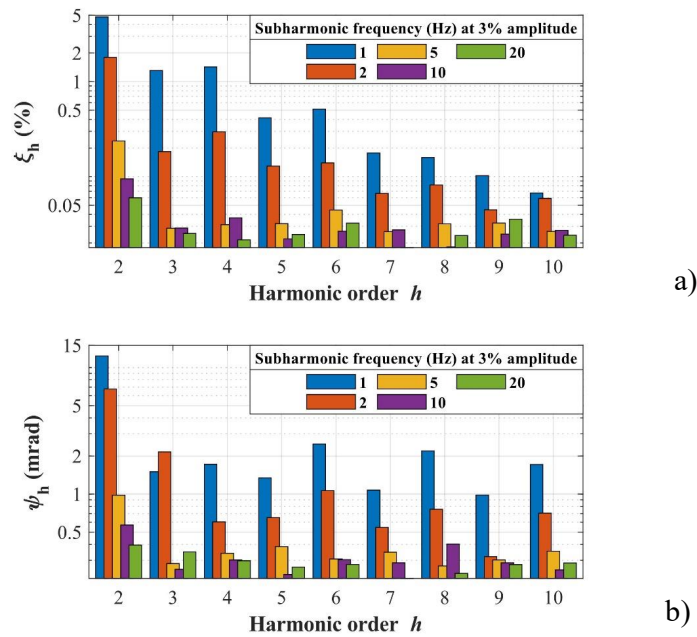
Fig. 4.26 Maximum absolute increments of VT$_B$ ratio errors (a) and phase errors (b) at harmonic order h in presence of subharmonics with 3% amplitude and various frequencies.

C. Impact of operating conditions

To quantify the subharmonic impact on the VT performance when it is used under operating conditions different from those assumed in the previous section, three different test quantities are considered in the following:

1. the amplitude of the fundamental component,

2. the amplitude of the harmonic tone,

3. the burden condition.

The subharmonic chosen for these additional analyses is the one that, according to the results shown in previous subsection, which has the greatest influence on the performance of the VTs, i.e., the subharmonic characterized by 0.1% amplitude and 0.01 Hz frequency. For sake of brevity, the analyses here shown refer only to the ratio error of VT$_A$ in harmonic measurement. Similar considerations can be done for VT$_B$ and are also valid for phase error.

Fundamental tone Amplitude

With respect to the analysis carried out in Section VI by considering the rated value for the fundamental component, other two fundamental tone amplitudes are here considered: 80% and 120% of the rated primary voltage. The harmonic component superimposed on the fundamental tone has amplitude equal to the 1% of the fundamental tone and order variable from 2 to 10. Tests are carried out with null burden. Results are shown in Fig. 4.27. For all the harmonic orders, ξ_h increases with the increase of the fundamental tone amplitude. When the fundamental tone is 80% of the rated value, the subharmonic influence leads to a ξ_2 equal to 5.48%, whereas the same quantity reaches 12.66% if the fundamental tone amplitude increases to 120% of the rated one. Consequently, the VT full operating range, that is from 80% to 120% [5], has to be accounted in the analysis, since the evaluated maximum error increments due to the subharmonic presence can vary up to an order of magnitude.
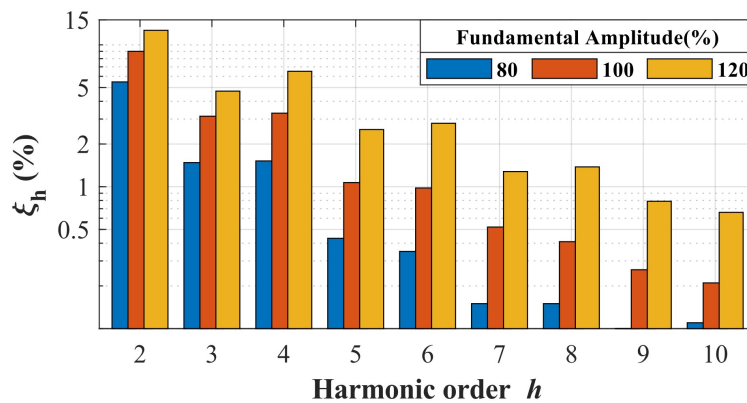
Fig. 4.27 Maximum absolute increments of VT_A ratio errors at harmonic order h, with various values of fundamental amplitude, in presence of a 0.1%, 0.01 Hz subharmonic component.

Harmonic Amplitude

This section aims at assessing the impact of the subharmonic presence on the VT when it is used to measure harmonics having different amplitude levels. For this purpose, FHS tests with three additional harmonic amplitudes are performed: 0.5%, 3% and 5% of the fundamental tone. The other test parameters and operating conditions are those assumed in the test previously presented.

Results are shown in Fig. 4.28, where also the maximum ratio errors increment at 1% harmonic amplitude case are reported. Looking at Fig. 4.28, it can be observed that the ratio error maximum increments significantly increase for low values of

harmonic amplitude. This is due to the fact that when the amplitude of the harmonic tone injected at the primary side is low, it is comparable to the amplitude of the correspondent spurious harmonic introduced at the secondary side by the presence of the subharmonic. Moreover, it can be observed that, especially for the first harmonics, the maximum error increments are inversely proportional to the amplitude of the injected harmonic. For instance, ξ_4 (i.e. the maximum ratio error increment at the fourth harmonic) doubles from 3.30% to 6.58% when the harmonic amplitude is halved from 1% to 0.5% and it is reduced to one fifth, from 3.30% to 0.63%, when the harmonic amplitude increases from 1% to 5%.
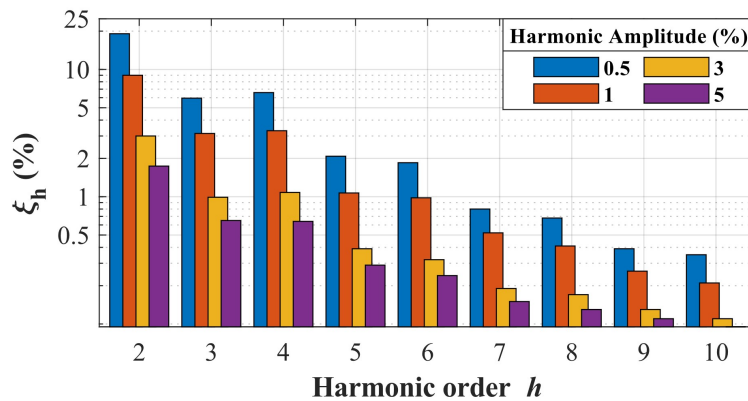
Fig. 4.28 Maximum absolute increments of VT_A ratio errors at harmonic order h, with various values of harmonic amplitude, in presence of a 0.1%, 0.01 Hz subharmonic component.

Burden Condition

The scope of this section is to quantify the impact of the subharmonic on VT performance when it is used at rated burden condition. For this purpose, VT_A has been characterized under its rated burden condition, i.e., using a 30 VA ohmic-inductive burden with a $cos\phi = 0.8$ power factor. The fundamental tone has rated amplitude and frequency. The harmonic component superimposed on the fundamental tone has amplitude equal to the 1% of the fundamental tone and order variable from 2 to 10. Fig. 4.29 shows that the burden condition does not represent a significant influence parameter since the results measured under the two different conditions are very similar. In particular, the maximum difference between the tests performed with zero burden and rated burden is found at the third harmonic where the two errors differ by 0.23%, whereas for the other harmonics, this difference is below 0.1%.
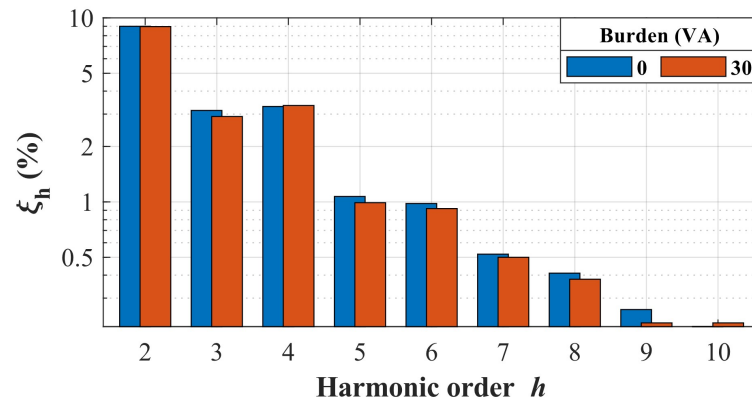
Fig. 4.29 Maximum absolute increments of VT$_A$ ratio errors at harmonic order h, with null and rated burden (30 VA), in presence of a 0.1%, 0.01 Hz subharmonic component

Chapter 5

Frequency characterisation of inductive VTs: Development of Simplified measurement procedures

5.1   Introduction

As well known, harmonic pollution is one of the most critical PQ phenomena because of its significant increase in recent years and the many problems it causes.

The primary sources of the harmonics are the phase angle controlled rectifiers and inverters, in particular switching-type power converters that are widely used in renewable power parks, EV chargers, energy storage facilities and HVDC systems. Arcing devices also inject the harmonics because of the high non-linearity of the electric arc's voltage-current characteristics. Transformers can also generate harmonics in case of iron core saturation or for the inrush current phenomenon that occurs when they are energized.

The presence of harmonic distortion in the supply voltage can cause different types of problems. For example, in three-phase systems, the third harmonics combine constructively, producing an excessive neutral current and, therefore, the overheating of the neutral conductor. Another problem due to the harmonics is the increase of the transformers' losses that depend on the input voltage frequency (skin effect, eddy current). The presence of harmonics also increases motor and transformer temper-

atures reducing their efficiency and life span. Moreover, the harmonic distortion compromises the proper function of protection devices based on the zero-crossing principle.

Against this background, it is clear that harmonic level monitoring is a matter of great importance, and a lot of work and research is done in this area.

From the metrological point of view, it is necessary to properly characterize the VTs included in the measurement chain for the measurement of harmonics at MV level. Recent literature [8–10, 44, 46, 50, 53, 90, 91] has highlighted that the performance of VTs in the harmonics measurement is affected by their intrinsic non-linearity and by stray capacitance. Because of these issues, VTs can introduce non-negligible ratio and phase errors in measuring both low and high-order harmonics. A simple and widely used approach for determining such errors is to test VTs at low voltage (LV) with a sinusoidal frequency sweep (SFS). However, because of the VTs non-linearity, the harmonic ratio and phase errors assessed under LV SFS can significantly differ from those measured by supplying them with actual waveforms [44, 43]. For this reason, the VT frequency characterization should be performed with waveforms representative of the real operating conditions, that is composed of one fundamental tone at rated voltage and frequency plus one or N superimposed harmonic tones with reduced amplitudes. However, the characterization of VT under such distorted conditions requires complex generations and measurement systems not always available in the characterization laboratories. In this scenario, it can be helpful to study and find simplified procedures to obtain an approximated frequency response of VTs. These simplified procedures aim to be a trade-off between complex test procedures, proposed in [8–10, 44, 46, 50, 53, 90, 91], and more simple but less accurate LV SFS ones.

To this end, two different simplified procedures have been studied, developed and compared. They have been published in [92, 93]. The techniques are both based on the same two measurement steps, that are:

1. measurement of the VT ratio and phase errors under AC power frequency supply and rated amplitude and the measurement of the first 10-15 harmonic spurious tones at VT primary and secondary sides. This step is necessary for applying the SINDICOMP (SINusoidal characterization for DIstortion COMPensation) compensation procedure to strongly reduce the harmonic error contribution due to the VT non-linearity.

2. Measurement of the VT harmonics errors under a LV sinusoidal frequency sweep (LV SFS).

As proved with experimental tests, both the techniques depend on the VT burden conditions so the measurement steps listed above have to be carried out with the VT actual burden conditions.

It is worth noting that both the measurement steps involve only the generation of sine waves. In particular, for the first step, the voltage test signal is the one that is already required by the standard [5] for the verification of the accuracy class. For the second step, it is necessary to generate sinusoidal voltages with amplitude lower than 50 V and with frequency in the range (0.1-9) kHz.

Starting from the data set obtained from the two measurement steps, it is possible to apply the two different procedures, E-SINDICOMP and SINDICOMP-LV, to build the VT approximated frequency response.

The first developed technique, E-SINDICOMP, provides a method for the approximation of the VT frequency ratio error response whereas SINDICOMP-LV also provides a method for the reconstruction of the VT both ratio and phase frequency behaviour.

The two techniques have been experimented in the approximation of the frequency responses of three commercial VTs and results have been validated by comparison with measurements results obtained by INRIM reference generation and measurement system. The reference system is the one presented in Chapter 3 and the reference test is the FH1 described in Chapter 4, along with the application of SINDICOMP [9] that is briefly recalled in the following.

Moreover, in the following after a brief discussion of the effects of magnetic iron core non-linearity in the harmonic measurements, the two developed techniques are described; results of their application to the measurement of the frequency response are reported.

5.2 VT Non-Linearity: Theoretical Background

 Inductive VTs introduce errors in the measurement of harmonics because of the non-linearity of their iron core. It is possible to identify two main effects of such a non-linearity, and in the following, a brief overview of them is provided.

The first non-linearity effect is described in Fig. 5.1 and Fig. 5.2. The curves respectively shown are the ratio and phase errors at the third harmonic measured supplying the VT with a signal composed of a fundamental tone at rated voltage, rated frequency and 0 rad phase plus the third harmonic with amplitude equal to 1% of the fundamental and phase angle varying in the range [-π, π]. As can be observed, the errors referring to the uncompensated case (blue curves) strongly depend on the third harmonic phase angle and show an almost sinusoidal behaviour. This effect is caused by the combination of the third harmonic applied to the VT input and the third harmonic generated at the VT secondary side by the fundamental tone because of the non-linearity of the *B-H* curve. Some compensation techniques have been proposed to reduce the ratio and phase error contributions due to the non-linearity [9, 50, 10]. One of these techniques is SINDICOMP [9] and it will be briefly recalled in next section.
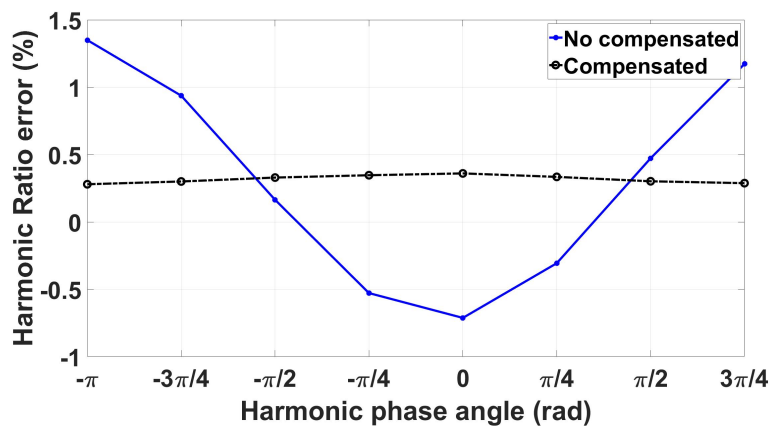
Fig. 5.1 Ratio error associated with the applied third harmonic versus its phase displacement without and with the compensation method SINDICOMP.
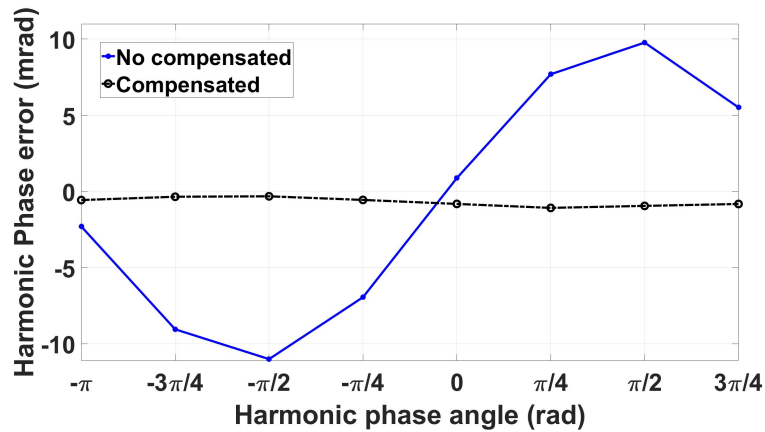
Fig. 5.2 Ratio error associated with the applied third harmonic versus its phase displacement without and with the compensation method SINDICOMP.

The second effect of the VT non-linearity is shown in Fig. 5.3 and it is also discussed in [44]. The figure provides the frequency responses of the same VT measured from rated frequency up to 3 kHz under different test conditions. In particular, the solid lines refer to the harmonic ratio errors measured under increasing LV SFS. In contrast, the black dotted line is obtained by supplying the VT with a fundamental component at rated voltage and frequency, with a superimposed harmonic frequency sweep (FH1).
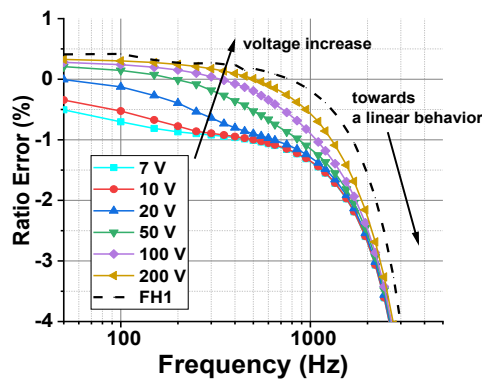
Fig. 5.3 Ratio errors frequency behavior obtained with various low voltage amplitudes and FH1 response (reference frequency response measured at rated voltage plus harmonic).

As can be observed, the two curves differ more than 1%, especially at the first harmonics. This means that the responses measured at very LV levels are not

able to accurately describe the VT behaviour under rated conditions, since they are quite far from the " true value" FH1. These differences are due to a different magnetization of the VT iron core for different amplitudes of the test waveforms and, therefore, different iron losses, which depend on the supply voltage and frequency. The differences among the curves reduce with the increase of the frequency. This is due to the effect of the stray capacitance among turns and between windings and ground that starts to dominate on the non-linear effects of the iron core.

5.3   SINDICOMP

Both the simplified procedures share the application of the SINDICOMP compensation techniques as a preliminary step. In this section, a brief recall of the method is given.

When a VT is working in no-load conditions and supplied with a pure sinusoidal voltage, it produces a sinusoidal flux sustained by a magnetization current. Because of the magnetic core hysteresis, the magnetization current is not described by a pure sinusoidal waveform but is distorted, as observed in Fig. 5.4. Analyzing the harmonic content of the magnetization current, the presence of the first odd harmonics (up to 11th -15th) can be noted, which are not included in the primary input signal.
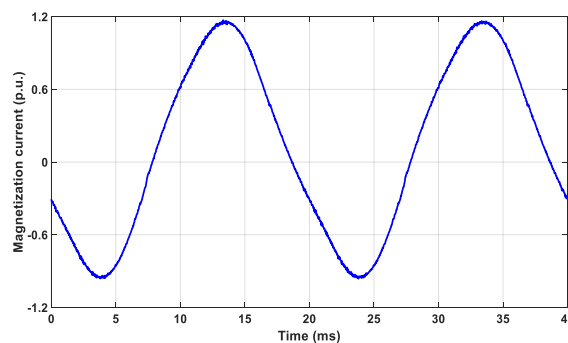
Fig. 5.4 Magnetizing current of a commercial inductive MV VT when a sinusoidal voltage is applied to the primary winding.

Under no-load conditions, the VT can be represented with the simplified circuit provided in Fig 5.5, where the harmonic components of the magnetization currents

are modelled with a current generator. The VT primary winding is represented by impedance $\overline{Z^*}$ consisting of the equivalent resistance R and the leakage inductance L series-connected. The magnetization current depends on the hysteresis loop characteristics, that is the peak value and the frequency of the input voltage. However, in normal operating conditions, the supply voltage is composed of a large component at the fundamental frequency with small superimposed harmonics, so it is reasonable to assume that the harmonic magnetization currents depend on the fundamental amplitude and frequency.
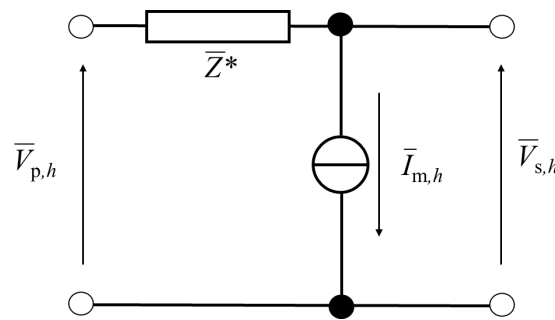
Fig. 5.5 VT simplified circuit.

Consequently, the voltage at the secondary windings when the VT is supplied with a sinusoidal voltage (superscript 'sin') can be expressed as in Equation 5.1:

$$\overline{V}_{s,h}^{sin} = -\overline{Z^*} \cdot \overline{I}_{m,h} \tag{5.1}$$

If the VT is operating in distorted conditions and it is supplied with a voltage signal composed of a fundamental plus one harmonic at frequency hf, the secondary voltage can be computed as:

$$\overline{V}_{s,h}^{d} = \overline{V}_{p,h}^{d} - \overline{Z^*} \cdot \overline{I}_{m,h} \tag{5.2}$$

As said before, the operating conditions allow assuming the magnetization current depending only on the fundamental component, and since $\overline{Z^*}$ is a parameter of the VT, it can be concluded that the error contribution due to nonlinear behavior can be measured by measuring the VT harmonic response under sinusoidal conditions.

Combining the Equations 5.1 and 5.2, the primary voltage in distorted conditions can be derived as described by Equation 5.3:

$$\overline{V}_{s,h}^{d} = \overline{V}_{p,h}^{d} - \overline{V}_{s,h}^{sin} \tag{5.3}$$

Equation 5.3 indicates that it is possible to use the secondary voltage harmonic components measured under sinusoidal conditions $\overline{V}_{s,h}^{sin}$ to correct the harmonic components measured in distorted conditions $\overline{V}_{s,h}^{d}$. In this way, the error contributions due to the iron core non-linearity are strongly reduced as can be observed in Fig 5.1 and 5.2. As the final result after the application of SINDICOMP, the ratio and phase error for the first harmonics assumes a quite flat response with values close to those measured at rated frequency.

To apply this compensation technique, it is necessary to supply the VT with sinusoidal waveforms as required by the standard [5], that is from 80% to 120% of the rated voltage; the only additional step is, for every sinusoidal input, the measurement of spurious harmonics phasors. Thereby, a correction lookup table is built and stored and it is used when the VT is used to measure real distorted waveforms.

5.4   E-SINDICOMP

The first simplified technique for the building of the VT approximated frequency response is E-SINDICOMP. The E-SINDICOMP simplified procedure provides a solution for the approximation of the VT ratio error frequency response and it does not cover the phase error.

This technique starts from the applications of SINDICOMP and extends it in frequency. After the application of SINDICOMP, the proposed procedure requires the execution of SFS at LV at harmonics frequency. For each generated harmonic frequency, ratio and phase errors are evaluated according to Equations 5.4 and 5.5, respectively:

$$\varepsilon_h = \frac{k_r \cdot U_{s,h} - U_{p,h}}{U_{p,h}} \tag{5.4}$$

$$\Delta\phi_h = \phi_{s,h} - \phi_{p,h} \tag{5.5}$$

where:

- $k_r = U_{p,r} \, / \, U_{s,r}$ is the rated transformation ratio ($U_{p,r}$ and $U_{s,r}$ are the rated primary and secondary voltages);

- $U_{p,h}$ and $U_{s,h}$ are the r.m.s. values of the primary and secondary h-order harmonic voltage;

- $\phi_{p,h}$ and $\phi_{s,h}$ are the phase angle the primary and secondary h-order harmonic voltage.

Starting from the data collected performing the sinusoidal test at rated conditions and the SFS, the approximated VT frequency response is constructed using three different curves in three different frequency regions.

The three curves are:

- ε_{50Hz} is a flat curve with value equal to the power frequency error measured at rated voltage;

- $\varepsilon_{LV}(f)$ is the measured frequency response under low voltage supply;

- $\tau(f)$ the tangent to the low voltage response.

The situation is depicted in Fig. 5.6, where the ratio errors versus frequency are shown.
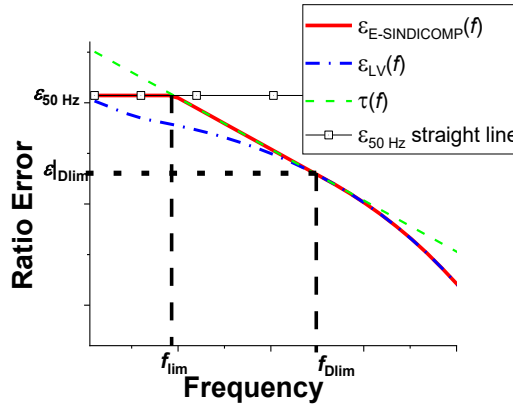
Fig. 5.6 Graphical description of the asymptotic fitting procedure for the identification of the VT frequency response.

The first region is from 50 Hz to the frequency f_{lim}. In this region, the VT response is approximated using a flat frequency response since a MV VT with primary voltage lower than 20 kV, after the compensation of non-linearity error, shows a quite flat frequency response up to the 10th -15th harmonic [9]. Therefore, the ratio error is assumed constant and equal to $\varepsilon_{50\text{Hz}}$ the value measured at 50 Hz up to the limit frequency f_{lim}:

$$\varepsilon(f) = \varepsilon_{50\text{Hz}}, \qquad 50\,Hz < f < f_{\text{lim}} \tag{5.6}$$

The frequency f_{lim} is identified by the intersection between two curves: the flat line $\varepsilon(f) = \varepsilon_{50\text{Hz}}$ and a straight line $\tau(f)$ with negative slope D_{lim}. In particular, $\tau(f)$ is the tangent in f_{Dlim} to the ratio error curve measured at low voltage $\varepsilon_{\text{LV}}(f)$. The second region is from the frequencies f_{lim} to f_{Dlim} and here the ratio error is approximated with $\tau(f)$, as in Equation 5.7:

$$\varepsilon(f) = \tau(f), \qquad f_{\text{lim}} < f < f_{\text{Dlim}} \tag{5.7}$$

$$\tau(f) = D_{\text{lim}} \cdot (f - f_{\text{Dlim}}) + \varepsilon_{\text{Dlim}} \tag{5.8}$$

$$D_{\text{lim}} = \left. \frac{d\varepsilon_{\text{LV}}(f)}{df} \right|_{f=f_{\text{Dlim}}} \tag{5.9}$$

Since f_{lim} is the frequency point where $\tau(f)$ is equal to $\varepsilon_{50\text{Hz}}$, the Equation 5.10 results:

$$f_{lim} = f_{Dlim} + \frac{\varepsilon_{50 \text{ Hz}} - \varepsilon_{Dlim}}{D_{lim}} \qquad (5.10)$$

The frequency f_{Dlim} is determined by analyzing the frequency behaviour of the derivative of the low voltage ratio error $\varepsilon_{\text{LV}}(f)$, D. Preliminary experimental tests on MV VTs with different features and primary voltage from 6 kV up to 20 kV have proved that D has a quite repetitive behaviour that is provided in Fig. 5.7: after a first flat part, it starts to decrease and from a specific frequency point, indicated as f_{Dlim}, the absolute value of the negative slope significantly increases.
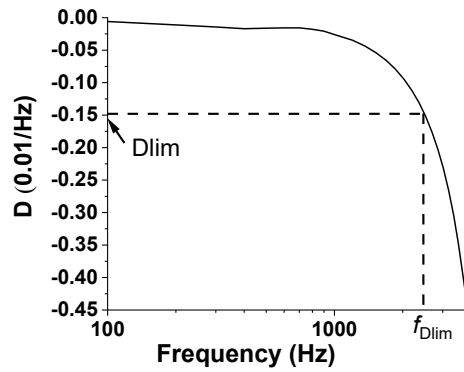
Fig. 5.7 Behavior of the frequency derivative of the VT ratio error. The point (f_{Dlim}, Dlim), which identifies the limit beyond which the linear effects affecting the ratio error are predominant on the non-linear ones, is highlighted.

The shape of D gives information on the frequency behaviour of the VT: the first flat part can be associated with the non-linear behaviour of the VT, whereas the region from f_{Dlim}, where the decreasing slope of D is more evident, can be related to the frequency region where stray capacitances between windings and ground are predominant. According to these considerations, for frequencies higher than f_{Dlim} the predominance of the linear effects allows assuming the VT as a linear device. Hence, its frequency response does not dependent on the input voltage, and therefore, the one measured at low voltage can be used. According to the experimental results, the proper value for D_{lim} ranges between - 0.10 (0.01/Hz) and - 0.2 (0.01/Hz). Additionally, information on the numerical selection of the optimum D_{lim} and, thus, the frequency f_{Dlim} is provided in subsection 5.8.1. The third region is defined for frequencies higher than f_{Dlim} and the ratio error $\varepsilon(f)$ is assumed equal to the ratio error $\varepsilon_{\text{LV}}(f)$ as indicated in Equation 5.11:

$$\varepsilon(f) = \varepsilon_{\text{LV}}(f), \qquad f > f_{\text{Dlim}} \tag{5.11}$$

It is worth underlining that the last equation applies up to the VT first resonance: in fact, the VT in correspondence of resonance and over shows very high variations making accurate measurements quite critical.

To summarize, the ratio error obtained by performing the E-SINDICOMP technique is 5.12:

$$\varepsilon_{E-SINDICOMP}(f) = \begin{cases} \varepsilon_{50\,Hz}, & 50\,Hz < f < f_{lim} \\ \tau(f), & f_{lim} < f < f_{Dlim} \\ \varepsilon_{LV}, & f > f_{Dlim} \end{cases} \tag{5.12}$$

5.5   SINDICOMP-LV

The SINDICOMP-LV (S-LV) procedure can approximate the VT frequency response in terms of ratio and phase errors. As well as the E-SINDICOMP technique, S-LV requires as the first step the application of SINDICOMP and then the measurement of the frequency response $\varepsilon_{\text{LV}}(f)$, $\Delta\phi_{\text{LV}}(f)$ by performing SFS at LV.

5.5.1   Ratio Error Approximation

According to S-LV, the approximation of the ratio error response is based on the fit of the low voltage response $\varepsilon_{\text{LV}}(f)$ to the following function:

$$\varepsilon_{\text{FIT}}(f) = \frac{\sqrt{(2\pi f a)^2 + b^2}}{\sqrt{\left(1 - \left(\frac{f}{f_R}\right)^2\right)^2 + \left(\frac{f}{2\pi f_R^2} \cdot \frac{b}{a}\right)^2}} \tag{5.13}$$

where:

- f_{R} is the first resonance frequency, whose value is obtained from the measured $\varepsilon_{\text{LV}}(f)$, and

- *a* and *b* are fit parameters determined by fitting the experimental frequency response data.

The structure of this function is obtained starting from the function that describes the impedance frequency behavior of a circuit simply constituted by the parallel connection of an inductor and a capacitor.

The fitting procedure is performed in a specific frequency range from f_{start} to f_{stop} where the VT can be considered linear. As regards f_{stop}, it is fixed 1 kHz before the resonance frequency f_{R}. The value of f_{R} can be easily determined by performing a LV SFS [23].

$$f_{\text{stop}} = f_{\text{R}} - 1\ kHz \tag{5.14}$$

Then, to exclude the lower frequencies where the VT is non-linear, f_{start} is chosen halving the interval [50 Hz,f_{R}].

$$f_{\text{start}} \approx (f_{\text{R}} - f_1)/m; with\ m = 2 \tag{5.15}$$

Experimental results on three different VTs sizes and accuracy classes (see Table 4.1) have been performed to refine the choice of the parameter m. In particular, m is varied in the range from 2 to 3, and in all the cases, it does not significantly affect the S-LV accuracy cases. However, a proper choice of f_{start} is:

$$f_{\text{start}} \approx (f_{\text{R}} - f_1)/m; with\ m = 2.5 \tag{5.16}$$

Compared to Equation 5.15, 5.16 corresponds to an extension of the frequency range where the fitting procedure is performed. After the definition of the frequency range [f_{start}, f_{stop}], the *a* and *b* parameters of the fitting function $\varepsilon_{\text{FIT}}(f)$ are found by the non-linear least-squares analysis using the $\varepsilon_{\text{FIT}}(f)$ measured data. After the fitting procedure, it is necessary to take into account the VT response at the lowest frequency, where the VT non-linearities are predominant. To this end, an offset correction $\varepsilon_{\text{OFS,a}}$, computed as in 5.17, is added to $\varepsilon_{\text{FIT}}(f)$:

$$\varepsilon_{\text{OFS,a}} = \varepsilon_{\text{MV}}(f_1) - \varepsilon_{\text{FIT}}(f_1) \tag{5.17}$$

where $\varepsilon_{\mathrm{MV}}(f_1)$ is the ratio error value obtained from the VT calibration at rated frequency and voltage carried out in the preliminary step. The final VT approximated ratio error $\varepsilon_{\mathrm{S-LV}}(f)$ is then assumed equal to $\varepsilon_{\mathrm{FIT}}(f) + \varepsilon_{\mathrm{OFS,a}}$ up to f_{start}. From f_{start} on, the VT can be considered linear and its ratio error frequency response $\varepsilon_{\mathrm{S-LV}}(f)$ is assumed equal to the $\varepsilon_{\mathrm{LV}}(f)$ shifted of the quantity $\varepsilon_{\mathrm{OFS,b}}$, obtained as:

$$\varepsilon_{\mathrm{OFS,b}} = \varepsilon_{\mathrm{FIT}}(f_{\mathrm{start}}) + \varepsilon_{\mathrm{OFS,a}} - \varepsilon_{\mathrm{LV}}(f_{\mathrm{start}}) \tag{5.18}$$

To summarize, the approximated ratio error $\varepsilon_{\mathrm{S-LV}}(f)$ is described by the following equation:

$$\varepsilon_{S-LV}(f) = \begin{cases} \varepsilon_{FIT}(f) + \varepsilon_{OFS,a}, & f_1 \leq f < f_{start} \\ \varepsilon_{LV}(f) + \varepsilon_{OFS,b}, & f_{start} \leq f < f_{stop} \end{cases} \tag{5.19}$$

The graphical representation of all the S-LV steps for identifying the VT ratio error are shown in Fig. 5.8 , where the involved ratio error curves versus frequency are provided. The ratio error frequency response obtained under FH1 test is also reported for comparison.
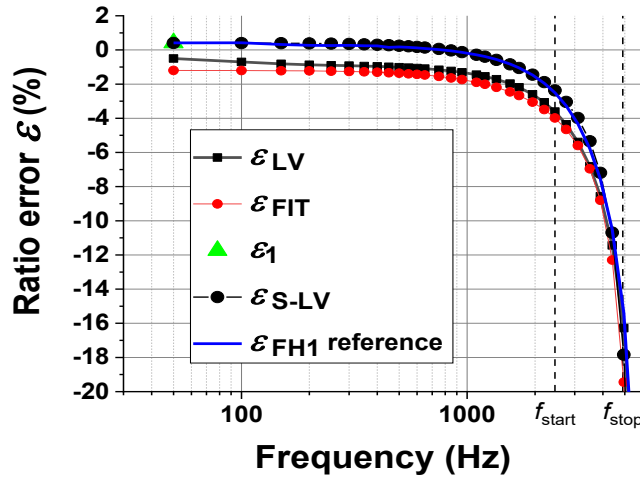
Fig. 5.8 Graphical description of the fitting procedure for the identification of the VT ratio error frequency response.

5.5.2 Phase Error Approximation

The same approach is adopted for the phase error approximation: $\Delta\phi_{\text{LV}}(f)$ and f_{R} quantities are those measured in the LV test, the parameters f_{start}, f_{stop}, a and b are the ones found in the ratio error fit procedure. The function used for phase error approximation is:

$$\Delta\phi_{\text{FIT}}(f) = \arctan\left(2\pi f \cdot \frac{a}{b}\right) - \arctan\left(\frac{\left(\frac{f}{2\pi f_R^2} \cdot \frac{b}{a}\right)}{\left(1 - \left(\frac{f}{f_R}\right)^2\right)^2}\right) + 2\pi f \cdot \frac{a}{b} \qquad (5.20)$$

Similarly to the ratio error case, $\Delta\phi_{\text{FIT}}(f)$ is shifted adding an offset $\Delta\phi_{\text{OFS,a}}$ that is computed in the same way:

$$\Delta\phi_{\text{OFS,a}} = \Delta\phi_{\text{MV}}(f_1) - \Delta\phi_{\text{FIT}}(f_1) \qquad (5.21)$$

Where $\Delta\phi_{\text{MV}}(f_1)$ is obtained from the tests under the sinusoidal rated conditions. Thus, the S-LV phase error is equal to $\Delta\phi_{\text{FIT}}(f) + \Delta\phi_{\text{OFS,a}}$ from the rated frequency up to f_{start}. From f_{start} up to f_{stop}, the VT phase frequency response is equal to $\Delta\phi_{\text{LV}}(f)$ shifted of $\Delta\phi_{\text{OFS,a}}$ obtained as:

$$\Delta\phi_{\text{OFS,b}} = \Delta\phi_{\text{FIT}}(f_{\text{start}}) + \Delta\phi_{\text{OFS,a}} - \Delta\phi_{\text{LV}}(f_{\text{start}}) \qquad (5.22)$$

Summarizing, the S-LV approximated phase error $\Delta\phi_{\text{S-LV}}(f)$ is:

$$\Delta\phi_{S-LV}(f) = \begin{cases} \Delta\phi_{FIT}(f) + \Delta\phi_{OFS,a}, & f_1 \leq f < f_{start} \\ \Delta\phi_{LV}(f) + \Delta\phi_{OFS,b}, & f_{start} \leq f < f_{stop} \end{cases} \qquad (5.23)$$

The graphical representation of the S-LV steps is provided in Fig. 5.9, where all the involved phase error curves are shown. The phase-frequency response obtained under FH1 test is also reported for comparison.
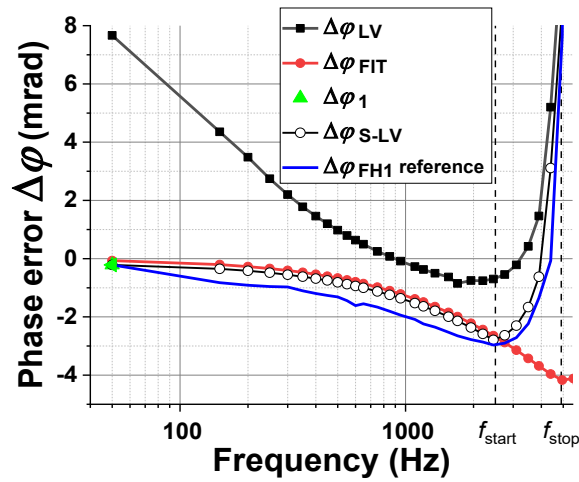
Fig. 5.9 Graphical representation of the S-LVs steps for the identification of the VT phase error frequency response.

5.6   Measurement Setups and Devices under test

5.6.1   Measurement setups

As said in Section 5.1, the two simplified procedures are based on the same two measurement steps, so for this reason, identical measurement setups can be used for their application.

In particular, two measurement setups with different generation and measurement capabilities are needed to perform the two measurement steps.

Regarding the first step, the VT test is carried out using the measurement setup shown in Fig. 5.10 and described in Chapter 3 as regards the calibration of inductive VTs.
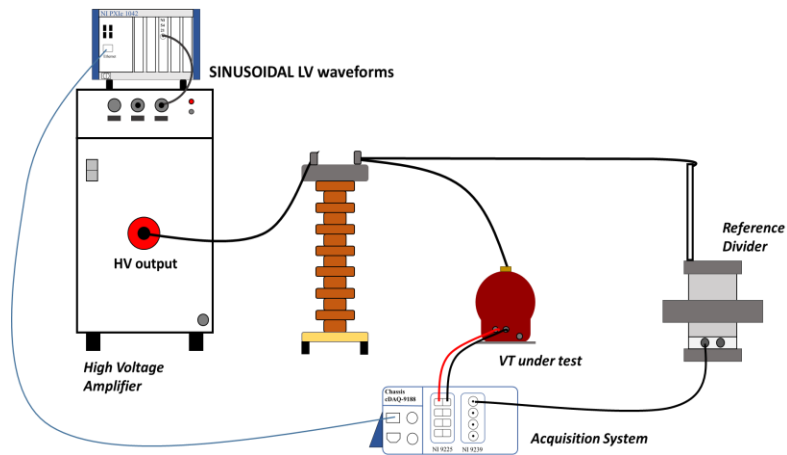
Fig. 5.10 Block diagram of the setup used for VT characterization in step 1 and for validation tests of E-SINDICOMP and SINDICOMP-LV.

It's worth noting that, as demonstrated in [94], this measurement step that is necessary for the quantification of the power frequency errors and the application of SINDICOMP, can be performed also by the means of more common measurement setup that does not include voltage amplifier but step up transformer.

For the second step, the LV SFS is performed using the measurement setup shown in Fig. 5.11. A Fluke 5500A calibrator, remotely controlled is used for the generation of LV SFS. No reference sensor is needed, since the generated LV signals are always compliant with the input stage of the acquisition system.
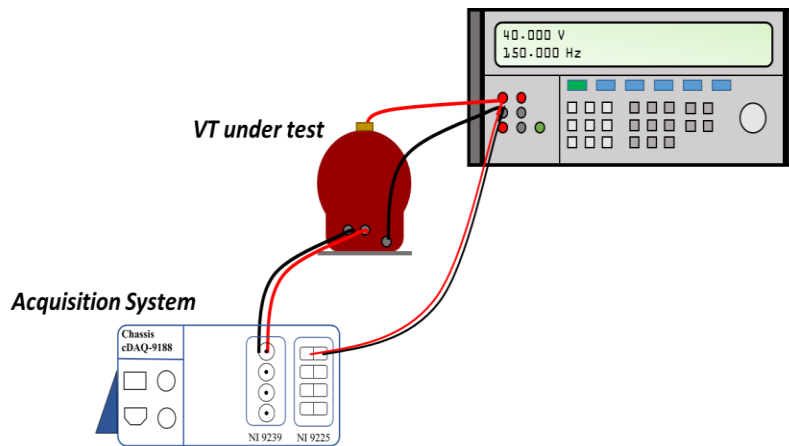
Fig. 5.11 Block diagram of the setup used for VT characterization in step 1 and for validation tests of E-SINDICOMP and SINDICOMP-LV.

Both the measurement setups share the same acquisition system that is a NI compact Data AcQuisition system (cDAQ) chassis with various input module as described in Section 3.6. As regards the setup for the low voltage frequency sweep, the sole uncertainty contribution source is due to the acquisition system since it is used to measure both primary and secondary voltages (see Chapter 3). Following its calibration, its uncertainty is estimated equal to 50 μV/V and 50 μrad at power frequency and reaches 100 μV/V and 120 μrad at 9 kHz for the ratio error and phase error respectively.

5.6.2   Devices under Test

  The two simplified techniques are applied to approximate the frequency responses of the same three VTs. In particular, the considered devices are commercial resin insulated VTs for MV phase to ground applications at 50/60 Hz. The main features of the analyzed VTs are summarized in Table 4.1.

5.7   E-SINDICOM and SINDICOMP-LV Validation

The simplified procedures are validated by comparing their characterization results with the results obtained by characterizing the three VTs with the FH1 tests, which are assumed as references. The FH1 tests are performed by using the reference generation and measurement system as described in Chapter 3. Fundamental tone with amplitude in the range 80% to 120% of the VT primary rated voltage and frequency 50 Hz, and one harmonic tone, with amplitude 1% of the fundamental one and frequency from 100 Hz up to 10 kHz, are used. For each generated harmonic tone, various phase angles in the range $\pm \pi$ rad are analyzed. The performances of E-SINDICOMP and SINDICOMP-LV are quantified as:

$$\delta_{\text{E-SINDICOMP}}(f) = \varepsilon_{\text{E-SINDICOMP}}(f) - \varepsilon_{\text{MV}}(f) \tag{5.24}$$

$$\delta_{\text{S-LV}}(f) = \varepsilon_{\text{S-LV}}(f) - \varepsilon_{\text{MV}}(f) \tag{5.25}$$

$$\Theta_{\text{S-LV}}(f) = \Delta\phi_{\text{S-LV}}(f) - \Delta\phi_{\text{MV}}(f) \tag{5.26}$$

Where $\delta_{\text{E-SINDICOMP}}(f)$, $\delta_{\text{S-LV}}(f)$, $\Theta_{\text{S-LV}}(f)$ are the deviations between the approximated and actual ratio and phase error respectively. To quantify the improvement provided by the proposed procedure with respect to the simple LV SFS, the deviations between the errors obtained at LV ($\varepsilon_{\text{LV}}(f)$, $\Delta\phi_{\text{LV}}(f)$) and the actual ones are also evaluated according to the following equations:

$$\delta_{\text{LV}}(f) = \varepsilon_{\text{LV}}(f) - \varepsilon_{\text{MV}}(f) \tag{5.27}$$

$$\Theta_{\text{LV}}(f) = \Delta\phi_{\text{LV}}(f) - \Delta\phi_{\text{MV}}(f) \tag{5.28}$$

5.8   E-SINDICOM Application

5.8.1   Identification of the D_{lim} value

 As the first step, for the three analyzed VTs it is identified the proper D_{lim} value by studying the SFS derivative D measured at 40 V. Fig. 5.12 provides the ratio error curves measured at LV versus normalized frequency, whereas the relative derivative curves are shown in Fig. 5.13
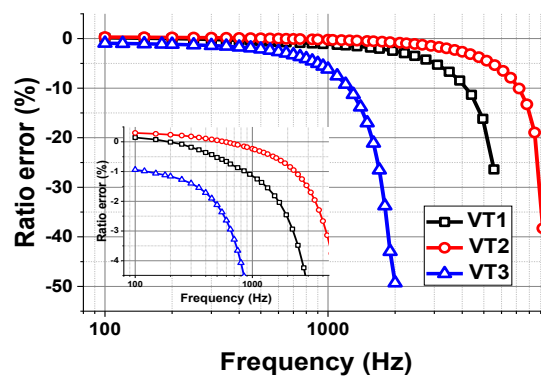
Fig. 5.12 VT1 (square marker), VT2 (circle marker) and VT3 (triangle marker): SFS ratio error before resonance frequency (inset: zoom up to f_{Dlim}).
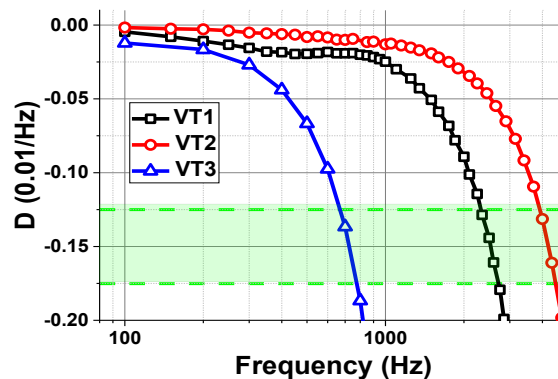

Fig. 5.13 VT1 (square marker), VT2 (circle marker) and VT3 (triangle marker): SFS ratio error derivative curves D (b).

    In particular, Fig. 5.13 shows the VTs SFS ratio error responses before their respective resonance frequencies and, in addition, zoom up their respective f_{Dlim}

frequency. In Fig. 5.13 it is highlighted in green the portion where D goes from 0.12 to 0.16 (0.01/Hz); that is the region where the absolute value of the D slope starts to increase significantly.

Table 5.1 reports the D_{lim} and f_{Dlim} values selected for the three investigated VTs.

Table 5.1 Selected D_{lim} and f_{Dlim} values.

DUT	D_{lim} (0.01/Hz)	f_{Dlim} (Hz)	f_{lim} (Hz)
VT1	-0.14	2500	800
VT2	-0.14	4000	1600
VT3	-0.14	800	300

In Fig. 5.12, it can be noticed that for VT1 (square marker) three different D_{lim} values are included in the green highlighted portion. Therefore, to quantify the impact of the D_{lim} choice on the E-SINDICOMP performance, the procedure is performed for all three D_{lim} values. In particular, three responses are built following the E-SINDICOMP procedure for each of the D_{lim} values, 0.12, 0.14 and 0.16 (0.01/Hz), that correspond to f_{Dlim} values of 2350 Hz, 2500 Hz and 2600 Hz, respectively. Regarding f_{lim} frequency, the three f_{Dlim} values identify three different f_{lim} values that are equal to 700, 800 and 900 Hz, respectively. Fig. 5.14 provides the results of the analysis on D_{lim} selection. In particular, it shows the deviations between the reference ratio error (REF) and the three ratio error curves (APP) obtained by applying E-SINDICOMP for the three different couples of D_{lim} and f_{Dlim} values. As it can be observed, the three curves are well overlapped below the lowest f_{lim} value, which is 700 Hz. From this frequency point, the three curves are distanced (maximum deviations of 5 mV/V among them) and the best result is obtained with $D_{\mathrm{lim}} = 0.14$ (0.01/Hz), identified by circle markers in Fig. 5.14. After 2.6 kHz, that is the higher f_{Dlim} value, the three curves come closer together, resulting again in overlap. For the rest of the analysis, a $D_{\mathrm{lim}} = 0.14$ (0.01/Hz) is chosen for VT1.
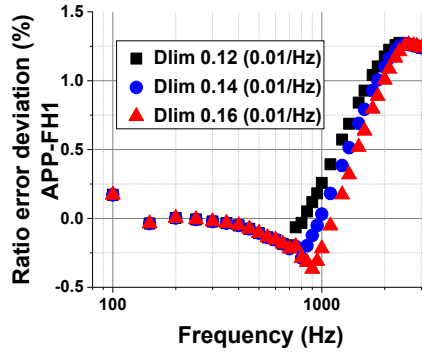
Fig. 5.14 VT1 ratio error deviation vs frequency with different values for D_{lim} and D_{Dlim}.

5.8.2 VTs characterization

This subsection provides the results of the E-SINDICOMP application to approximate the ratio error frequency responses of the three analyzed VTs when they operate in zero burden condition. The results here provided are also presented in [92].

VT1 characterization

For VT1, some experimental results have been already presented in Sections 5.8.1. Here, the complete characterization is shown. All the three ratio error curves, the REF, the SFS and the E-SINDICOMP are shown in Fig. 5.15. Table 5.2 shows the deviations $\delta_{\text{E}-\text{SINDICOMP}}(f)$ and $\delta_{\text{LV}}(f)$. Good improvements, up to one order of magnitude for the ratio error deviations up to hundreds of hertz, are obtained by using the E-SINDICOMP frequency response with respect to the use of the SFS response.

Fig. 5.15 VT1 comparison of ratio errors obtained with REF (FH1 with SINDICOMP), SFS and E-SINDICOMP.

Table 5.2 VT1 deviations between SFS and REF responses and between E-SINDICOMP and REF responses.

Frequency (Hz)	$\delta_{LV}(f)$ (%)	$\delta_{E-SINDICOMP}(f)$ (%)
100	-0.36	0.03
200	-0.54	-0.0039
300	-0.72	0.022
700	-1.19	0.22
1000	-1.27	-0.031
1250	-1.28	-0.38
1500	-1.29	-0.69
1750	-1.29	-0.93
2000	-1.27	-1.0

VT2 characterization

The second VT (VT2) has been selected with a primary voltage half of the VT1 one, same manufacturer, lower transformation ratio (100 against 200) and higher first resonance frequency (9.2 kHz against 5.5 kHz). Fig.5.16 shows the comparison of the REF, the SFS and the E SINDICOMP ratio and phase errors, respectively. Table 5.3 shows the deviations on ratio obtained between SFS and REF responses

and between E-SINDICOMP and REF responses. Again, as already seen for VT1, E-SINDICOMP gives good results compared to the use of SFS.

Fig. 5.16 VT2 comparison of ratio errors obtained with REF (FH1 with SINDICOMP), SFS and E-SINDICOMP.

Table 5.3 VT2 deviations between SFS and REF responses and between E-SINDICOMP and REF responses.

Frequency (Hz)	$\delta_{LV}(f)$ (%)	$\delta_{E-SINDICOMP}(f)$ (%)
100	-0.24	-0.03
500	-0.47	-0.01
1000	-0.62	0.12
1500	-0.68	0.31
2000	-0.69	-0.01
2500	-0.69	-0.21
3000	-0.69	-0.43
3500	-0.67	-0.56

VT3 characterization

The third investigated VT, VT3, is a resin insulated transformer from a different manufacturer. It has higher primary voltage and two different ratios, 50 kV / 100 V and 20 kV / 100 V; here, only the 20 kV / 100 V configuration was used. As in the previous cases, Fig. 5.17 show the comparison among the REF, the SFS and the E

SINDICOMP ratio errors, respectively, whereas the deviations with respect to REF are quantified in Table 5.4.
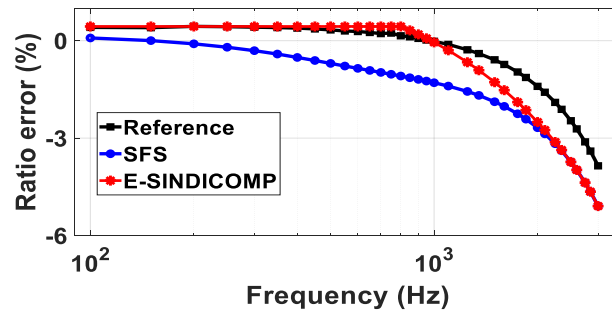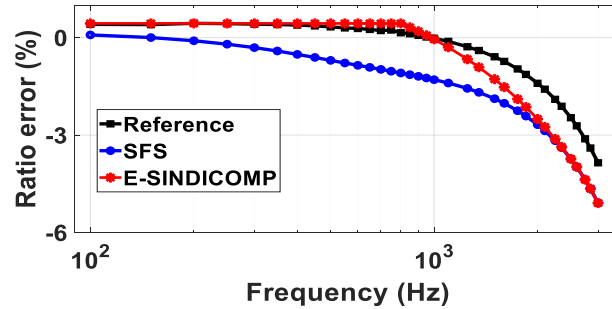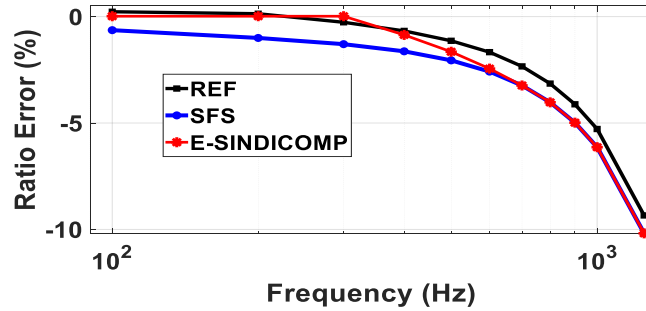

Fig. 5.17 VT3 comparison of ratio errors obtained with REF (FH1 with SINDICOMP), SFS and E-SINDICOMP.

Table 5.4 VT3 deviations between SFS and REF responses and between E-SINDICOMP and REF responses.

Frequency (Hz)	$\delta_{LV}(f)$ (%)	$\delta_{E-SINDICOMP}(f)$ (%)
200	-0.86	-0.21
300	-1.14	0.120
500	-0.96	-0.19
700	-0.91	-0.77

Burden effect

This section aims to study the VT burden effect on the E-SINDICOMP performance. For convenience, only the results related to VT2 at its rated burden, 50 VA, are shown. However similar considerations also apply to the other two analyzed VTs. The burden is a ohmic-inductive burden with a $cos\phi_b = 0.8$ power factor. The study of the derivative D of the VTs SFS, measured in the rated burden condition, provides a f_{Dlim} equal to 4350 Hz, corresponding to D_{lim} equal to 0.16 (0.01/Hz), whereas f_{lim} is fixed to 1500 Hz. By comparing the resulting values of f_{lim} and f_{Dlim} (1500 Hz and 4350 Hz) with the values obtained in zero burden conditions (1600 Hz and 4000

Hz), a slight enlargement of the second frequency region can be noticed. Results related to the burden effect on E-SINDICOMP performance are provided in Fig. 5.18. In this case, the E-SINDICOMP method also reduces the ratio error deviations by giving values below 0.1% up to 1 kHz and a maximum error of -1.1% at 4350 Hz.
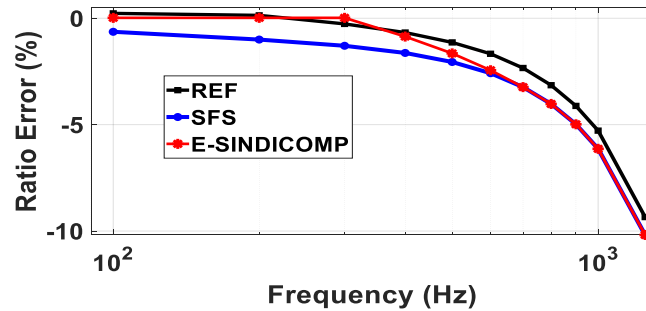
Fig. 5.18 VT2 REF, SFS and E SINDICOMP ratio error curves measured under rated burden condition.

5.9   SINDICOMP-LV Application

This subsection provides the results of the SINDICOMP-LV application to approximate the ratio error and phase error frequency responses of the three analyzed VTs described in Table 4.1. The results here provided have been also published in [93]. For each VT, the two steps required by S-LV are performed. As regards the LV test, the sinusoidal frequency sweep is executed at harmonic frequencies hf_1 from f_1 up to 10 kHz with a 7 V applied voltage. Table 5.5 summarizes, for each analyzed VT, the selected fit frequency region and the fit parameters, obtained according to the procedure described in Section 5.5.

Table 5.5 Fit parameters of the analyzed VTs.

Name	f_R (Hz)	f_{start} (Hz)	f_{stop} (Hz)	a (s)	b
VT1	5900	2450	4900	0.2	1.7
VT2	9500	4000	8500	1	1
VT3	2000	750	1000	0.65	1.5

5.9.1 VT1 characterization

The deviations $\delta_{S-LV}(f)$ and $\delta_{LV}(f)$ versus frequency are shown in Fig. 5.19. The VT ratio errors measured by the FH1 reference test are given in the same figure (red triangular marker). Related numerical results for a limited number of frequencies are given in Table 5.6.

Fig. 5.19 Comparison between the VT1 ratio error deviations obtained by the LV (square marker) and the S-LV (circle marker) characterization. VT1 reference ratio error obtained performing the FH1 test (triangle marker) is also shown.

Table 5.6 VT1 ratio error results.

Frequency (Hz)	$\varepsilon_{\text{FH1}}(f)$ (%)	$\delta_{\text{LV}}(f)$ (%)	$\delta_{\text{S-LV}}(f)$ (%)
150	-0.092	1.14	-0.08
400	-0.17	1.22	-0.09
1200	-0.79	1.18	-0.15
3500	-6.16	1.10	-0.50
4900	-15.76	1.05	-0.75

The VT1 ratio error $\varepsilon_{\text{FH1}}(f)$ is quite low (a few parts in 10^3) at the first harmonics and then increases up to -15.76% at 4.9 kHz (f_{stop}). Considering the LV deviation $\delta_{\text{LV}}(f)$ results, it is observed a reduction $\delta_{\text{LV}}(f)$ at highest frequencies, but worst results for the first harmonics, f.i. at the third harmonic, where $\delta_{\text{LV}}(f)$ is over one order of magnitude higher than the reference error. It can be seen, instead, that the S-LV approach gives better results for all the analyzed frequencies. In particular, for the first ten harmonics, the deviation values are lower than 0.1%, whereas an increase can be observed at the highest frequencies. Nevertheless, the highest absolute value is well below 1% and it is reached only at f_{stop}, i.e. 4.9 kHz. The corresponding phase error deviations $\Theta_{\text{S-LV}}(f)$ and $\Theta_{\text{LV}}(f)$ and the VT reference phase error $\Delta\phi_{\text{FH1}}(f)$ versus frequency are shown in Fig. 5.20, whereas related numerical results are given in Table 5.7.
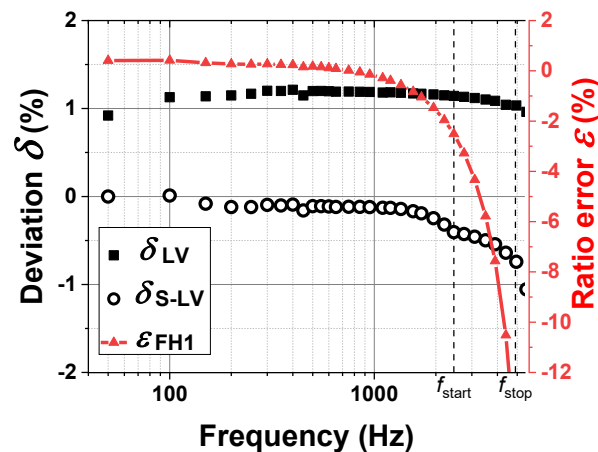
Fig. 5.20 Comparison between the VT1 phase error deviations obtained by the LV (square marker) and the S-LV (circle marker) characterization. VT1 reference phase error obtained performing the FH1 test (triangle marker) is also shown.

Table 5.7 VT1 phase error results.

Frequency (Hz)	$\Delta\varphi_{FH1}(f)$ (mrad)	$\vartheta_{LV}(f)$ (mrad)	$\vartheta_{S-LV}(f)$ (mrad)
150	-0.66	-5.23	-0.52
400	-0.99	-2.67	-0.50
1200	-2.03	-1.88	-0.54
3500	-2.02	-2.65	-0.58
4900	2.99	-3.10	-1.05

Looking at Fig. 5.20 it can be noted that the deviations obtained with the LV characterization are the highest almost for every analyzed frequency, but especially for the first harmonics. On the contrary, the S-LV approach gives better results for each analyzed frequency and the absolute value of the phase error deviation remains lower than 1.1 mrad up to 4.9 kHz where the actual error is 8 mrad.

5.9.2   VT2 characterization

The VT2 reference ratio errors $\varepsilon_{FH1}(f)$, and the deviations $\delta_{S-LV}(f)$ and $\delta_{LV}(f)$ versus frequency are shown in Fig. 5.21, whereas numerical results are given in Table 5.8. Looking at the two ratio error deviation trends in Fig. 5.21, it can be noted that also for VT2, the use of the S-LV procedure leads to the best results. For instance, at 2.1 kHz the deviation with respect to the FH1 value, obtained by using the LV measurement is 0.66%, and it reduces to about one third (-0.23%) by using the proposed procedure. The VT2 phase errors $\Delta\phi_{FH1}(f)$ and the deviations $\Theta_{S-LV}(f)$ and $\Theta_{LV}(f)$ versus frequency are shown in Fig. 5.22, whereas the related numerical results are given in Table 5.9.
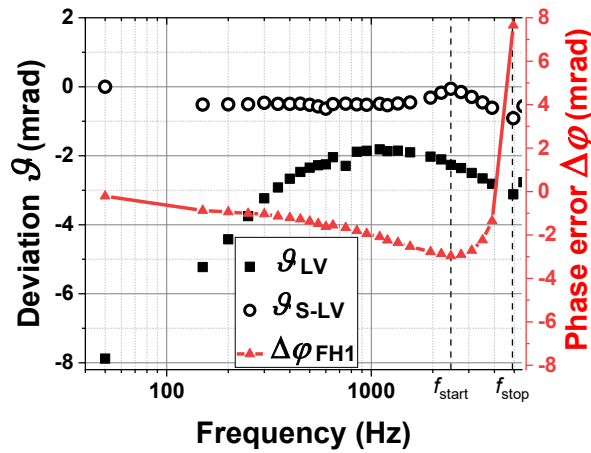

Fig. 5.21 Comparison between the VT2 ratio error deviations obtained by the LV (square marker) and the S-LV (circle marker) characterization. VT2 reference ratio error obtained performing the FH1 test (triangle marker) is also shown.

Table 5.8 VT2 ratio error results.

Frequency (Hz)	$\varepsilon_{FH1}(f)$ (%)	$\delta_{LV}(f)$ (%)	$\delta_{S-LV}(f)$ (%)
150	0.040	0.60	0.044
1500	-0.32	0.76	-0.094
2100	-0.65	0.66	-0.23
6100	-6.40	0.52	-0.42

In this case, the application of S-LV to VT2 allows obtaining a phase error deviation (absolute value) lower than 1 mrad up to 7.2 kHz. In particular, for VT2, the improvement obtained for the phase error, as the frequency increases, is more evident than the one obtained with VT1.

Fig. 5.22 Comparison between the VT2 phase error deviations obtained by the LV (square marker) and the S-LV (circle marker) characterization. VT2 reference phase error obtained performing the FH1 test (triangle marker) is also shown.

Table 5.9 VT2 phase error results.

Frequency (Hz)	$\Delta\varphi_{FH1}(f)$ (mrad)	$\vartheta_{LV}(f)$ (mrad)	$\vartheta_{S-LV}(f)$ (mrad)
150	0.38	-2.51	0.51
1500	-0.95	-1.76	0.66
2100	-1.53	-2.05	0.60
6100	-2.80	-3.80	0.19

5.9.3   VT3 characterization

The VT3 ratio errors $\varepsilon_{FH1}(f)$ and the deviations $\delta_{S-LV}(f)$ and $\delta_{LV}(f)$ are shown in Fig. 5.23. Some numerical results are also given in Table 5.10. The application of the S-LV method to VT3 leads to a significant reduction of the ratio error deviation, whose maximum value is -0.36%.
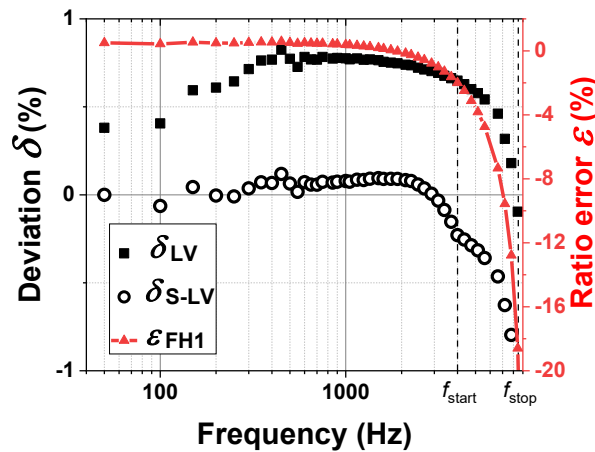
Fig. 5.23 Comparison between the VT3 ratio error deviations obtained by the LV (square marker) and the S-LV (circle marker) characterization. VT3 reference ratio error obtained performing the FH1 test (triangle marker) is also shown.

Table 5.10 VT3 ratio error results.

Frequency (Hz)	$\varepsilon_{FH1}(f)$ (%)	$\delta_{LV}(f)$ (%)	$\delta_{S-LV}(f)$ (%)
200	0.11	1.33	0.36
400	0.70	1.07	0.26
800	-3.18	0.97	0.066
1000	-5.31	0.95	-0.35

The corresponding phase errors deviations and the reference response versus frequency are shown in Fig. 5.24; related numerical results are given in Table 5.11. As regards the phase error deviation, $\Theta_{S-LV}(f)$ is within 0.5 mrad up to 1 kHz, whereas, in the same frequency range, $\Theta_{LV}(f)$ reaches a maximum value of -5.20 mrad.
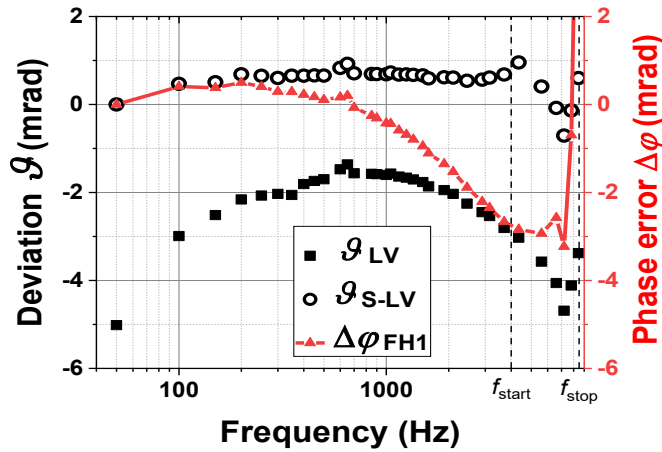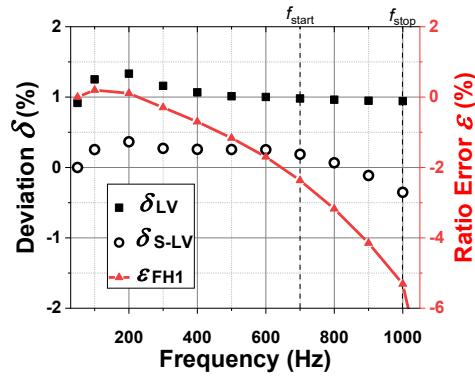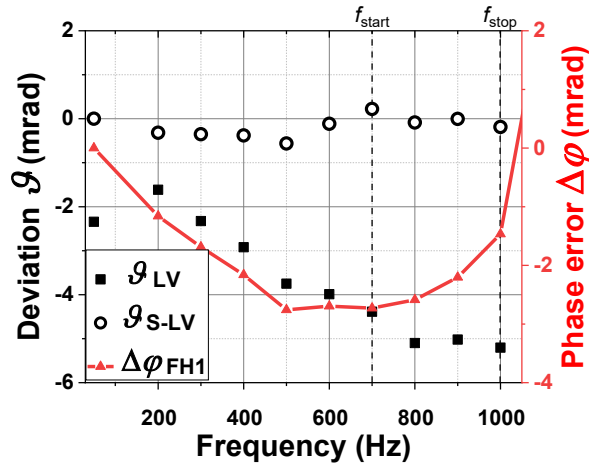
Fig. 5.24 Comparison between the VT3 phase error deviations obtained by the LV (square marker) and the S-LV (circle marker) characterization. VT3 reference phase error obtained performing the FH1 test (triangle marker) is also shown.

Table 5.11 VT3 phase error results.

Frequency (Hz)	$\Delta\varphi_{FH1}(f)$ (mrad)	$\vartheta_{LV}(f)$ (mrad)	$\vartheta_{S-LV}(f)$ (mrad)
200	-1.16	-1.61	-0.32
400	-2.16	-2.92	-0.38
800	-2.10	-5.10	-0.084
1000	-0.87	-5.20	-0.19

5.9.4 Sensitivity Analysis of S-LV

The accuracy performance of the S-LV procedure, as investigated in the previous section, can be affected by influence quantities. In this section, three quantities are considered in the following: two of them are parameters of the method, f_{start} and the amplitude of the sinusoidal voltage used in the LV test, and the third is the burden used in the VT operation. For sake of brevity, the analyses here shown refer only to the ratio error of VT1. Similar results can be found for the other two VTs and are also valid for phase error.

S-LV sensitivity to f_{start} selection

  The scope of this section is to quantify the impact of the f_{start} choice on the S-LV accuracy performance.

  For this purpose, the factor m, indicated in equation (5.13) as the value that allows obtaining the best results, is varied in the range (2, 3) with a step equal to 0.25. Thus, five different f_{start} values are used in the S-LV technique application, given in Table 5.12. The assessment of the f_{start} impact on the S-LV performance is shown in Fig. 5.25. The triangle represents the reference ratio error $\varepsilon_{\text{FH1}}(f)$, whereas the circle represents, for each frequency, the mean value of the deviation $\delta_{\text{S-LV}}(f)$ obtained with the five different f_{start} values. The bars superimposed to the circles are the maximum deviation from the mean value. It can be observed that the bars are practically null up to 2 kHz, where they start to be detectable. The maximum bar amplitude, found at f_{stop}, is below 0.2% against a deviation value of 0.75%. This proves the substantial insensitivity of S-LV to f_{start} at low frequencies and the quite limited effect when approaching the resonance frequency.

Table 5.12 Values of f_{start} chosen to verify S-LV sensitivity.

m	2	2.25	2.5
f_{start} **(Hz)**	3000	2750	2450
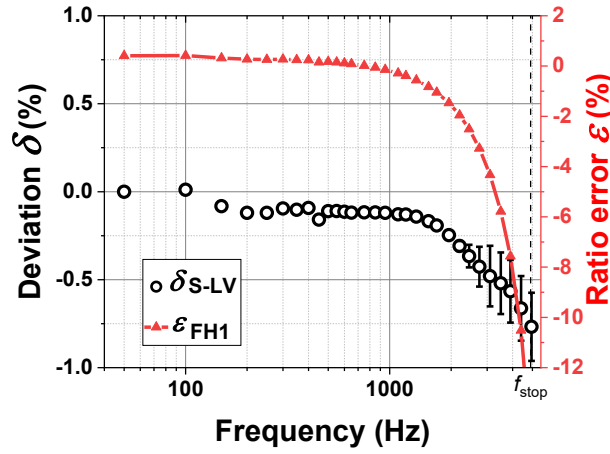
Fig. 5.25 Sensitivity analysis of S-LV to f_{start}. Reference ratio error of VT1 $\varepsilon_{FH1}(f)$ (triangle marker) and mean values of $\delta_{S-LV}(f)$ (circle marker) of the f_{start} values. The bars over the circle marker represent the maximum deviations from the mean values.

S-LV sensitivity to LV amplitude selection

The analysis carried out in the previous sections refers to LV tests carried out at the lower considered value (7 V). Six low voltage amplitudes are here considered: 7 V, 10 V, 20 V, 50 V, 100 V and 200 V and the S-LV procedure is executed for each considered voltage amplitude. As regards the identification of f_R, no difference is found and, consequently, the values of f_{start} and f_{stop} are the same for each considered low voltage level. As to the fit parameters, they slightly decrease with the increase of the low voltage amplitude. In particular, b and a found at 7 V are 1.7 and 0.2 s, whereas they drop to 1.58 and 0.19 s at 200 V. The resulting S-LV ratio error deviation curves are shown in Fig. 5.26, along with $\varepsilon_{FH1}(f)$. Fig. 5.27 shows, a zoom of Fig. 5.26, depicting only the $\delta_{S-LV}(f)$ curves.
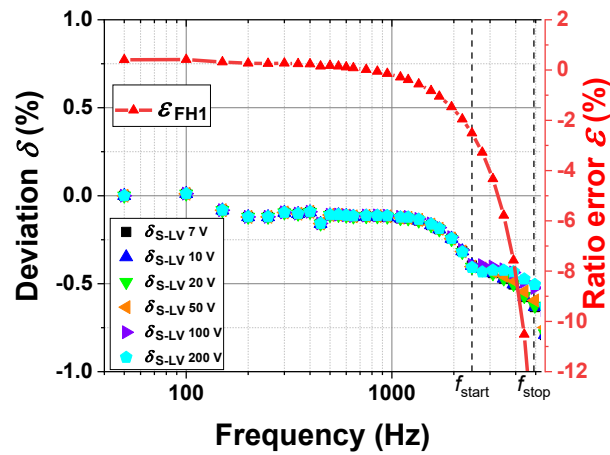
Fig. 5.26 Comparison between the $\varepsilon_{FH1}(f)$ ratio error of VT1 (triangle marker) and the ratio error deviations $\delta_{S-LV}(f)$ (various triangle markers) obtained with different LV amplitudes.
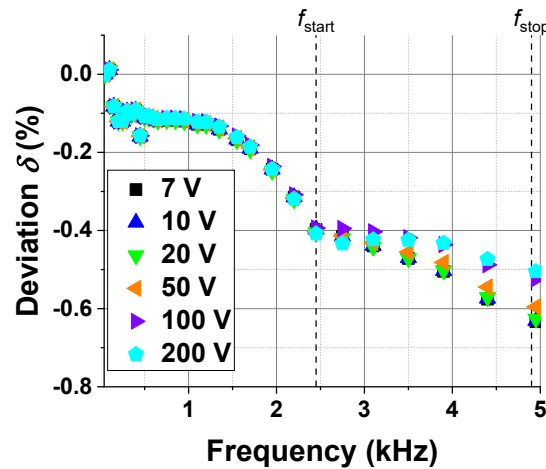
Fig. 5.27 Ratio errors deviations $\delta_{S-LV}(f)$ obtained with increasing LV voltage amplitude (zoomed data).

All the S-LV deviations curves are well overlapped from 50 Hz up to 2450 Hz and no significant differences are measured. From 2450 Hz up to 4900 Hz the difference among the curves can be appreciated: in particular, at 4900 Hz the reduction of $\delta_{S-LV}(f)$ can be clearly observed. However, the maximum deviation between 7 V and 200 V, at 4900 Hz, is equal to 0.12% that represents a relative benefit, compared

to the eventual rising cost if the instrumentation necessary to increase the test voltage
over 7 V has to be purchased.

S-LV sensitivity to VT burden condition

The aim of this section is to assess the impact of the VT burden condition on the
S-LV performance.

For this purpose, VT1 has been characterized under its rated burden condition,
i.e. using a 50 VA ohmic-inductive burden with a $cos\phi_b = 0.8$ power factor. As a
preliminary verification, the deviation is evaluated between the ratio error $\varepsilon_{S-LV}(f)$,
found with zero burden condition, and the reference response $\varepsilon_{FH1,rb}(f)$ measured
when the VT1 supplies its rated burden. Results related to this analysis are shown in
Fig. 5.28. Looking at Fig. 5.28, it is evident that the results are unsatisfactory. In fact,
for the first harmonics the S-LV deviation error is equal to 0.5%, that is about seven
times higher than the results obtained with zero burden condition. This result is
mainly due to an evident performance variation of the VT in presence of the burden.
In this regard, it is sufficient to point out that burden strongly varies the ratio error at
power frequency from 0.41% (zero burden) to -0.09% (rated burden).

Fig. 5.28 Ratio error of VT1 with rated burden $\varepsilon_{FH1,rb}(f)$, obtained by performing the FH1
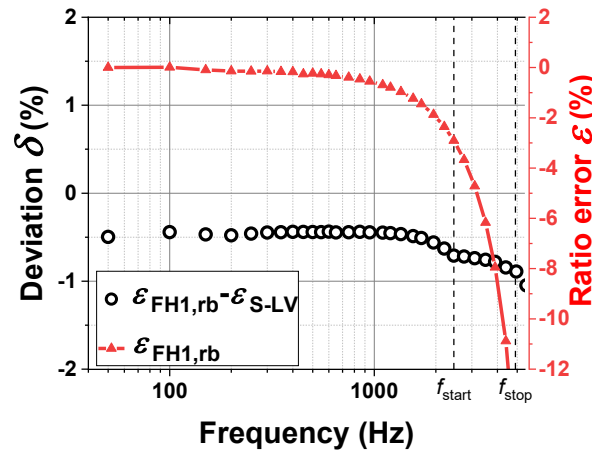test (triangle marker), and the deviation between $\varepsilon_{S-LV}(f)$ and $\varepsilon_{FH1,rb}(f)$ (circle marker).

As expected, it is necessary to carry out the S-LV procedure for each rated
burden condition under which the VT is designed to operate. As regards the fit

frequency region identification, it should be taken into account that the burden does not change the first frequency resonance point [45], so it is not necessary to repeat the identification of f_R, f_{start} and f_{stop} since the values are the same as those found with zero burden. As to the fit parameters, b and a have higher value in the presence of00 the burden: b increases from 1.7 to 2.40 whereas a goes from 0.2 s to 0.21 s. Results of this analysis are shown in Fig. 5.29, where the reference ratio errors $\varepsilon_{FH1,rb}(f)$, $\delta_{S-LV,rb}(f)$ and $\delta_{LV}(f)$ are shown. Similarly to the zero burden case, the S-LV method strongly reduces the ratio error deviations by giving values below 0.1% up to 1500 Hz, whereas the maximum error is found at 4950 Hz and equal to -0.6%.
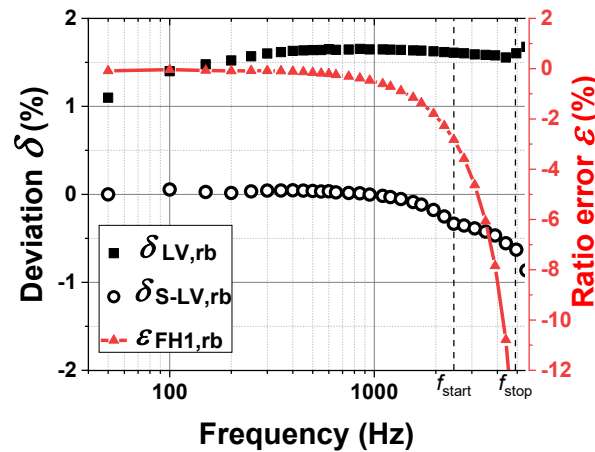
Fig. 5.29 Ratio error deviation of VT1 with rated burden, obtained by the LV (square marker) and S-LV (circle marker) procedure.

Comparison among the E-SINDICOMP and SINDICOMP-LV

In this section, the comparison among the two techniques is provided. For this analysis, only VT1 is considered. The approximated responses are built using the same data set, that is the response measured at 100% of the rated voltage and rated frequency and the response measured under SFS at 7 V. The deviations of the two techniques concerning the REF conditions are shown in Fig. 5.30. As can be observed in all the considered frequency range, SINDICOMP-LV produces results more accurate, being the deviations lower than those relative to E-SINDICOMP. Generally, SINDICOMP-LV deviations are within $\pm0.5\%$ up to 5 kHz, whereas E-SINDICOMP deviations exceed $\pm1\%$ at 2 kHz.

However, the E-SINDICOMP method can still be considered a valid technique:
it can be applied when only the frequency behavior of VT ratio error is needed, and
from the computational point of view, it is preferred to perform an easier operation,
that is, a numerical derivative instead of a fit.
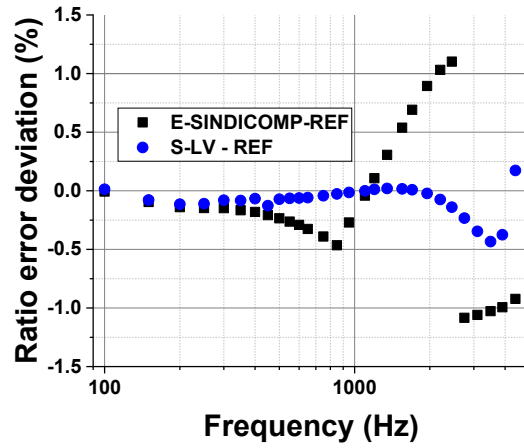
Fig. 5.30 Comparison between E-SINDICOMP and SINDICOMP-LV procedures.

Chapter 6

Conclusions and Future work

The evolution of the electrical network in terms of extensions and complexity has exacerbated the associated problem of PQ degradation, making it a critical topic. The measurement chain for PQ monitoring at levels other than low must include ITs to scale down the voltage and current to amplitude fitting with the PQ measuring units.

A thorough examination of recent literature and standards dealing with PQ phenomena and ITs revealed a normative and knowledge gap concerning the performance of ITs used in PQ applications. In this context, this thesis has presented a novel characterization setup and measurement procedures for quantifying the error contribution of voltage sensors when they are involved in PQ or PMU measurements.

The measurement setup has been designed to be modular and flexible. It can be used to characterise different types of voltage sensors, including those with digital output (IEC 61850-9-2 compliant).

The measurement system has been characterized in all its parts. The relative expanded uncertainties (level of confidence 95%) for the VT ratio error and phase error are equal to 70 µV/V and 70 µrad for measurement at power frequency and 185 µV/V and 320 µrad for measurement from 100 Hz to 9 kHz and from 5 kV to 20 kV.

An extensive set of test waveforms has been implemented for investigating voltage sensors performances in presence of several PQ event and combinations of events. In particular, the PQ phenomena available and already tested are:

- fundamental plus one or *N* harmonics and interharmonics,

- amplitude and phase modulated signals,

- frequency ramps,

- voltage dip,

- PQ events reconstructed from available database of on-site recorded signal (comtrade files).

As first applications, commercial inductive VTs, LPVTs and inductive VT coupled with commercial SAMU have been characterized under PQ events listed above. From these characterization tests, one of the most significant result is related to the harmonic measurement in presence of subharmonics phenomenon. It has been found that the presence of subharmonics impacts very negatively on the inductive VT performance in the measurement of harmonics, especially the first ones. In particular, in same cases subharmonics at low frequency lead the VT harmonics ratio and phase errors to increases of 20% and 30 mrad, respectively.

The thesis presented two simplified procedures (E-SINDICOMP and SINDICOMP-LV) for the measurement of the frequency response of the MV VTs in common industrial laboratories.

The E-SINDICOMP technique provides a method for the only approximation of VT ratio error response whereas SINDICOMP-LV allows to build the VT frequency response in terms of both amplitude and phase. The simplified methods have been applied for the frequency characterization of three different VTs and validated by comparison with results obtained using the developed reference generation and measurement set up.

Both the simplified procedures allow reaching an accuracy improvement with respect to the use of a conventional LV SFS technique up to one order of magnitude for the ratio error.

The results provided by the two simplified techniques are then compared with each other and it is found that SINDICOMP-LV produces a better approximation of the VT ratio error frequency response. In particular, SINDICOMP-LV accuracy performance in the VT ratio error evaluation is found within 0.4% up to 20th harmonic, and within 1% close to the resonance frequency; as to the phase error, it is always within 0.8 mrad.

Future developments of this research activity will include the analysis of the impact of external influence factors such as temperature, on-site burden, grounded, floating or energized structures on VT performance in the measurement of PQ phenomena. Sensors with different features (from different manufacturers, with different types of insulation, different accuracy class at power frequency etc) will be tested under PQ phenomena other than those presented, such as slow transients, voltage swells, and other phenomena combinations (for example, simultaneous modulation of amplitude and phase). In particular, a massive and systematic measurement campaign will be carried out in order to:

1. identify an extension of the VT accuracy classes for measuring PQ phenomena,

2. identify a minimum set of tests for the VT test.

Finally, it will be investigated how to extend the developed system to include PQ phenomena with spectral content greater than 9 kHz up to 150 kHz.

References

[1] IEC 61869-6 - Instrument Transformers - part 6: Additional general requirements for low-power instrument transformers. Standard, TC38, April 2011.

[2] Roman Targosz and Jonathan Manson. Pan-european power quality survey. In *2007 9th International Conference on Electrical Power Quality and Utilisation*, pages 1–6, 2007.

[3] R. Targosz. Evaluating cost of inadequate quality of supply. In *IEEE PES General Meeting*, pages 1–8, 2010.

[4] IEC 61869-2 - Instrument Transformers - part 2 : Additional requirements for inductive current transformers. Standard, TC38, April 2011.

[5] IEC 61869-3 - Instrument Transformers - part 3: Additional requirements for inductive voltage transformers. Standard, TC38, April 2011.

[6] IEC 61869-103 - Instrument Transformers - part 103: The use of instrument transformers for power quality measurement». Technical report, IEC, April 2012.

[7] Alessandro Mingotti, Lorenzo Peretto, and Roberto Tinarelli. A smart frequency domain-based modeling procedure of rogowski coil for power systems applications. *IEEE Transactions on Instrumentation and Measurement*, 69(9):6748–6755, 2020.

[8] T. Pfajfar, J. Meyer, P. Schegner, and I. Papič. Influence of instrument transformers on harmonic distortion assessment. In *2012 IEEE Power and Energy Society General Meeting*, pages 1–6, 2012.

[9] Antonio Cataliotti, Valentina Cosentino, Gabriella Crotti, Antonio Delle Femine, Dario Di Cara, Daniele Gallo, Domenico Giordano, Carmine Landi, Mario Luiso, Mohammad Modarres, and Giovanni Tinè. Compensation of nonlinearity of voltage and current instrument transformers. *IEEE Transactions on Instrumentation and Measurement*, 68(5):1322–1332, 2019.

[10] Marco Faifer, Christian Laurano, Roberto Ottoboni, Sergio Toscani, and Michele Zanoni. Harmonic distortion compensation in voltage transformers for improved power quality measurements. *IEEE Transactions on Instrumentation and Measurement*, 68(10):3823–3830, 2019.

[11] Yeying Chen, Gabriella Crotti, Alexander Dubowik, Palma Sara Letizia, Enrico Mohns, Mario Luiso, and Jorge Bruna. Novel calibration systems for the dynamic and steady-state testing of digital instrument transformers. In *2021 IEEE 11th International Workshop on Applied Measurements for Power Systems (AMPS)*, pages 1–6, 2021.

[12] EURAMET. Measurement methods and test procedures for assessing accuracy of instrument transformers for power quality measurements, 19NRM05 IT4PQ, 2019.

[13] G. Crotti, H.E. van den Brom, E. Mohns, R. Tinarelli, M. Luiso, R. Styblikova, M Agazar, H. Cayci, P. Mazza, J. Meyer, and M. Almutairi. Measurement methods and procedures for assessing accuracy of instrument transformers for power quality measurements. In *2020 Conference on Precision Electromagnetic Measurements (CPEM)*, pages 1–2, 2020.

[14] S. Zhao, H. Y. Li, P. Crossley, and F. Ghassemi. Testing and modelling of voltage transformer for high order harmonic measurement. In *2011 4th International Conference on Electric Utility Deregulation and Restructuring and Power Technologies (DRPT)*, pages 229–233, 2011.

[15] EN 50160 - Voltage characteristics of electricity supplied by public distribution networks, May 2011.

[16] IEC TS 62749 - Assessment of power quality - characteristics of electricity supplied by public networks, February 2020.

[17] IEC 61000-2-12 - Part 2-12: Compatibility levels for low-frequency conducted disturbances and signalling in public medium-voltage power supply systems. Standard, April 2011.

[18] IEC 61000-4-30 - Electromagnetic compatibility (emc) - part 4-30: Testing and measurement techniques - power quality measurement methods, February 2015.

[19] IEC 61000-4-7 - Electromagnetic compatibility (emc) - part 4-7: Testing and measurement techniques - general guide on harmonics and interharmonics measurements and instrumentation, for power supply systems and equipment connected thereto, August 2002.

[20] IEEE 1159 - Recommended practice for monitoring electric power quality. *IEEE Std 1159-2019 (Revision of IEEE Std 1159-2009)*, pages 1–98, 2019.

[21] IEC 61000-4-11 - Electromagnetic compatibility (emc) part 4-11: Testing and measurement techniques - voltage dips, short interruptions and voltage variations immunity tests for equipment with input current up to 16 a per phase, August 2020.

[22] IEEE/IEC 60255-118 - International standard - measuring relays and protection equipment - part 118-1: Synchrophasor for power systems - measurements. *IEC/IEEE 60255-118-1:2018*, pages 1–78, 2018.

[23] IEC 61869-10 - Instrument Transformers - part 10: Additional requirements for low-power passive current transformers, July 2018.

[24] IEC 61869-11 - Instrument Transformers - part 10: Additional requirements for low-power passive voltage transformers, June 2018.

[25] IEC 60044-7 - Instrument Transformers- part 7: Electronic voltage transformers, November 2001.

[26] IEC 60044-8 - Instrument Transformers - part 8: Electronic current transformers, June 2004.

[27] Gabriella Crotti, Giovanni D'Avanzo, Carmine Landi, Palma S. Letizia, Mario Luiso, Fabio Muñoz, and Helko van den Brom. Instrument transformers for power quality measurements: a review of literature and standards. In *2021 IEEE 11th International Workshop on Applied Measurements for Power Systems (AMPS)*, pages 1–6, 2021.

[28] Kaspirek Martin, Mikula Ladislav, Mezera David, Prochazka Karel, Santarius Pavel, and Krejci Petr. Analysis of voltage quality parameters in MV distribution grid. In *2014 16th International Conference on Harmonics and Quality of Power (ICHQP)*, volume 2017, page 517–521, 2017.

[29] Denisa Rusinaru, Leonardo Geo Manescu, Marius Merfu, and Petru Postolache. Power quality general levels in distribution networks. In *2014 16th International Conference on Harmonics and Quality of Power (ICHQP)*, pages 58–62, 2014.

[30] Martin Kašpírek. Voltage quality in the medium voltage distribution grid with connected wind power plants. In *2016 17th International Scientific Conference on Electric Power Engineering (EPE)*, pages 1–5, 2016.

[31] E. A. Mertens, L. F. S. Dias, F. A. Fernandes, B. D. Bonatto, J. P.G. Abreu, and H. Arango. Evaluation and trends of power quality indices in distribution system. In *2007 9th International Conference on Electrical Power Quality and Utilisation*, pages 1–6, 2007.

[32] CIGRE/CIRED JWG C4.112. *GUIDELINES FOR POWER QUALITY MONITORING – MEASUREMENT LOCATIONS, PROCESSING AND PRESENTATION OF DATA.* CIGREEditor: CIGREISBN: 978-2-85873-297-5, 2014.

[33] Petr Krejci, Pavel Santarius, Radomir Gono, and Zdenek Brunclik. Long-term monitoring of flicker and some other parameters of voltage quality. In *2016 IEEE 16th International Conference on Environment and Electrical Engineering (EEEIC)*, pages 1–6, 2016.

[34] Etienne Gasch, Max Domagk, Jan Meyer, Sami Abdelrahman, Huilian Liao, and Jovica V. Milanović. Assessment of power quality performance in distribution networks part i - measurement campaign and initial analysis. In *2016 17th International Conference on Harmonics and Quality of Power (ICHQP)*, pages 164–169, 2016.

[35] David Mezera. Voltage quality in the low voltage distribution grids with the high penetration of distributed energy sources. In *2015 16th International Scientific Conference on Electric Power Engineering (EPE)*, pages 292–295, 2015.

[36] Zuriayati Zainal, S.P. Ang, M. A. Salam, Pg Jamra Weira, and R. Goh. Measurement of harmonics in different sectors on 11 kv distribution networks. In *2013 IEEE International Conference of IEEE Region 10 (TENCON 2013)*, pages 1–5, 2013.

[37] Gil de Castro Westman Mailn Brodin Magnus Rönnberg Sarah, Gutiérrez Ballesteros. Long-term power quality measurements in medium voltage networks. In *2016 17th International Conference on Harmonics and Quality of Power (ICHQP)*, page 5, 2019.

[38] A. Testa, M. F. Akram, R. Burch, G. Carpinelli, G. Chang, V. Dinavahi, C. Hatziadoniu, W. M. Grady, E. Gunther, M. Halpin, P. Lehn, Y. Liu, R. Langella, M. Lowenstein, A. Medina, T. Ortmeyer, S. Ranade, P. Ribeiro, N. Watson, J. Wikston, and W. Xu. Interharmonics: Theory and modeling. *IEEE Transactions on Power Delivery*, 22(4):2335–2348, 2007.

[39] A. Honrubia-Escribano, A. Molina-García, E. Gómez-Lázaro, and E. Muljadi. Power quality survey of a photovoltaic power plant. In *2013 IEEE 39th Photovoltaic Specialists Conference (PVSC)*, pages 1799–1804, 2013.

[40] Kjetil Uhlen Jorun Irene Marvik, John Olav Giæver Tande. Wind farm voltage dip measurements. In *CIRED 2015*, pages 1137–1145, 2015.

[41] M. Tesarova and M. Kaspirek. Evaluation of long-term voltage dip monitoring in HV,MV and LV networks. In *CIRED 2015*, pages 1–5, 2015.

[42] Abbas Ghaderi, Alessandro Mingotti, Lorenzo Peretto, and Roberto Tinarelli. Low-power voltage transformer smart frequency modeling and output prediction up to 2.5 kHz, using sinc-response approach. *Sensors*, 20(17), 2020.

[43] G. Crotti, D. Gallo, D. Giordano, C. Landi, M. Luiso, and M. Modarres. Calibration of mv voltage instrument transformer in a wide frequency range. In *2017 IEEE International Instrumentation and Measurement Technology Conference (I2MTC)*, pages 1–6, 2017.

[44] R. Stiegler, J. Meyer, and P. Schegner. Portable measurement system for the frequency response of voltage transformers. In *2012 IEEE 15th International Conference on Harmonics and Quality of Power*, pages 745–750, 2012.

[45] Christoph Buchhagen, Markus Fischer, Lutz Hofmann, and Holger Däumling. Metrological determination of the frequency response of inductive voltage transformers up to 20 kHz. In *2013 IEEE Power and Energy Society General Meeting*, pages 1–5, 2013.

[46] M. Klatt, J. Meyer, M. Elst, and P. Schegner. Frequency responses of mv voltage transformers in the range of 50 Hz to 10 kHz. In *Proceedings of 14th International Conference on Harmonics and Quality of Power - ICHQP 2010*, pages 1–6, 2010.

[47] S. Zhao, H. Y. Li, P. Crossley, and F. Ghassemi. Testing and modelling of voltage transformer for high order harmonic measurement. In *2011 4th International Conference on Electric Utility Deregulation and Restructuring and Power Technologies (DRPT)*, pages 229–233, 2011.

[48] Michal Kaczmarek and Ryszard Nowicz. Application of instrument transformers in power quality assessment. In *2010 Modern Electric Power Systems*, pages 1–5, 2010.

[49] T. Pfajfar, J. Meyer, P. Schegner, and I. Papič. Influence of instrument transformers on harmonic distortion assessment. In *2012 IEEE Power and Energy Society General Meeting*, pages 1–6, 2012.

[50] Adam J. Collin, Antonio Delle Femine, Daniele Gallo, Roberto Langella, and Mario Luiso. Compensation of current transformers' nonlinearities by tensor linearization. *IEEE Transactions on Instrumentation and Measurement*, 68(10):3841–3849, 2019.

[51] A. E. Emanuel, R. Langella, and A. Testa. Limiting low frequency interharmonic distortion and voltage fluctuations. In *IEEE PES General Meeting*, pages 1–6, 2010.

[52] A. Testa and R. Langella. Power system subharmonics. In *IEEE Power Engineering Society General Meeting, 2005*, pages 2237–2242 Vol. 3, 2005.

[53] G. D'Avanzo, A. Delle Femine, D. Gallo, C. Landi, and M. Luiso. Impact of inductive current transformers on synchrophasor measurement in presence of modulations. *Measurement*, 155:107535, 2020.

[54] M. Kaczmarek. Secondary current distortion of inductive current transformer in conditions of dips and interruptions of voltage in the power line. *Electric Power Systems Research*, 137:1–5, 2016.

[55] Gabriella Crotti, Antonio Delle Femine, Daniele Gallo, Domenico Giordano, Carmine Landi, and Mario Luiso. Measurement of the absolute phase error of digitizers. *IEEE Transactions on Instrumentation and Measurement*, 68(6):1724–1731, 2019.

[56] IEC 61850-9-2 - Communication networks and systems in substations- part 9-2: Specific communication service mapping (scsm) – Sampled values over ISO/IEC 8802-3. Standard, April 2004.

[57] International Organization for Standardization. *Guide to the expression of uncertainty in measurement (GUM)*.

[58] G. Crotti, D. Giordano, G. D'Avanzo, A. Delle Femine, D. Gallo, C. Landi, M. Luiso, P.S. Letizia, L. Barbieri, P. Mazza, and D. Palladini. Measurement of dynamic voltage variation effect on instrument transformers for power grid applications. In *2020 IEEE International Instrumentation and Measurement Technology Conference (I2MTC)*, pages 1–6, 2020.

[59] Gabriella Crotti, Giovanni D'Avanzo, Palma Sara Letizia, and Mario Luiso. Measuring harmonics with inductive voltage transformers in presence of sub-harmonics. *IEEE Transactions on Instrumentation and Measurement*, 70:1–13, 2021.

[60] Meng Wu, Le Xie, Lin Cheng, and Rongfu Sun. A study on the impact of wind farm spatial distribution on power system sub-synchronous oscillations. *IEEE Transactions on Power Systems*, 31(3):2154–2162, 2016.

[61] Z. Leonowicz. Power quality in wind power systems. *REPQJ*, 1(07):234–238, 2009.

[62] Gang Chen, Chang Liu, Guanhong Wang, Dongping Ai, Huabo Shi, and Yan Li. Research on simulation accuracy of ultra-low frequency oscillation in power system with high proportion of hydropower. In *2019 IEEE 3rd International Electrical and Energy Conference (CIEEC)*, pages 834–838, 2019.

[63] Qin LIU, Gang CHEN, Baisi LIU, Yudong ZHANG, Chuyu LIU, Zhuolin ZENG, Chengwei FAN, and Xiaoyan HAN. Emergency control strategy of ultra-low frequency oscillations based on wams. In *2019 IEEE Innovative Smart Grid Technologies - Asia (ISGT Asia)*, pages 296–301, 2019.

[64] Yiping Chen, Yingshang Liu, Zhuoyao Tang, Jun Hou, Yong Zhang, Weike Mo, and Haoyong Chen. Analysis of ultra-low frequency oscillation in yunnan asynchronous sending system. In *2017 IEEE Power Energy Society General Meeting*, pages 1–5, 2017.

[65] Nurashikin Jamil. Low frequency oscillations of hydroelectric power plant. In *2015 50th International Universities Power Engineering Conference (UPEC)*, pages 1–6, 2015.

[66] R. Langella, A. Testa, S. Z. Djokic, J. Meyer, and M. Klatt. On the interharmonic emission of pv inverters under different operating conditions. In *2016 17th International Conference on Harmonics and Quality of Power (ICHQP)*, pages 733–738, 2016.

[67] Md. Rabiul Islam, A. M. Mahfuz-Ur-Rahman, Kashem M. Muttaqi, and Danny Sutanto. State-of-the-art of the medium-voltage power converter technologies for grid integration of solar photovoltaic power plants. *IEEE Transactions on Energy Conversion*, 34(1):372–384, 2019.

[68] Selcuk Sakar, Sarah K. Rönnberg, and Math Bollen. Interharmonic emission in ac–dc converters exposed to nonsynchronized high-frequency voltage above 2 kHz. *IEEE Transactions on Power Electronics*, 36(7):7705–7715, 2021.

[69] Zbigniew Leonowicz. Analysis of sub-harmonics in power systems. In *2010 9th International Conference on Environment and Electrical Engineering*, pages 125–127, 2010.

[70] Joaquin Garrido-Zafra, Antonio Moreno-Munoz, Aurora R. Gil-de Castro, Francisco José Bellido-Outeirino, Ricardo Medina-Gracia, and Elena Gutiérrez-Ballesteros. Load scheduling strategy to improve power quality in electric-boosted glass furnaces. *IEEE Transactions on Industry Applications*, 57(1):953–963, 2021.

[71] R.F. Chu and J.J. Burns. Impact of cycloconverter harmonics. *IEEE Transactions on Industry Applications*, 25(3):427–435, 1989.

[72] P. Syam, P.K. Nandi, and A.K. Chattopadhyay. An improved feedback technique to suppress subharmonics in a naturally commutated cycloconverter. *IEEE Transactions on Industrial Electronics*, 45(6):950–953, 1998.

[73] P. Syam, G. Bandyopadhyay, P.K. Nandi, and A.K. Chattopadhyay. Simulation and experimental study of interharmonic performance of a cycloconverter-fedsynchronous motor drive. *IEEE Transactions on Energy Conversion*, 19(2):325–332, 2004.

[74] F. De Rosa, R. Langella, A. Sollazzo, and A. Testa. On the interharmonic components generated by adjustable speed drives. *IEEE Transactions on Power Delivery*, 20(4):2535–2543, 2005.

[75] J.P.G. De Abreu and A.E. Emanuel. The need to limit subharmonics injection. In *Ninth International Conference on Harmonics and Quality of Power. Proceedings (Cat. No.00EX441)*, volume 1, pages 251–253 vol.1, 2000.

[76] Francesco Bonavolontà, Luigi Pio Di Noia, Annalisa Liccardo, Salvatore Tessitore, and Davide Lauria. A pso-mma method for the parameters estimation of interarea oscillations in electrical grids. *IEEE Transactions on Instrumentation and Measurement*, 69(11):8853–8865, 2020.

[77] A. Testa, M. F. Akram, R. Burch, G. Carpinelli, G. Chang, V. Dinavahi, C. Hatziadoniu, W. M. Grady, E. Gunther, M. Halpin, P. Lehn, Y. Liu, R. Langella, M. Lowenstein, A. Medina, T. Ortmeyer, S. Ranade, P. Ribeiro, N. Watson, J. Wikston, and W. Xu. Interharmonics: Theory and modeling. *IEEE Transactions on Power Delivery*, 22(4):2335–2348, 2007.

[78] M. Klein, G.J. Rogers, and P. Kundur. A fundamental study of inter-area oscillations in power systems. *IEEE Transactions on Power Systems*, 6(3):914–921, 1991.

[79] J. Barros, M. de Apraiz, and R. I. Diego. Measurement of subharmonics in power voltages. In *2007 IEEE Lausanne Power Tech*, pages 1736–1740, 2007.

[80] Luigi Feola, Roberto Langella, and Alfredo Testa. On the effects of unbalances, harmonics and interharmonics on pll systems. *IEEE Transactions on Instrumentation and Measurement*, 62(9):2399–2409, 2013.

[81] José Matas, Miguel Castilla, Jaume Miret, Luis García de Vicuña, and Ramon Guzman. An adaptive prefiltering method to improve the speed/accuracy tradeoff of voltage sequence detection methods under adverse grid conditions. *IEEE Transactions on Industrial Electronics*, 61(5):2139–2151, 2014.

[82] Roberto Langella, Alfredo Testa, and Alexander E. Emanuel. On the effects of subsynchronous interharmonic voltages on power transformers: Single phase units. *IEEE Transactions on Power Delivery*, 23(4):2480–2487, 2008.

[83] Roberto Langella, Alfredo Testa, Jan Meyer, Friedemann Möller, Robert Stiegler, and Sasa Z. Djokic. Experimental-based evaluation of pv inverter harmonic and interharmonic distortion due to different operating conditions. *IEEE Transactions on Instrumentation and Measurement*, 65(10):2221–2233, 2016.

[84] IEEE 519 - Recommended practice and requirements for harmonic control in electric power systems. *IEEE Std 519-2014 (Revision of IEEE Std 519-1992)*, pages 1–29, 2014.

[85] IEC 61000-2-12 - Electromagnetic compatibility (emc) - part 2-12: Environment - compatibility levels for low-frequency conducted disturbances and signalling in public medium-voltage power supply systems, July 2003.

[86] IEC TR 61000-3-6 - Electromagnetic compatibility (emc) "smart city"., July 2008.

[87] IEC 61000-2-4 - Electromagnetic compatibility (emc) - part 2-4: Environment - compatibility levels in industrial plants for low-frequency conducted disturbances, June 2002.

[88] Paul Kinsler. Faraday's law and magnetic induction: Cause and effect, experiment and theory. *Physics*, 2(2):150–163, 2020.

[89] IEC 60050 - International electrotechnical vocabulary - details for iev number 411-47-02: "magnetization characteristic"», May 2002.

[90] Antonio Cataliotti, Dario Di Cara, Alexander E. Emanuel, and Salvatore Nuccio. A novel approach to current transformer characterization in the presence of harmonic distortion. *IEEE Transactions on Instrumentation and Measurement*, 58(5):1446–1453, 2009.

[91] Marco Faifer, Christian Laurano, Roberto Ottoboni, Sergio Toscani, Michele Zanoni, Gabriella Crotti, Domenico Giordano, Luca Barbieri, Marco Gondola, and Paolo Mazza. Overcoming frequency response measurements of voltage transformers: An approach based on quasi-sinusoidal volterra models. *IEEE Transactions on Instrumentation and Measurement*, 68(8):2800–2807, 2019.

[92] Gabriella Crotti, Giovanni D'Avanzo, Domenico Giordano, Palma Sara Letizia, and Mario Luiso. Extended sindicomp: Characterizing mv voltage transformers with sine waves. *Energies*, 14(6), 2021.

[93] G. Crotti, D. Giordano, G. D'Avanzo, P.S. Letizia, and M. Luiso. A new industry-oriented technique for the wideband characterization of voltage transformers. *Measurement*, 182:109674, 2021.

[94] Giovanni D'Avanzo, Marco Faifer, Carmine Landi, Christian Laurano, Palma Sara Letizia, Mario Luiso, Roberto Ottoboni, and Sergio Toscani. Theory and experimental validation of two techniques for compensating vt nonlinearities. *IEEE Transactions on Instrumentation and Measurement*, 71:1–12, 2022.